NASA

Technical Memorandum 86137

MHD PROCESSES IN THE OUTER HELIOSPHERE

L. F. Burlaga

AUGUST 1984

National Aeronautics and
Space Administration

Goddard Space Flight Center
Greenbelt, Maryland 20771

MHD Processes in the Outer Heliosphere

by

L. F. Burlaga
NASA/Goddard Space Flight Center
Laboratory for Extraterrestrial Physics
Greenbelt, MD 20771

CONTENTS

8. Radial Evolution of Large-Scale Fluctuations

   A. Velocity Fluctuations
   B. Magnetic Field Strength Fluctuations
   C. Filtering and Entrainment
   D. Turbulence

9. Discussion

1. Introduction

Exploration of the outer heliosphere (the region beyond Mars) began with the launches of Pioneers 10 in 1972 and Pioneer and 11 in 1973. Measurements of the magnetic field and solar wind plasma are available from the instruments of Smith and Wolfe, respectively, and the results of these measurements have been reviewed by Smith (1974, 1979, 1981, 1983), Smith and Wolfe (1977, 1979) Smith and Barnes (1983) and Intriligator (1976, 1977, 1980). The spacecraft Voyager 1 and Voyager 2 were launched into the outer heliosphere nearly half a solar cycle later, on September 5, 1977 and August 20, 1977, respectively. The choice of topics and the selection of figures in this review emphasize Voyager observations and analyses. Some of the plasma observations from Voyagers 1 and 2 were summarized by Gazis (1983), and Gazis and Lazarus (1983), but this is the first review of the magnetic field measurements from Voyager and the MHD processes in the outer heliosphere. An attempt was made to give a complete bibliography of the experimental and theoretical work concerning magnetic fields and plasmas observed in the outer heliosphere.

Emphasis in this review is on basic concepts and dynamical processes involving the magnetic field. The theory that serves to explain and unify the interplanetary magnetic field and plasma observations relating to phenomena with scales $\gtrsim$ 100 km is magnetohydrodynamics (MHD), which is summarized briefly in the next section. Basic physical processes and observations that can be directly related to solutions of the MHD equations are emphasized, but one must remember that obtaining solutions of this complex system of equations involves various assumptions and approximations. It is natural to be enamoured by the attractiveness of simple results, but the outer heliosphere does not always behave and appear as one would like. The spatial and temporal complexity of the outer heliosphere, and some approaches for dealing with this complexity are discussed, but the existing descriptions and explanations of complex phenomena are still inadequate.

The Voyager 1 and 2 trajectories projected onto the ecliptic plane are shown in Figure 1. Bends in the trajectories occur where the spacecraft encountered Jupiter and Saturn. Voyager 2 will encounter Uranus in January 24, 1986 and Neptune in August 24, 1989, and Voyager 1 is moving away from the

sun at a faster rate than Voyager 2. This review will emphasize the results obtained inside of the orbit of Saturn, $\lesssim$ 10 AU.

The Voyager spacecraft were designed primarily for planetary studies, so they are 3-axis stabilized (Pioneer 10 and 11 were spin-stabilized). A brief description of the spacecraft, an overview of its mission, and a complete list of its scientific instruments is given by Kohlhase and Penzo (1977). Additional information on the spacecraft and trajectories may be found in the references of their paper.

The magnetometer and solar wind plasma analyzer on Voyagers 1 and 2 are described by Behannon et al. (1977) and Bridge et al. (1977), respectively. The Principal Investigators are N. F. Ness and H. S. Bridge, respectively. The magnetometer is a dual-sensor system with a wide dynamic range, from 0.006 nT (nanoteslas) to 20 G (gauss). The sensors are light-weight fluxgate magnetometers and the low field system has a sensor noise of 0.006 nT RMS over a bandpass of 0-8.3 Hz. The instrument is capable of making accurate measurements of the interplanetary magnetic fields well beyond 10 AU even in the presence of a weak spacecraft field, which is measured and corrected for using the dual magnetometer concept (Ness et al., 1971, and Neubauer, 1975). The magnetometers on Voyager 1 and 2 are all operating at the time of this writing. The plasma analyzer consists of two Faraday cups. One of these cups is designed for studies of the solar wind and magnetosheath flows. It has a large field of view and an energy range from 10 to 5950 volts with a resolution of $\Delta E/E \geq 0.29$ (L mode). A large sensor area makes it possible to measure very low fluxes ($\lesssim 6 \times 10^3$ cm^{-2} sec^{-1}), giving accurate density (3%) and speed (1%). The solar wind velocity direction is measured to $\sim 0.15°$. The Voyager 2 instrument has operated without problems from launch to present. The Voyager 1 plasma analyzer failed after encounter with Saturn and for a period in 1978, but it operated satisfactorily during the encounters with Jupiter and Saturn and throughout most of the primary interplanetary cruise phase of the mission.

2. Basic Equations

Many interplanetary phenomena can be interpreted in the framework of magnetohydrodynamics. There have been numerous attempts to "justify" this theory on the basis of a plasma model which treats the medium in terms of particles and electromagnetic fields (see references in Cuperman, 1980), but a rigorous justification does not exist. We simply accept MHD as a set of postulates, a physical model, and we use it to organize and relate as many interplanetary observations and phenomena as possible. It is recognized that the model must not be applied on scales where particle phenomena manifest themselves, such as the gyroradius, gyroperiod, Debye length, interparticle spacing, etc. The gyroradius R_L is the largest of these scales, and it is of the order of 50 km at 1 AU. Since the scale of our system is of the order of 30 AU = 4.5×10^9 km $\sim 10^8$ R_L, there is ample scope for the application of MHD theory.

A. Dynamics

The MHD equation of motion in Eulerian form is:

$$\rho \frac{\partial \underset{\sim}{V}}{\partial t} + \rho(\underset{\sim}{V}\cdot\nabla)\,\underset{\sim}{V} = -\nabla p - (\nabla \times \underset{\sim}{B}) \times \underset{\sim}{B} + \rho \nu \nabla^2 \underset{\sim}{V} \qquad (1)$$

The left-hand side represents inertial effects, and the acceleration is written as the familiar sum of a "nonstationary" term $\frac{\partial \underset{\sim}{V}}{\partial t}$, and a "convective term" $(\underset{\sim}{V}\cdot\nabla)\,\underset{\sim}{V}$. The convective term is nonlinear, and it is the source of many interesting physical phenomena (such as stream steepening, "overtaking", and shock formation) as well as the principal source of mathematical difficulties in obtaining solutions. The right-hand side of Eq. 1 shows two types of terms, a dissipation term $\rho \nu \nabla^2 \underset{\sim}{V}$ and 2 force terms. The dissipation term may be important at small scales, e.g., in shocks, boundary layers and turbulence, but it is usually neglected in discussing large-scale processes. Only 2 forces are considered: a gas dynamic force per volume, ∇p, and a

magnetic (Lorentz) force per volume, $(\nabla \times \underset{\sim}{B}) \times \underset{\sim}{B} = \underset{\sim}{J} \times \underset{\sim}{B}$. In the absence of a magnetic field, the only force is ∇p and the equation of motion reduces to that of ordinary gas dynamics. Applications of gas dynamic theory to the solar wind have been reviewed by Parker (1963) and Hundhausen (1972, 1984). The magnetic force introduces new dynamical processes in the solar wind. One can write

$(\nabla \times \underset{\sim}{B}) \times \underset{\sim}{B} = \nabla \frac{B^2}{8\pi} + \frac{(\underset{\sim}{B} \cdot \nabla)\underset{\sim}{B}}{4\pi}$, which shows that the magnetic force may be regarded as the sum of a magnetic "pressure" force $\nabla \frac{B^2}{8\pi}$ that acts normal to the magnetic field direction and a "curvature force" that is present when the magnetic field lines have a non-zero curvature. Most applications of Eq. (1) to the solar wind have neglected the curvature force, in which case the effect of the magnetic field is essentially the same as that of the gas pressure. One then speaks of the "total pressure" $P = p + B^2/8\pi$, and the equation of motion reduces to

$$\rho \frac{\partial \underset{\sim}{V}}{\partial t} + \rho(\underset{\sim}{V} \cdot \nabla)\underset{\sim}{V} = -\nabla P. \qquad (2)$$

This has the same form as the gas dynamic equation, and it can therefore be treated by the standard methods of gas dynamics.

The equation of motion (1) shows that we are considering two vector fields ($\underset{\sim}{B}$ and $\underset{\sim}{V}$) and two scaler fields (ρ and p). Thus, we describe the system by a set of functions, the components of $\underset{\sim}{B}$ and $\underset{\sim}{V}$ together with ρ and p; i.e., we describe it as a field, with no reference to particles or bodies. Additional equations are needed to describe the system completely and self-consistently.

The density ρ is related to the velocity field $\underset{\sim}{V}$ very simply through a constraint expressing conservation of mass:

$$\frac{\partial \rho}{\partial t} + \nabla \cdot (\rho \underset{\sim}{V}) = 0 \qquad (3)$$

The absence of a source term expresses the neglect of reactions that might convert matter from one form to another.

B. Thermodynamics

The gas pressure p implies a link to thermodynamics. It is usually assumed that the gas is polytropic, in which case the thermal conductivity and heat flux are not considered explicitly. The electrical resistivity and viscosity are assumed to be zero everywhere except possibly at singular points. This exception is very important, for it means the phenomena such as reconnection and shocks can be treated in the framework of ideal MHD, but they must be treated separately, e.g., by identifying a singular shock surface and applying the Rankine-Hugoniot equation across it. Thus everywhere except at singularities it may be assumed that the equation of state $p = p(S,\rho)$ can be written in the separated form $p = A(S)\ \rho^{\gamma}$, where γ is the adiabatic constant and S is the entropy. Different volume elements (e.g., those coming from different regions on the sun or those ahead of and behind a shock) may have different entropy, hence different A, but for any given volume element, $p \propto \rho^{\gamma}$. In this way even irreversible processes can be introduced within the formalism of ideal MHD. This type of equation of state implies that the entropy of a given volume element is constant everywhere except at singularities, i.e., entropy is conserved. In other words $A(S) = p\rho^{-\gamma}$ is a constant following a volume element, which gives the constraint

$$\left(\frac{\partial}{\partial t} + \underset{\sim}{V} \cdot \nabla\right)\ (P\ \rho^{-\gamma}) = 0. \qquad (4)$$

An additional complication arises because in the solar wind one measures temperature rather than pressure. It is usually assumed that $p = nkT = \rho/m\ kT$, where n is the number density, but one must recognize that the solar wind is made of not one component, as assumed up till now, but primarily two components--protons and electrons. In general, their number densities are nearly equal--$n_e \approx n_p$ but their temperatures are different $T_e \neq T_p$. Thus we should replace $p = nkT$ by $p = n_e\ kT_e + n_p\ kT_p \approx n_p k(T_e + T_p)$ where n_p is the proton number density. For various practical reasons, electron measurements are not always available. In this case, it is often assumed that $T_e \propto T_p$, so $P \propto 2\ nkT$ where T is the proton temperature and n is the proton density. Observations of the radial variations of the temperature of protons and electrons have been reported by Sittler and Scudder (1980), Gazis and Lazarus (1982), Kayser (1984), and Mihalov and Wolfe (1978).

C. Electrodynamics

The absence of magnetic charge is expressed by Gauss' law

$$\nabla \cdot \underset{\sim}{B} = 0, \tag{5}$$

which asserts that the magnetic field lines never begin or end--except at singular points, where B = 0 or the field is discontinuous. This exception is rarely mentioned, but it is very important, for it allows the introduction of processes such as reconnection and shocks without requiring resistivity or dissipation in the medium as a whole, provided one introduces singularities and discontinuties in the field. There is no fundamental mathematical problem in doing this; it simply enriches the topology. The magnetic field is coupled directly to the velocity field by Faraday's law in the form

$$\frac{\partial \underset{\sim}{B}}{\partial t} = \nabla \times (\underset{\sim}{V} \times \underset{\sim}{B}). \tag{6}$$

In writing this equation, it is assumed that $\underset{\sim}{E} = -\underset{\sim}{V} \times \underset{\sim}{B}$ in an inertial frame, or equivalently that E = 0 in a frame moving with velocity $\underset{\sim}{V}$. Again, this is a good approximation everywhere except at isolated singularities in a fully ionized plasma. In general, one should add the term $\eta \nabla^2 \underset{\sim}{B}$, where η is the electrical resistivity. This term can be important on very small scales, for example near neutral points or in shocks.

Equations 2-6 are a complete set of equations for the 2 vector fields $\underset{\sim}{V}$, $\underset{\sim}{B}$, and the 2 scalar fields ρ and p. Note that the equations form a system of first order partial differential equations. Such systems allow geometrical interpretations in a natural way. The presence of the operator $\left(\frac{\partial}{\partial t} + \underset{\sim}{V} \cdot \nabla\right)$ implies that propagation phenomena are important. In the interplanetary medium the bulk flow speed is greater than the characteristic speeds, i.e., the flow is "supersonic", and the equations are hyperbolic, which has further mathematical and physical implications. We shall not discuss these

implications here, but simply emphasize that Equations 2-6 embody a great wealth of mathematical ideas and physical phenomena.

D. Coordinates

All of the functions of interest, as well as the locations of the spacecraft, depend on position and time. It is necessary to adopt a single inertial coordinate system so that positions can be given by a consistent set of numbers. Our choice of an inertial coordinate frame is the "inertial heliographic system" (IHG) which is illustrated in Figure 2. This is based on the following considerations. Since the sun is the source of interplanetary plasma and magnetic fields, a mathematical singularity to first approximation, it is natural to put the origin of the coordinate system at the center of the sun. The rotation of the sun singles out one line (the rotation axis), and its sense of rotation gives a natural orientation. Thus, the $\hat{Z}_{IHG}$ axis is chosen to point northward along the rotation axis. Choosing an orthonormal basis, the X_{IHG} and Y_{IHG} axes are then in the solar equatorial plane. The intersection of the solar equatorial plane with the ecliptic plane gives a line, the longitude of the ascending mode, which we shall take as the X_{IHG}-axis. This drifts slowly with time ($\sim 1°/72$ yrs). and we shall take the X_{IHG}-axis along the direction of the ascending node in 1900. The Y_{IHG}-axis is then choosen to complete an orthonormal triad. Thus, the basis of the inertial coordinate system which we choose is that illustrated in Figure 2. In particular, we specify the location of the Voyager 1 and 2 spacecraft with reference to this basis, and the field variables will be considered to be functions of the coordinates (X_{IHG}, Y_{IHG}, Z_{IHG}) relative to this basis. For brevity we shall drop the subscripts and understand that (X,Y,Z) refers to the inertial heliographic coordinate.

Since we are considering two vector fields $\underset{\sim}{V}$ and $\underset{\sim}{B}$, it is necessary to adopt a basis at every point in the heliosphere in order to specify components of the fields. The orientation and position of each of these bases is given relative to the inertial system described above. One natural direction is along the line joining a given point (X,Y,Z) with the center of the sun, i.e., the radial direction. Thus we choose one of the 3 basic vectors, $\hat{X}_{HG}$ (X,Y,Z), where (X,Y,Z) is the origin of the basis in relation to the inertial frame, to

be a unit vector directed radially from the sun to the observer at (X,Y,Z) (Figure 3). The $\hat{Y}_{HG}$ (X,Y,Z) direction is assumed to be parallel to the solar equatorial plane (normal to $\hat{Z}_{IHG}$), normal to $\hat{X}_{HG}$, and pointing in the direction of motion of the planets. The $\hat{Z}_{HG}$ (X,Y,Z) axis is chosen to complete an orthonormal triad. Thus, at each point in the heliosphere one has a triad $\hat{X}_{HG}$, $\hat{Y}_{HG}$, $\hat{Z}_{HG}$, and one can specify the components of any vector at that point relative to this basis. It is convenient to describe the direction of a vector $\underset{\sim}{B}$ at a point in terms of two angles λ and δ, where δ is the elevation angle relative to the X_{HG}-Y_{HG} plane and λ is the angle measured in the plane relative to the X_{HG}-axis, and considered to be positive for rotations of $\underset{\sim}{B}$ in the same sense as the sun's rotation.

3. Large-scale Variations

A. Magnetic Field Strength

The radial variation of the strength of the interplanetary magnetic field between 1 AU and ~ 9.5 AU, measured by Voyager 2 between August 21, 1977 and August 10, 1981, is shown in Figure 4. The center of each bar represents a 25 day average of the magnetic field (25 days being approximately the solar rotation period in an inertial frame) and the length of the bar gives the uncertainty of the average. The solid curve in Figure 4 (from Burlaga et al., 1984a) is a theoretical curve derived by Parker (1958, 1963), with the constant 4.75 chosen to minimize the deviation between the observations and the theoretical curve. The curve is derived on the basis of the following assumptions: 1) The solar wind velocity is radial and of constant speed; 2) The medium is axially symmetric, i.e., the equations are invariant with respect to rotations about the solar rotation axis; and 3) The solar magnetic field does not change with time. Equation 5 implies that the radial component of the field is $B_R \sim R^{-2}$ and Equation 6 implies that the azimuthal component of the field is $B_T \sim R^{-1}$. Combining these two components gives the formula shown in Figure 4. Considering the simplicity of the assumptions and the resulting formula, Parker's curve gives a remarkably good fit to the data. This is certainly a satisfactory zeroth order description of the magnetic field strength. There is significant scatter of the observations relative to this curve which is a hint of complexities that will be discussed below.

The radial variation of B(R) was also measured by the Pioneer 10 and 11 spacecraft, at a different epoch of the solar cycle. Smith (1974) reported agreement with Parker's theory to first order between 1 AU and 4.3 AU, but he noted significant systematic second order deviations. Similar results were reported for Pioneer 10 observations between 1 AU and 8.5 AU by Smith and Wolfe (1979). On the other hand, Smith and Barnes (1983) found that Pioneer 10 and 11 observations of B(R) between 1 AU and ~ 11 AU were consistent with Parker's model, but they argued that this was a coincidence. On the basis of a comparison of 1 AU data with Pioneer data, they suggested that the field strength actually decreased significantly more rapidly with R than Parker's model predicts, but this just happened to be compensated by an increase of the

solar magnetic field with time in the interval in which the measurements were made. Long term variations of the interplanetary magnetic field strength were reported by King (1979, 1981), Burlaga et al. (1982b), and Slavin et al. (1984). Smith and Barnes (1983) suggested that the systematic decrease of B with respect to Parker's curve might be due to a latitude effect. Slavin et al. (1984) observed that the B_T component of $\underset{\sim}{B}$ measured by Pioneer apparently decreased with R faster than predicted. A similar effect over shorter distances has been reported by various authors (see the review of Behannon, 1978, and the paper by Jokipii, 1976). Slavin et al. (1984) suggested that the effect is due to the transport of magnetic flux away from the equatorial plane by meridional flow. Parker's model predicts a higher magnetic pressure in the equatorial plane than over the poles, because the spiral is "tighter" in the equatorial plane. The resulting pressure gradient would tend to drive a meridional flow (Suess and Nerney, 1973); Nerney and Suess, 1975; Suess and Nerney, 1975) but it was not expected that this effect should be as large as the one reported by Slavin et al. (1984), and Smith and Barnes (1983).

Measurements of the radial variation of B(R) using simultaneous data from 1 AU (IMP-8 data from the experiment of Ness et al. and ISEE-3 data from the experiment of Smith) and from Voyager 1 and 2) do not show large systematic ($\sim$ 20%) deviations from the spiral model within 10 AU. Figure 5 from Burlaga et al. (1984a) shows the 1 AU observations together with Voyager observations of B, normalized to 1 AU by dividing by the fit to Parker's model given in Figure 4. There are large fluctuations of the Voyager magnetic field strengths, related to dynamical processes in the solar wind, but no significant systematic differences between the two curves is evident. The reason for the apparent disagreement between the Voyager results and the Pioneer results is not yet clear. The difference might be real, since the Pioneer and Voyager measurements at a given distance were made at significantly different times and at different latitudes. It might also be due to the use of different averaging methods (which are important in dealing with large-amplitude fluctuations about the mean) or possibly to instrumental effects.

B. Magnetic Field Direction

Parker's model gives the direction of the field as well as the magnitude. Figure 6 (Burlaga et al., 1982b) shows daily average Voyager 2 observations

between 1 AU and 5 AU. The δ angle (see Figure 3) should be zero according to Parker's model, and on average that is observed. Note that there are large fluctuations about the average, corresponding to phenomena which are not included in Parker's model for the large-scale field. Of greater interest is the λ-angle, or azimuthal direction of the field (see Figure 3). The directions predicted by Parker's model are shown by the 2 solid curves; there are two curves because the magnetic field can have either of two orientations, "toward the sun" or "away from the sun". The "sector" structure can be seen clearly between 3 AU and 4 AU, but it is less evident elsewhere. The observed values of λ are generally close to the theoretical values, particularly when the sectors are well-defined, but there are times when significant departures from the theoretical values occur and the sector structure is not clear. These are found to be times when there were many transients, i.e., non-stationary flows, as discussed below. The early Pioneer 10 and 11 observations showed very good agreement with the theoretical spiral directions (Thomas and Smith, 1980) but these observations were made when the sun was quiet and the flows were relatively steady.

C. Components of B

Instead of considering the magnitude and direction of $\underset{\sim}{B}$ one can equivalently consider the components B_R, B_T, B_N, with respect to the HG basis vectors $\hat{X}_{HG}$, $\hat{Y}_{HG}$, $\hat{Z}_{HG}$, respectively (see Figure 3). Voyager 1 observations of 24-hr averages of these components obtained between 1 AU and 5 AU are shown in Figure 7, from Burlaga et al., 1982b. Note the very large scatter in the observations at a given R, which reflects the variability of the solar wind due to dynamical processes on many different scales. Clearly, in drawing conclusions from fits to those data or averages of them, one must take care to consider the fluctuations, which represent physical processes that are not considered in Parker's model. Consider $|< B_N >|$ for example. According to Parker's model this should be zero for all R, and Figure 6 shows that the field does fluctuate randomly about $\delta = 0$. Yet Figure 7 shows relatively large values of $|< B_N >|$ decreasing as $R^{-0.2}$. This represents small and intermediate scale phenomena, and it has nothing to do with the large-scale field. These effects are also superimposed on the B_T and B_R components. For example, at 5 AU $|< B_R >|$ is comparable to $|< B_N >|$ and we may conclude that

the measured average component at that distance is largely due to fluctuations rather than the large-scale Parker field. The best fit to $|< B_R >|$ implies a decrease as $R^{-1.6}$ rather than R^{-2}, probably because the effects of small and intermediate scale fluctuations become increasingly important at larger R. The B_T component is the largest component at large distances, and the fluctuations in this component are less important out to 5 AU. Thus $|< B_T >|$ varies as $R^{-0.92}$, in close agreement with the theoretical value $R^{-1.0}$. Using Pioneer 10 data, Rosenberg et al. (1978) found that $B_T \propto R^{-1.29 \pm 0.06}$ and $B_R \propto R^{-2.1 \pm 0.03}$ between 1 AU and 5 AU. Thus, these authors found that the azimuthal field component decreases significantly more rapidly than Parker's model predicts. A similar result was found in Mariner data obtained between 1 AU and 1.5 AU by Coleman et al. (1969).

D. Sectors

The interplanetary magnetic field may have one of two possible orientations at any point and time, either toward the sun or away from the sun. One can describe the pattern of polarities on successive solar rotations by assigning a polarity for each day when the data coverage is sufficiently complete. If the field is directed away from (toward) the sun on more than 2/3 of the hours for which data are available, the polarity is designed + (-). If no dominant polarity is observed on a given day, due to a mixture of inward and outward fields on that day, the polarity is said to be mixed, and it is denoted by a dot. The polarities derived in this way from the Voyager 1 data are shown in Figure 8 from Burlaga et al. (1984a); similar results were obtained from Voyager 2. Sector boundaries are outlined in Figure 8, but note that they are only approximate, owing to data gaps and regions of mixed polarity. The essential point is that a 4-sector pattern was observed between day 268 of 1977 and day 200 of 1978, and a 2-sector pattern was observed thereafter until $\sim$ day 51 of 1979. Essentially the same pattern was observed at 1 AU (Sheeley and Harvey, 1981), indicating that the change from 4-sectors to 2-sectors was a temporal effect rather than an effect of radial evolution or spacecraft latitude. It is possible that stream interactions alter the position and shape of the sector boundary, as suggested by Smith (1981), and Hakamada and Akasofu (1982) but this is at most a perturbation of the underlying pattern. Pizzo (1982) argued that the effect is smaller than these

authors suggested, and certainly not large enough to produce a very large meridional component of the field. To first approximation, we can assume that the sector pattern mapped from 1 AU to at least 5 AU with no significant qualitative change in the pattern as a whole.

The relation between the orientation of the sector boundary surface observed by Voyager within $\sim$ 3 AU and that observed in the corona was investigated by Behannon et al. (1983). The footpoints of the current sheet in the corona were identified with the maximum intensity of white-light polarization brightness (see Hundhausen, 1977). When the white-light data indicated that the current sheet was near to the equatorial plane, Voyager 1 and 2 observed mixed polarities (Figure 9a). When the white-light data indicated a highly inclined sector boundary surface, Voyager 1 and 2 observed a sector boundary crossing after an interval corresponding to the propagation time from the sun to the spacecraft. It was found that the observed inclination of the thin highly inclined sector boundary was consistent with that computed from a "minimum variance analysis" of high resolution magnetic field measurements in that boundary, but minimum variance analysis of current sheets in the horizontal (equatorial) sector boundary surface did not give the expected normal. Thus, the minimum variance method must be used with great caution in determining sector boundary orientations.

E. Large-scale Field Strength Fluctuations

It was shown above that the average field strength is given to good approximation by Parker's model, which is a kinematic model involving no forces or energy transfer processes. Figure 6 shows that large fluctuations about this average are generally present even when daily averages are considered. These fluctuations represent the results of dynamical interplanetary processes, which will be the subject of the following sections in this review.

One can exhibit the fluctuations most clearly by removing the large-scale spiral field variation, e.g., by dividing the observed field strength B by the nominal spiral model field strength at that distance, B_p. Regarding B as the spiral field plus a perturbation field B', one obtains $B/B_p = 1 + B'/B_p$. In

other words, the relative disturbance B'/B_p is given by $B/B_p - 1$, or simply B/B_p. Figure 10 shows daily averages of B/B_p for successive 27 day intervals in the same format as Figure 8. The approximate profile of sector boundaries shown in Figure 8 is reproduced in Figure 10. Typically, there are 2 or 3 regions of enhanced field strength on each solar rotation, and these are frequently observed near sector boundaries. This pattern is less clear in 1977, when 4-sectors and many transients were observed, and it is more clear in 1978 when there was a 2-sector pattern. The enhancements rarely recur at regular intervals (e.g., $\sim$ 27 days), i.e., the pattern is not stationary, but there does appear to be a relatively slow evolution of the pattern and a tendency to persist from one rotation to the next. The speed profiles for the same period are shown on the right of Figure 10, again with the approximate sector pattern from Figure 8. The streams tend to occur within sectors, and the speed tends to be low at sector boundaries, as expected from 1 AU observations (see Hundhausen, 1972), but the pattern is not as clear as that observed at 1 AU when the sun is not very active. Examination of Figure 8 shows that the perturbations in B are related to the streams, which is an indication that the perturbations represent the result of dynamical processes. A major question is, how do the streams and B/B_p profiles evolve with distance? The question must be answered within the context provided by Figure 10 which indicates that the pattern is evolving with time as well as with distance. Thus, in general one should use simultaneous data from two or more spacecraft to study the dynamical evolution of magnetic field fluctuations.

F. Shocks and Interfaces

Shocks and discontinuities are two fundamental features of supersonic MHD flows. Figure 11 provides an overview of the patterns of shocks and certain non-propagating discontinuities called "interfaces", in a format similar to that of Figure 10. A stream interface is a discontinuity across which the density decreases and the temperature increases. It is an indication of a corotating flow (Belcher and Davis, 1971; Burlaga, 1974; Gosling et al. 1978; and Burlaga and King, 1979), and an interface bounded by a forward-reverse shock pair indicates a corotating interaction region in which B/B_p and the total pressure are generally high. Interaction regions were defined by Burlaga and Ogilvie (1970) as regions with a scale of $\gtrsim$ several hours in which

the total pressure is significantly higher than average. Smith and Wolfe (1976) called those interaction regions which tend to recur "corotating interaction regions", "CIR's". A shock which is not followed by an interface (S) or a magnetic cloud (C) is an indication of a transient flow which shows no tendency to recur. Owing to data gaps, not all of the shocks or interfaces that were present in the solar wind are identified in Figure 11, but it does serve to illustrate the general situation. From launch to mid-1978, when the 4-sector pattern was observed, there were many transients, but corotating interaction regions were more prominent in the second half of 1978. This is another indication that time variations were important in this epoch of the solar cycle.

Figure 11 together with Figure 10 are maps of the locations of major dynamical processes in the solar wind. They are related to one another and to the large scale structure of the sun through the sector pattern. Thus, the sector pattern and its evolution in time is basic for understanding the global ordering or "partitioning" of the large scale magnetic field perturbations. This is controlled by dynamical processes in the solar interior. However, this will not be pursued further in this review.

We turn now to specific dynamical phenomena in the solar wind. Sections 4, 5 and 6 discuss dynamical processes associated with one or two isolated large-scale magnetic field strength fluctuations, identified by discontinuities and maxima in B/B_p. Sections 7 and 8 discuss $B/B_p(t)$ as an extended time series with many irregular variations. In both cases, one can speak of dynamical processes involving forces and energy transfer processes. For processes involving no more than a few discontinuities and extrema in B, deterministic models may be used. For processes involving complex time series, one must turn to statistical models. We begin with the simplest phenomenon, a corotating stream, and proceed to discuss flows of increasing complexity.

4. Corotating Configurations

A. Corotating Streams

The concept of a corotating stream in the solar wind has been discussed in many places, (see e.g., Parker, 1958, 1963, 1965; Hundhausen, 1972 and 1984; Suess, 1979; Burlaga, 1979; and Pizzo, 1982, 1983a, 1984). The essential ideas were expressed clearly by Parker (1963), and it is worth reproducing his diagram (Figure 12) and his words: "... A slight difference in coronal temperature over opposite hemispheres of the sun will lead to somewhat different quiet-day solar wind velocities in opposite directions from the sun. If such a condition is maintained for half a solar revolution or longer, then there will be at least one direction in space where the slower solar wind of say 250 km/s is pursued some 14 days later by a faster wind, of say 400 km/sec. A simple calculation shows that the faster solar wind overtakes the slower wind in about 24 days at a radial distance of 5.4 AU. It is obvious, of course, that the overtaking is gradual at first, probably beginning some 2 or 3 AU from the sun and developing into a strong shock in the vicinity of 5 or 6 AU as a result of the supersonic overtaking velocity of 150 km/sec. Considerable heating will occur, to perhaps 10^{6}°K, as a result of the shock transition. The smooth spiral interplanetary fields... for a uniform solar wind, become distorted and pinched, perhaps in a manner similar to the sketch shown in Figure 12."

Dessler and Fejer (1963), and Sonnett and Colburn (1965) suggested that a reverse shock would form as well as a forward shock, and an analytical gas dynamical model of such a system was presented by Simon and Axford (1966). The formation of shock pairs was discussed qualitatively by Formisano and Chao (1972), and a numerical gas dynamic model was used to identify shock pairs in Pioneer speed profiles by Hundhausen and Gosling (1976). The theory of MHD shocks in the solar wind was reviewed by Colburn and Sonett (1966) and Burlaga (1971). The evolution of a stream with the formation of a shock pair was reviewed by Hundhausen (1984). The importance of generating a corotating stream by means of a temperature perturbation near the sun, in order to explain the temperature-speed relation, was discussed by Burlaga et al. (1971).

A corotating reverse shock was observed at 1 AU by Burlaga (1970), and observations of a shock pair at 1 AU were reported by Chao et al. (1972). Corotating shock pairs between 1 AU and 5 AU were observed by Smith and Wolfe (1976) and by Gazis and Lazarus (1983). Thus, the existence of corotating shock pairs is now firmly established.

Stationary MHD models of corotating streams were developed by Matsuda and Sakurai (1972), Goldstein and Jokipii (1977), Whang (1980, 1984), Whang and Chien (1981), and Pizzo (1982, 1983a). Non-stationary models were applied to the study of corotating flows by Steinolfson et al. (1974, 1975) and Dryer et al. (1978b). These papers have been reviewed by Pizzo (1981, 1983a, 1984). The equation of motion used in all of these models is Equation 2. Viscous stresses are neglected and the magnetic curvature force plays no significant role.

Isolated stationary corotating streams between 1 AU and 5 AU have been studied extensively, motivated by the frequent observations of such streams by Pioneer 10 and 11 in the years of declining solar activity. The results of Dryer et al. (1978b) and Smith et al. (1981) show that a time-dependent MHD code can describe the basic qualitative features of stationary flow although quantitative agreement with the observed magnetic field strengths is not as good as one would like. The difficulty in using such an "R-T" code for corotating flows is that it assumes spherical symmetry and considers the fields to be functions of distance from the sun and time. Thus, the spiral structure of the magnetic field and azimuthal inhomogeneities in the flows cannot be modeled without some approximations. This limitation is overcome in stationary MHD models such as those of Matsuda and Sakurai (1972), Pizzo (1982), Whang (1980, 1984), and Whang and Chien (1981).

An application of Pizzo's stationary MHD code to the analysis of an isolated corotating stream observed by Voyager 1, was discussed by Burlaga et al. (1984b). With data from IMP-8 at 1 AU as the inner boundary conditions, the model predicts radial evolution of a small corotating stream as shown in Figure 13. Note the expected formation of a shock pair, the surprisingly rapid erosion of the speed profile, and the growth of the magnetic field

strength in the interaction region between the shocks. A comparison of the model with observations made by Voyager 1 at 1.7 AU is shown in Figure 14 from Burlaga et al. (1984b). There is good agreement between the observed and predicted speed profiles. A shock pair was observed, as predicted, but the calculated arrival time is somewhat earlier than the observed time, possibly due to latitudinal gradients or temporal variations of the source. The temperature is not modeled very accurately, because a 1-fluid model is used, and there are significant differences between the observed and predicted density profiles. However, the field strength and total pressure are modeled satisfactorily when allowance is made for an offset in arrival times. The essential characteristics of the evolution of an isolated corotating stream between 1 AU and 5 AU may be regarded as well-understood.

B. Filtering

One of the earliest and most important results from Pioneer 10 was the observation of Collard and Wolfe (1974) that the amplitudes of the streams diminished with increasing distance, with a "decay length" of 7-10 AU. In general, the speed profile at large distances showed less variability than the speed profiles at smaller distances. This has been confirmed with more extensive Pioneer observations by Collard et al., 1982, and with Voyager data by Gazis, 1983. In searching for an explanation of such results, it was natural to turn to the gas dynamic models which had been discussed prior to 1974.

Holzer (1979), describing some unpublished calculations made by Hundhausen and Pizzo, showed that disturbances produced by short-duration velocity pulses near the sun evolve more rapidly than those produced by long-duration velocity pulses near the sun, as illustrated in Figure 15. Note that these results refer to isolated streams moving through an undisturbed solar wind. Holzer describes the evolution by saying that the small streams are more strongly "damped" than the large streams. If near the sun the solar wind consisted of a number of streams with different durations, then at large distances only the large streams would survive. The more rapid "damping" of small streams is referred to as "filtering". Note that filtering does not involve 1) the collision of one stream with another stream, 2) the coalescence of interaction

regions from different streams, or 3) the transfer of energy from a small scale to a larger scale. These phenomena are associated with a different process called "entrainment", which is discussed in Section 6.

A somewhat different concept of "filtering" was introduced earlier by Gosling et al. (1976). They considered an isolated stream, presumably from a single source on the sun, and they noted the presence of large-amplitude speed fluctuations superimposed on the underlying speed profile. The nature of these fluctuations is not clear from the data they presented, but the authors regard them as small streams. Based on a comparison of Pioneer 10 speed observations at $\sim$ 4.5 AU with corresponding IMP-7 speed observations at 1 AU, they observed that "the large-amplitude speed fluctuations on the leading edge of the profile at 1 AU are not readily apparent at the greater heliospheric distance". An example of this effect is shown in Figure 16, from the paper of Gosling et al. (1976). They refer to this observation as "the filtering out of short wavelength structures". The physical mechanism which they propose for this "filtering" phenomenon is described by them as follows: "... these short-wavelength speed fluctuations disappear because they quickly steepen to form successive shock pairs that overtake one another". In other words, the energy of the speed fluctuations is converted into heat by means of shocks, and the fluctuations are thereby "damped out". An alternative explanation is suggested by the discussion of Burlaga (1975), who noted that the evolution of a velocity disturbance depends on the size of the velocity change ΔV relative to the magnetoacoustic speed, V_M. He suggested that when $\Delta V < V_M$ the pressure gradient might significantly alter the speed profile of such "irregular fluctuations" without the formation of shocks.

C. Pressure Waves without Fast Streams

Up to this point, attention was focused on the speed profiles of streams, and on the "decay" ("smoothing", "damping", "erosion") of the amplitude of a speed profile with increasing distance from the sun. This process is described schematically on the left side of Figure 17, which is essentially the same as a figure in Gosling (1981). On the basis of this result alone, one might expect the solar wind at large distances from the sun to be rather uniform and dynamically uninteresting. However, the right side of Figure 17

shows that the decay of the speed profile is accompanied by a growth in the amplitude of the pressure perturbations. Near 1 AU, the region of high pressure occurs ahead of a fast stream and is produced by the interaction of the fast stream with slower plasma ahead of it, hence the term "interaction region" (Burlaga and Ogilvie, 1970) or "corotating interaction region" (Smith and Wolfe, 1976). The pressure disturbances themselves have the physical nature of non-linear waves, and they can exist independently of fast streams (Burlaga, 1983b). The existence of "pressure waves without fast streams" was demonstrated with Voyager data, and examples of them are shown in Figure 18. Burlaga (1983b) suggested that at large distances from the sun ($\gtrsim$ 10 AU) such "pressure waves without fast streams" might be the dominant feature, and that interactions among these waves might be a dominant dynamical process in the outer heliosphere.

Corotating compression waves, with or without accompanying streams, are often bounded by shocks beyond 2 or 3 AU (Smith and Wolfe, 1976, 1979; and Gazis, 1983). The forward and reverse shocks in each pressure wave move apart, as indicated in Figure 19 from Burlaga et al. (1984b), so the size (radial extent) of a compression wave increases with distance from the sun.

D. Large-scale Patterns

Whereas streams near 1 AU have a structure that carries memory of the source (e.g., low densities and high temperatures in corotating streams from coronal holes), the pressure waves far from the sun have a structure which carries less memory of the source. This is illustrated by the results in Figure 20 from Burlaga et al. (1984a). At 1 AU, the magnetic field strength and density are uncorrelated, but at large distances they may be strongly correlated, which is a characteristic of the strong compression and rarefaction waves. One expects and finds a similar relation between density and temperature with increasing distance (Gazis, 1983). Thus, at distances of $\sim$ 10 AU, the organization of the solar wind reflects the dominance of pressure waves that were produced in the interplanetary medium, whereas at distances of $\sim$ 1 AU the organization of the solar wind reflects the dominance of streams that are related to coronal structure. The pressure waves at $\sim$ 10 AU carry less memory of the source than the streams at $\sim$ 1 AU.

Pressure waves will begin to interact beyond $\sim$ 10 AU as a result of their expansion, and Burlaga (1983b) estimated that the reverse shock from a pressure wave generated by a stream on one solar rotation will have passed through a pressure wave from the following solar rotation beyond $\sim$ 20 AU. Thus, at such large distances pressure waves will have interacted very extensively with one another and a new organization of the solar wind will result from these non-linear wave interactions, forming a third zone with distinctive properties. This "wave interaction zone" (Figure 21) may carry little memory of the sources in the solar corona and photosphere. In general, most of the material in the wave interaction zone, will be "shocked" at least once. The time for the solar wind to move 20 AU is $\sim$ 80 days. The sun is rarely stationary over such a time scale, so additional variability and complexity must be introduced. Thus, the wave interaction zone can be very complex, especially on small scales. Burlaga (1983b) suggested that it might be necessary to resort to statistical descriptions and models for the solar wind at distances $\gtrsim$ 25 AU.

5. Magnetic Clouds

A. Transients

Magnetic clouds belong to one of several classes of transient flows in the solar wind. A transient flow is presumably produced by an impulsive event on the sun, such as a solar flare or an eruptive prominence. It is conceivable that some interplanetary shocks are produced by solar explosions that release energy but do not expel plasma directly, in which case one would observe a shock behind which the speed, density and temperature decrease monotonically (Parker, 1963; Hundhausen, 1972, 1984). In many cases a solar explosion expells a mass of plasma, which was originally called a "plasma cloud" in the old literature and is now generally referred to as "ejecta" (Hundhausen, 1972 and 1979). Ejecta carry along solar magnetic fields, because of the high electrical conductivity of the plasma, and they move past an observer at 1 AU in a few days and out through the heliosphere. Most ejecta have filamentary density and temperature profiles, but the magnetic field may be ordered in some cases and irregular in others. Transient ejecta may move either supersonically with respect to the ambient solar wind, in which case the ejecta drives a shock wave ahead of it, or subsonically. Most studies of ejecta consider the more spectacular shock-associated flows. A driven shock is usually followed by a fast stream (Parker, 1963; Burlaga, 1972; Hundhausen, 1972 and 1984). Acuña et al. (1981) reported a shock at Voyager 1 that was followed by a fast stream, and they found that the corresponding shock observed nearby at a higher latitude by Voyager 2 was not followed by a fast stream. They suggested that the shock extended over a wide range of latitudes whereas the stream was sharply bounded in latitude, the boundary being between Voyager 2 and Voyager 1. Another possibility is that a stream may decelerate as it moves away from the sun, in which case a shock produced near the sun may become detached from the stream at larger distances (Burlaga et al., 1980).

Several studies of unusually fast shock-associated transient flows observed by Pioneers 10 and 11 (Dryer, 1975, 1976; Dryer et al., 1978a; Intriligator, 1976, 1977; Smith and Wolfe, 1977, 1979, and Smith et al., 1977) show that shocks do not decelerate appreciably beyond 1 AU that shocks may be appreciably curved. Observations of unusually fast transient streams beyond

20 AU have been reported by Kayser and Barnes (1984). Some isolated shocks at large heliocentric distances were discussed by Mihalov and Wolfe (1979).

B. Nature of Magnetic Clouds

There have been several speculations about the configuration of the magnetic field in a transient plasma cloud (ejecta): e.g., ordered, turbulent, connected to the sun, or disconnected from the sun. The early papers and recent ideas based on indirect observations (such as energetic particle anisotropies and temperatures) concerning possible "loop-like" configurations are referenced in Klein and Burlaga (1982) and Burlaga (1983c). We use the term "magnetic cloud" to denote the specific kind of flow system shown in Figure 22, which describes an event observed by Voyager 2 at $\sim$ 2 AU. This event is similar to magnetic clouds observed near 1 AU by Burlaga et al. (1981), Klein and Burlaga (1982), and Burlaga et al. (1982a). The most distinguishing figure of a magnetic cloud is a large-scale rotation of magnetic field vector that is observed as the cloud moves past a fixed observer. Magnetic clouds defined in this way should not be confused with the numerous observations of ejecta, "magnetized plasma clouds" or "hydromagnetic clouds" discussed in the early literature (see, e.g., Ivanov and Harshiladze, 1983). Magnetic clouds are magnetized plasma clouds (ejecta) in which the magnetic fields have a special order suggestive of large-scale loops (Burlaga et al., 1981).

Figure 22 shows rotation from a southern direction to a northern direction occurring over $\sim$ 39 hours. The limits of the cloud were arbitrarily taken as the largest and smallest δ angle, simply because these can be identified objectively, but the cloud may be even larger. The magnetic field strength is typically higher inside the magnetic cloud than outside, particularly $\lesssim$ 1 AU. The density and temperature are typically lower inside the magnetic cloud than outside, particular $\gtrsim$ 1 AU. Note that in Figure 22 the speed of the cloud is the same as that of the ambient medium, i.e., it is embedded in the solar wind flow, and it is being carried passively away from the sun at the position of Voyager. Magnetic clouds observed closer to the sun are often in a fast stream that is preceded by a shock. There was possibly a shock ahead of the magnetic cloud in Figure 22 (in the data gap!). This shock was clearly not

driven by the magnetic cloud at the location of Voyager 2, since there was no stream, but one can conjecture that it was driven by a fast moving magnetic cloud near the sun and became detached as the cloud decelerated.

The momentum flux, total (magnetic plus thermal proton) pressure, and $\beta = nkT_p/(B^2/8\pi)$ for the event in Figure 22 are shown in Figure 23. Note that the momentum flux is low, again indicating that if a shock was present, it was not driven at the time of the observation. The total pressure is high inside the magnetic cloud, which is a general property of magnetic clouds. Thus, it is conceivable that the magnetic cloud would tend to expand in order to reduce the pressure. Expansion would produce low temperatures and densities (as observed), and it would reduce the momentum flux, thereby causing a deceleration of the stream (consistent with the low speed and "detached shock" observed in Figure 22). This concept is essentially a hypothesis, which can only be tested by simultaneous measurements by several spacecraft. The β inside the cloud was nearly an order of magnitude lower than that outside the cloud. This is another general characteristic of magnetic clouds. It indicates that the dominant energy in the cloud is that of the magnetic field, which thus gives the principal contribution to the pressure.

C. Size

In order to determine the size of a magnetic cloud (or any other transient flow) one needs simultaneous measurements by several suitably spaced spacecraft; consequently few studies of this sort have been made. Figure 24 from Burlaga et al. (1981) shows the results of observations made by IMP-8, Helios 1 and 2 and Voyagers 1 and 2. A magnetic cloud (preceded by a shock) was observed by all of the spacecraft except Helios 1. From the time interval over which the cloud moved past a given spacecraft, one can estimate the radial extent of the cloud along the spacecraft-sun line. Four such segments were determined by IMP-8, Helios 2 and Voyagers 1 and 2. The estimated geometry of the magnetic cloud on January 26, hour 22, 1978 is indicated by the shaded region in Figure 24, which shows that the azimuthal extent of the magnetic cloud was $\gtrsim 30^\circ$. Nothing is known about the latitudinal extent of magnetic clouds. The radial dimension of clouds observed at 1 AU is typically $\sim$ 0.25 AU (Klein and Burlaga, 1982).

Klein and Burlaga (1982) suggested that magnetic clouds might expand between the sun and earth at a rate of the order of $V_A/2$, where V_A is the Alfvén speed. Parker (1957) introduced a model of a very general type of "magnetized plasma cloud", and he found that it tends to increase in size at a rate of the order of the Alfvén speed. The relation between the structures that he modeled and the magnetic clouds considered here is unclear. If magnetic clouds expand, then the Voyager spacecraft should observe increasingly larger clouds at larger distances. Figure 25 from Burlaga and Behannon (1982) shows 4 magnetic clouds observed between 3 AU and 4 AU by Voyagers 1 and 2. The quadrilaterals give a limit on the size of the clouds, the width being determined by the azimuthal separation of the two spacecraft and the length by the time required to move past the spacecraft and the observed speed. This figure does show larger clouds at larger distances, consistent with expansion at a rate $\sim V_A/2$ in the radial direction, but the sample is very small and further data on the size of clouds should be sought. The data in Figure 25 give a very weak limit on the azimuthal extent of the clouds. One expects the azimuthal size to increase at least linearly with distance due to the radial motion of the solar wind, and possibly faster due to expansion caused by excess internal pressure.

Also shown in Figure 25 are arrows indicating the direction normal to the plane of rotation of $\underset{\sim}{B}$. This direction is within 30° of the radial direction, which puts a constraint on the possible field geometry. Another constraint is given by the line joining the points where the field direction is parallel to the solar equator, which are shown by the open circles in Figure 25. In 3 of the 4 cases this line is nearly in the plane of rotation of $\underset{\sim}{B}$, i.e., normal to the arrows.

D. Magnetic Field Configuration

Magnetic clouds have been selected on the basis of north-south variations of the magnetic field direction, in order to avoid confusion with sectors. Thus, the magnetic field lines in these magnetic clouds extend above and below the ecliptic, except at one point where the magnetic field lines rotate through the ecliptic. This means that one cannot unambiguously determine the

magnetic field line configuration with any number of spacecraft in the ecliptic, and one is forced to invent configurations which are constrained to be consistent with the observations made in the ecliptic and the condition $\nabla \cdot \underset{\sim}{B} = 0$.

Figure 26 shows three possible magnetic field configurations for a magnetic cloud (Burlaga and Behannon, 1982). In Figures 26a and 26c, each magnetic field line is topologically equivalent to a circle, and the cloud is essentially a cylinder which is fibered by these circles. Figure 26a resembles the disconnected "magnetic bottles" that have appeared in the cosmic ray literature. This implies that the normal to the rotation plane is nearly orthogonal to the radial direction, which is not consistent with observations (Figure 25). Figure 26c is consistent with observations, but this and any other configuration based on "circular" lines of force implies a neutral line, hence a low field region, somewhere in the magnetic cloud. Low field regions have never been observed in a cloud, so it is unlikely that the circular field models are generally valid. Another configuration, which is not subject to this difficulty and which is consistent with the observations is shown in Figure 26b. Recently, Goldstein (1983) has given a magnetic cloud configuration which is consistent with observations and which satisfies the static equation of motion (Equation 2 with $\partial \underset{\sim}{V}/\partial t = (\underset{\sim}{V} \cdot \nabla)\, \underset{\sim}{V} = 0$). This is a cylinder which is fibered by helical magnetic field lines, with the limiting forms of circles at the outer boundary and a straight line on the axis of the cylinder. In this model, the gas pressure is balanced by the magnetic curvature force. The validity of this attractive model remains to be determined. Clearly, the geometry and topology of magnetic fields in magnetic clouds is a subject which merits further theoretical and experimental study.

6. Stream Interactions

A. Classification

Consider two streams. There are basically two different ways in which they can interact: 1) If the streams have different amplitudes, then the faster stream may overtake and interact directly with the slower stream; 2) If the streams are nearly identical, with the same amplitude and size, there is no overtaking, but each stream produces a pressure wave (interaction region) and these pressure waves will expand and they may eventually interact with one another. The former process was referred to as "entrainment" by Burlaga et al. (1983), and the latter process will be called "twin-stream interactions" following Dryer and Steinolfson (1976). Although both types of interactions may be described by the same set of equations (Equations 2-6 above), the detailed dynamics and the resulting effects on the large-scale solar wind structure are different in the two cases, so it is best to make a clear distinction between them.

One can further classify stream interactions on the basis of the nature of the streams involved. For example, with 2 streams there are at least 4 possibilities: 1) two corotating streams, 2) a corotating stream overtaking a transient, 3) a transient overtaking a corotating stream, and 4) two transients. Each of these interactions will evolve differently, because of the different initial conditions.

B. Entrainment

Consider 2 or more flows, each from a different source (e.g., a transient stream from a coronal mass ejection, a shock wave from a flare, and a corotating stream from a coronal hole), and suppose that the last of the flows is moving faster than the others. The fast stream will obviously tend to "overtake" and "sweep-up" the slower flows ahead of it. This "overtaking process" is illustrated in Figure 27 with some Helios and Voyager data. The speed profiles from Helios 1, obtained between 1 AU and 0.3 AU, show a number of distinct streams of various amplitudes as well as some fluctuations that are associated with shocks and other transient disturbances. The speed

profile measured at Voyager 1 near 8.5 AU shows less variability both in the amplitude of the streams and in the time profile. The bottom panel shows the Helios 1 speed profile mapped to the Voyager 1 assuming stationary flows and constant speed, i.e., neglecting dynamics. The projected speed profiles are multivalued--a nonsensical result which is a consequence of neglecting the dynamics. Nevertheless, this illustrates very clearly the tendency of the fast streams to "overtake" the slower streams, shocks, etc. This "overtaking"" is a kinematic process involving 2 or more different streams from different sources. "Overtaking" is one aspect of the process that Burlaga et al. (1983) called "entrainment".

The process of "overtaking" of a slow stream by a fast stream should be distinguished from another kinematic process called "kinematic steepening" (Gosling, 1981; Hundhausen, 1984; Burlaga and Barouch, 1976). In order to make this distinction clear, consider the following two extreme situations: 1) two closely separated streams, each with the shape of a square wave, but with different amplitudes, and 2) one stream with the form of a sine wave. In the latter case, the crest of the sine wave will overtake the trough, compressing the material and fields between them and resulting in a "steepening" of the speed profile. In the former case, both streams are initially infinitely steep, so further steepening is impossible. Instead, the faster stream tends to move ahead as a unit until it overtakes the slower stream. This "overtaking" process is more appropriately regarded as a "collision" of a fast stream with another slower stream.

A geometrical picture of the overtaking of a corotating interaction region in a slow flow by an interaction region in a faster flow is given in Figure 28. This is a mapping based on Voyager 1 magnetic field and speed observations made between 1.85 AU and 2.12 AU from day 359, 1977 to day 386, 1977. The mapping assumes corotating flows and no change of speed with distance. It extends the observations both toward the sun and out to 10 AU. The solid (dashed) curves indicate magnetic fields stronger (weaker) than the nominal spiral field. Each spiral represents a field line whose pitch is that appropriate for the speed measured by Voyager. The figure is purely schematic, and it is not intended to describe an actual configuration, but it serves to illustrate how two interaction regions from opposite sides of the

sun tend to come together at a sufficiently large distance from the sun if one has a higher speed than the other. This is a kinematic result, a "tendency" which will inevitably be opposed by dynamical forces.

The dynamical aspect of "entrainment" is illustrated by a solution of the MHD equations obtained from Pizzo's model of stationary corotating streams with IMP-8 data as input. (The details are discussed in Burlaga et al., 1984b.) Figure 29 shows the speed and magnetic field strength from IMP-8 at 1 AU. The stream is a "compound stream" in the classification of Burlaga and Ogilvie (1973) and Burlaga (1975), consisting of a fast corotating stream which is overtaking a slower corotating stream. These streams must have different origins since they have different magnetic polarities, and they are distinct corotating streams because two stream interfaces were observed at IMP-8 (see Burlaga et al., 1984b). The magnetic field profile in Figure 29 shows that there were 2 maxima in B at 1 AU, i.e., 2 interaction regions, one in each stream. The computed magnetic field profile at 2 AU shows only 1 maximum. Thus, there is a qualitative change in the field profile as a result of the dynamical mapping of the compound stream from 1 AU to 2 AU. Two narrow interaction regions coalesce to form one broader interaction region. There is a transfer of magnetic energy from one scale to a larger scale. This coalesence and transfer of energy from small scales to large scales is the essential dynamical feature of entrainment (Burlaga et al., 1983). The cause of coalescence is twofold: 1) the interaction region in the faster stream is convected kinematically toward that of the slower stream; and 2) each interaction region is expanding as a pressure wave. Thus, they eventually interact, giving strong fields and a maximum in B(t) in the region where the two pressure waves overlap.

Pizzo's model was used to describe Voyager 1 observations that were made near 1.44 AU and close to a line connecting IMP-8 with the sun (Burlaga et al., 1984b). The dots in Figure 30 are Voyager 1 observations, and the curves are results of the model obtained with the IMP-8 data described above as input. In general, agreement between the model and observations is good, except for the temperature. The pressure profile shows two pressure waves in the region of increasing speed, and they are just beginning to interact. (Note that Voyager is nearly midway between the two positions discussed in the

preceding paragraph.) A forward shock and a reverse shock have formed in front of the first interaction region seen at IMP-8. There is a region marked (RS) in which a reverse shock from the second interaction region appears to be likely to form, but the corresponding site for the formation of a forward shock is less evident. The two stream interfaces can be seen in Figure 30. They are still separated significantly at 1.44 AU, but one is moving faster than the other, so they are tending to approach one another. The density between the two interfaces is higher than outside the region, because material between them is being compressed as a result of the overtaking of one interface by the other.

Let us now consider another example of entrainment, a very different case, in which a fast corotating stream is overtaking a shock wave that is not accompanied by a fast stream of its own. The IMP-8 speed and magnetic field strength profiles at 1 AU are shown in Figure 31 from Burlaga et al. (1984b), where the stream is evident and the shock is labeled F1. Using the IMP data as input to Pizzo's steady 2-D 1-fluid-MHD model, the speed and field strength profiles at 2 AU and 3 AU were computed (Figure 31). A forward-reverse shock pair (F2 and RS) formed ahead of the stream somewhere within 1.6 AU. The forward shock F2 was necessarily moving faster than F1, and they coalesced somewhere beyond 3 AU. The interaction region of the stream and the high pressure region behind the shock F1 coalesced to form one broad interaction region near 2 AU. Note that a third fast forward shock F3 advanced into the stream, and it interacted with the expanding "merged interaction region" between 2 AU and 3 AU forming a still larger interaction region, which is the result of the coalescence of three separate smaller interaction regions.

The process just described was observed by Voyager 2 at 1.6 AU near a line joining IMP-8 and the sun (Figure 32). The shocks F2 and RS had formed between 1 AU and 1.6 AU; the shock F1 observed at 1 AU was observed again at Voyager 2; and the shock F3 is expected to occur in a data gap at Voyager 2. Note that the two pressure waves associated with F1 and with the stream interaction region were close to one another, and they were just beginning to coalesce. Figure 21 shows that the stream seen at 1 AU was severely eroded by the pressure wave at only 1.6 AU. This is unusual, but it is possible to understand it as a consequence of the interaction with the post shock flow.

The density behind the shock (F1) was very high, > 100/cm^3, so the stream was "colliding" with a region with unusually high inertia. The reaction propagated back through the stream, decelerating it much more rapidly than would have been the case if the stream were isolated and moving through a typical ambient flow.

We now give a third example of entrainment, in which a fast stream with an associated shock pair overtakes a pressure wave without a fast stream (Figure 33). The flows were observed by Voyager 2 at ~ 4.0 AU and by Voyager 1 at ~ 4.3 AU; the speed and field strength profiles are shown in Figure 32 from Whang and Burlaga (1984), Whang (1984) has developed a 1-fluid, "R-T", MHD code based on the theory of characteristics. This code is better suited for describing discontinuities and their interactions than the models of Pizzo (1983a) or Dryer et al. (1978b), which treat shocks by means of an artifical viscosity. The model of Pizzo is optimized for stationary flows near the sun, whereas the model of Whang is optimized for non-stationary flows at large distances. With Voyager 2 data as input, the Voyager 1 profiles were computed by means of Whang's model, and the results are shown in Figure 32. The 2 shock pairs have widened significantly over the relatively small distance involved, but the shock positions as well as the speed and field strength profiles, are modeled very accurately.

The subsequent interaction of the two flows, which are entirely separate in Figure 33, is illustrated in the T-R diagram in Figure 34, based on an extension of the solution discussed above. Two shock pairs are shown, one (RA-FA) associated with the fast stream and another (RB-FB) associated with a "corotating pressure wave without a fast stream" ahead of it. As distance increases, RA moves away from FA and RB moves away from FB. Just beyond 6 AU, RB interacts with FA; both shocks are weakened by the interaction and slow down, and a tangential discontinuity, CS, forms between RB and FA. This interaction is very important in the structure and dynamics of the outer heliosphere. Rather than viewing the interaction as simply the collision between 2 shocks, one can think of it as an interaction between two pressure waves. This is illustrated in Figure 35, where the computed total pressure profiles for the case considered are shown at various times in the evolution of the flow. Initially (at the time of the Voyager 2 observations) two

separate pressure waves were observed. The pressure wave in front of the fast stream advances toward the other pressure wave, and during this time both pressure waves are expanding rapidly. By day 8 the two pressure waves overlap, i.e., they are beginning to interact and coalesce. On day 20 one observes a single broad pressure wave in which is an intense "merged pressure wave", in contrast to the situation on day 0 where 2 separate and narrower pressure waves were observed. This then, is an example of the coalescence of pressure waves associated with the entrainment of a slow flow by a faster flow at large distances from the sun.

An example of the process just described is shown in Figure 36, based on observations reported by Burlaga et al. (1983, 1984c). Helios 1 observed two distinct corotating streams within 1 AU, each of which was preceded by an interaction region, i.e., two distinct pressure waves were observed by Helios 1. Voyager 1, at $\sim$ 8.5 AU and close to a line joining Helios 1 and the sun, observed qualitatively different magnetic field and pressure profiles. The Voyager 1 pressure profile is very similar to that in Figure 35 for day 20, with two overlapping interaction regions and the shock sequence F-F-R-R. A single broad pressure wave formed from the interaction of two narrow pressure waves, and there was a corresponding transfer of magnetic energy from small scales to larger scales.

We conclude that "entrainment" is observed under a variety of circumstances. It involves 1) the overtaking of slow streams, shocks, etc., by faster streams, 2) the coalescence of two or more pressure waves, and 3) the transfer of energy from small scales to larger scales. Entrainment is very basic in modifying the structure of the interplanetary magnetic field.

C. Twin Streams

We have been discussing the interaction of two streams with different magnitudes. Now consider two identical streams. In this case overtaking is much less important, because stream A tends to move away from stream B as rapidly as stream B moves toward stream A. The left panel in Figure 37, is a kinematic result, showing the magnetic field lines and magnetic field strength for two identical streams from opposite sides of the sun. The panel on the

right shows interaction regions (shaded) bounded by forward and reverse shocks. In this case the dynamical interaction is associated with the expansion and interaction of the interaction regions rather than the overtaking of one stream by another.

The MHD evolution between 0.3 AU and 5 AU of each of two identical streams was discussed by Dryer and Steinolfson (1976). They noted the possibility that the reverse shock from one stream might interact with and pass through the forward shock from the following stream somewhere beyond 5 AU. This is illustrated in Figure 38 from their paper, showing the azimuthal magnetic field component. Note that the magnitude of this component is considerably lower than one expects. Unfortunately, the authors give no additional information about the flows, so one cannot verify that the indicated shocks have the correct signatures. The results suggest the existence of the interaction, but they provide no information on the interaction itself.

D. Recurrent Streams

In his review, Pizzo (1983a) discusses results of his MHD model for the evolution of two similar recurrent streams, originating on opposite sides of the sun and moving from 1 AU to 30 AU. The input data for Pizzo's computation were IMP-8 data, and his computed speed and pressure profiles are shown in Figure 39. Additional details of the results have not been published, but the model is described by Pizzo (1983a, 1984). Two shock pairs are illustrated in Figure 39, viz. F_1-R_1 and F_2-R_2. Each of the streams and interaction regions in Figure 39 evolves independently out to $\sim$ 10 AU. Then F_2 interacts with R_1 and R_2 interacts with F_1, as suggested by Dryer and Steinolfson (1976). The interaction of a forward shock with a reverse shock was originally investigated in the gas dynamic case by von Neumann (1943) and its possible relevance to the solar wind was discussed by Parker (1963, p. 110). The F_2-R_1 shock interaction was modeled by Whang and Burlaga (1984), who give details of the shock strengths, speeds, etc. Note that for a model involving two recurrent streams originating 180° apart on the sun (Figure 39), a fixed observer between $\sim$ 10 AU and $\sim$ 20 AU sees the signature RFRF... rather than the signature FFRR found by Whang and Burlaga for the entrainment of a slower flow by a nearby fast stream (Figures 35 and 36).

7. Flow Systems and Large-Scale Fluctuations

A. Scales

Most solar wind models and observations concern individual flows, or at most a few streams. As discussed in the two previous sections, the dynamics of such flows and binary flow interactions can be satisfactorily described by deterministic MHD models. However the time required to fill a volume with a radius of order 30 AU (the interplanetary medium) at an outflow speed of ∿ 400 km/sec is ∿ 120 days. The sun and its output usually vary considerably on such a large time scale. Typically there will be many streams in the volume, some changing slowly, others short-lived, and most interacting in one way or another with neighboring flows. Thus, in dealing with the large scale structure of the interplanetary medium, one must consider extended time series (∿ 120 days), preferably from several widely spaced spacecraft. This approach is also required in considering the modulation of galactic cosmic rays which move through a large volume of the heliosphere before being detected at 1 AU. Burlaga et al. (1982, 1983b, 1984c) and McDonald et al. (1982) emphasized the need to speak of "systems of flows" and the need to distinguish between two extreme types of systems of flows--"transient systems" (made up of transient flows) and "corotating systems" (made up of corotating flows). Intermediate types of flow systems, "mixed systems" consisting of both transient and corotating flows, are frequently observed. One can also view the solar wind with time series of say 1 year or more and examine their statistical properties. Such series will generally include all types of flows, although one type may be more dominant at one part of the solar cycle than another.

B. Corotating Systems

A system of corotating flows is illustrated in Figure 40 from Goldstein et al. (1984), which shows a quasi-periodic pattern in the measurements of magnetic field, strength, density and temperature from Voyager 1 at ∿ 5.7 AU. The enhancements represent corotating interaction regions which, are usually bounded by shock pairs at the distance considered. One can picture the corotating system as a result of the recurrence of corotating flows for

several solar rotations. A similar system of corotating flows is shown in Smith et al. (1981).

The spectral signatures of the magnetic field for the data in Figure 40 are shown in Figure 41 which is a plot of power versus frequency for fluctuations in the components of $\underset{\sim}{B}$ (top curve), in the magnitude of B (lower curve) and in the magnetic helicity (circles and triangles). Magnetic helicity is defined as $\underset{\sim}{A}\cdot\underset{\sim}{B}$, where $\underset{\sim}{A}$ is the magnetic vector potential. A method for computing the helicity spectrum was described by Matthaeus et al. (1982) and applied to the solar wind by Matthaeus and Goldstein, 1982a,b. For our purposes, one may visualize helicity as a measure of the extent to which the magnetic field lines are twisted, ranging from 0 for straight lines to 1, say, for cylindrical helices. This is discussed in more detail by Montgomery, 1983.

At frequencies $\gtrsim 2 \times 10^{-5}$ Hz, corresponding to a solar wind convection time of $\sim$ 14 hours, power in the components of $\underset{\sim}{B}$ has a $f^{-5/3}$ spectrum, and power in the magnetic field strength is nearly an order of magnitude lower. This behavior is representative of Alfvénic fluctuations, which have been studied extensively at 1 AU (see, e.g., the reviews by Barnes, 1979a,b and Behannon and Burlaga, 1981). These fluctuations will not be considered further in this review.

At frequencies $\lesssim 2 \times 10^{-5}$ Hz, the slope of the power in the fluctuations of the components of $\underset{\sim}{B}$ (the trace of the power spectral matrix) is flatter than at higher frequency, with a power law exponent close to minus 1 (see Figure 41). This behavior is expected to be a characteritic of the "inverse cascade" at frequencies lower than the correlation length for MHD turbulence (Matthaeus and Goldstein, 1983, Matthaeus and Montgomery, 1980; Montgomery, 1983). However, in the corotating flow system under consideration there is relatively little magnetic helicity at these frequencies, so it is unlikely that one is seeing a turbulent flow. Rather, the turbulence signatures in the spectra of the components is more likely to be the remnant of a turbulent cascade that took place near the sun, e.g., in the corona, but this is only a hypothesis. The power in the fluctuations of $|\underset{\sim}{B}|$ below $\sim 2 \times 10^{-5}$ Hz in Figure 41 is not described by a straight line, again suggesting that the

corotating flow system is not turbulent. A significant feature of this spectrum is the high ratio of power at 2×10^{-6} Hz ($\sim$ 5 days) relative to that at $\sim 2 \times 10^{-5}$ Hz ($\sim$ 1/2 day). This may be a signature of dynamical processes characteristic of corotating stream interactions near $\sim$ 5 AU.

C. Transient and Mixed Systems

A transient or mixed flow system observed by Voyager 2 at 2.4 AU is shown in Figure 42 from Goldstein et al. (1984). This transient system seems to have more variability on all scales than the corotating system in Figure 40. Whereas in the corotating system high speeds were associated with high temperatures, low densities and low field strengths, no such pattern appears in the transient system.

The spectrum of fluctuations in the components of $\underset{\sim}{B}$ for the transient system in Figure 42 is given in Figure 43. At frequencies $\gtrsim 2 \times 10^{-5}$ Hz the power in the components, magnitude and helicity of $\underset{\sim}{B}$ have the characteristics of Alfvénic fluctuations or turbulence. At frequencies $\lesssim 2 \times 10^{-5}$ Hz one again sees a f^{-1} dependence in the power. Insofar as fluctuations in the direction of the magnetic field are concerned, transient systems look very much like corotating systems. An important implication is that the different effects which corotating systems and transient systems have on cosmic rays are probably not due to fluctuations in the direction of the field, contrary to the prevailing ideas on cosmic ray diffusion (Burlaga, 1983c; Burlaga et al., 1984c).

The time series of the strength the magnetic field B(t) for a transient system is typically very complex, as illustrated in Figure 42. However, in frequency space (Figure 43) the description of the magnetic field strength for transient flows is remarkably simple--the power in B versus frequency is a straight line on a log-log scale! This is sufficient justification for using spectral methods to describe the magnetic field over a wide range of scales. The simple spectrum of B(t) and the large power in magnetic helicity below the correlation length suggest that the transient system is turbulent.

From the time series for a transient system, one derives the picture of a collection of different types of non-stationary flows of various shapes and sizes (e.g., shocks, ejecta, magnetic clouds, varying corotating streams, etc.), each of which has a characteristic "fine structure". This view presents a hopelessly complicated problem for anyone who would like to model the flows using deterministic MHD codes such as those mentioned above and reviewed by Pizzo (1983a, 1984). However, the simplicity of the spectra in Figure 43 suggests that an alternative approach is possible, which takes advantage of the complexity--a statistical approach. In particular, the observations suggest that the theory of MHD turbulence might be applicable. This implies that one cannot neglect the magnetic curvature force and vorticity in Equation 1, or the dissipative terms in Equations 1 and 6. Thus, the dynamics of transient systems is likely to be very interesting, but both the theory and interplanetary observations of MHD turbulence are very limited.

Data discussed in the preceding paragraphs were obtained between 4 AU and 5 AU. Flow systems and the corresponding spectra change with distance from the sun. For example, Goldstein et al. (1984) found that the correlation length in transient systems tends to increase with distance, possibly because larger scale structures are forming owing to the inverse cascade. Thus, at 1 AU transient systems have smaller correlation lengths than corotating systems, but at $\sim$ 5 AU the correlation lengths tend to be the same for both systems. Similarly, at 1 AU transient systems tend to have more power in $|\underset{\sim}{B}|$ at low frequencies than corotating systems, whereas at $\sim$ 5 AU this difference is not seen. The change is due in part to growth in the amplitude of low frequency perturbations in $|\underset{\sim}{B}|$ caused by the evolution of corotating streams.

D. Shells

Parker (1963, p. 129) noted that successive blast waves ejected at one month intervals would overtake and smear out preceding blast waves so that "the blast waves, which appear so violent at the orbit of Earth, must be almost completely obliterated by the time they reach r_D... a great deal of momentum and energy is being poured into the solar wind beyond the orbit of Earth by the degradation of blast waves into a smooth and very hot gas after several AU where successive waves begin to merge". The concept of a very

large ("tens of AU") "turbulent cloud" enveloping the sun, was suggested by Morrison (1954) before the existence of the solar wind was established, in an attempt to explain the 11-year cosmic ray variations. A stationary diffusive shell beyond 1 AU was also postulated by Meyer et al. (1956) to explain observations of a solar cosmic ray event. Evidence for a propagating shell, surrounding the sun and moving away from it at ∿ 400 km/s, was found in cosmic ray observations made by Helios, IMP, Voyager and Pioneer (McDonald et al., 1981a,b).

Direct evidence for large turbulent shells in the solar wind was presented by Burlaga et al. (1984c), who identified them with transient systems. Figure 44 is a very schematic illustration of such a shell. It is assumed that initially the sun is quiet and the heliospheric flows are stationary. Then, the sun becomes active for approximately 3 solar rotations, expelling transient streams, shocks, ejecta, coronal mass ejections, magnetic clouds, etc. This debris will occupy a shell of thickness ∿ 15 AU. The sun is assumed to return to its quiet state, and the ring moves out through the heliosphere as in Figure 44c,d. As described above such a complex flow shows order in the frequency spectrum which suggests the presence of MHD turbulence. One thus has a turbulent shell propagating away from the sun, and cosmic rays can diffuse in it by mirroring and drifting in the inhomogeneous magnetic field (Goldstein et al., 1984).

A very different kind of a magnetic shell was proposed by Hakamada and Akasofu (1983) and Hakamada and Akasofu (1983). This is illustrated in Figure 45, where the curves represent magnetic field lines and the black areas represent regions in which the magnetic field strength is strong. This is essentially a deterministic model in which the shell is made up of a set of nearly identical shock-flows that are released in succession from the sun over an interval of ∿ 25 days. Each of these shock-flows is like the "blast wave" described by Parker (1961, 1963, page 143), except that the shock is assumed to have a radius of curvature of ∿ 0.5 AU rather than 1 AU, and the model is kinematic rather than dynamic. Akasofu's model was criticized by Pizzo (1983b), and defended by Akasofu (1983). This model is clearly not consistent with the magnetic field observations in shells corresponding to systems of transients. It does not express the complexity of the magnetic field

profiles, which show a mixture of disturbances on all scales, and it does not account for the simple spectrum of magnetic field strength fluctuations that is observed. It should be noted that despite a number of strong assumptions, the construction of Figure 47 required the choice of 36 parameters. The observations of transient systems suggest the need for a statistical dynamical model such as MHD turbulence, whereas Akasofu's model is deterministic, simply ordered and kinematic. Akasofu's model might prove to be useful in visualizing the geometry of two or three non-interacting transient flows.

E. Stationarity and Homogenity

Theories of turbulence deal with ensemble averaged quantities, whereas measurements deal with time averaged quantities. According to the ergodic theorem, these averages converge when sufficiently long time averages are considered, if the random process is "stationary". A condition for "weak" stationary of fluctuations of the components of the interplanetary magnetic field was written by Matthaeus and Goldstein (1982b) and tested by them using data from 1 AU and from Voyager. Their criteria for stationarity was found to be satisfied for data sets containing $\gtrsim$ 10 correlation times when "significant organized structures are not undersampled". It is of interest to extend these results to other data sets representing different flow conditions at different distances from the sun, and to other time series such as those of magnetic field strength, speed, etc.

It was argued by Matthaeus and Goldstein (1982b, 1983) that time stationarity implies spatial homogeneity, provided the scale of the fluctuations is much less than the local heliocentric radial coordinate of the observer. To one who is accustomed to looking at solar wind data, the statement that the solar wind is spatially homogeneous seems unreasonable. For example, systems of recurrent corotating streams are clearly not homogeneous. On the other hand, systems of transients may well be homogeneous in some statistical sense. Thus, the meaning of statistical homogeneity and the circumstances under which this concept is meaningful merit further study. Independent measures of homogeneity should also be sought.

8. Radial Evolution of Large-Scale Fluctuations

A. Velocity Fluctuations

Referring to time series of daily averages of the solar wind speeds, Collard and Wolfe (1974) observed that the range of solar wind velocities decreases with increasing radial distance from the sun, between 1 AU and 5 AU, and they attributed this to exchange of momentum between high and low speed streams. These Pioneer 10 and 11 observations have been confirmed with data out to 15 AU by Collard et al. (1982). Radial variations of the speed profiles based on hour averages of measurements made simultaneously by IMP-8 and ISEE-3 at 1 AU and Voyager 1 near 5 AU are shown in Figure 46, from Burlaga and Goldstein (1984). The panels on the left represent a system of mixed flows, while the panels on the right represent a system of corotating flows. On can see both a reduction in the range of speeds as observed by Pioneer and an apparent loss of speed fluctuations at higher frequencies. Both of these effects are included in the term "velocity filtering". The velocity filtering appears to be stronger for corotating flows in Figure 46 than for transient flows. A systematic spectral analysis of this phenomenon has not been made.

B. Magnetic Field Strength Fluctuations

The magnetic field strength profiles at 1 AU and $\sim$ 5 AU corresponding to the speed observations discussed in the preceding paragraph are shown in Figure 47. In contrast to the behavior of the speed profiles, the range of magnetic field strength increases with distance. However, there is an apparent decrease in the power at high frequencies and increase in the power at low frequencies for the corotating system. A more objective description of the change in the distribution of power in frequency space as a function of radial distance is shown in Figure 48 from Burlaga and Goldstein (1984). The absolute power at a given frequency diminishes with distance as the mean field strength decreases, but this is not the main point of interest. More important is the observation that there is an increase in the power at $\sim$ 10 days relative to that at 1 day for the corotating system. Burlaga and Goldstein attribute it primarily to the transfer of energy from high

frequencies to low frequencies. In particular, they suggested a deterministic explanation in which two neighboring narrow peaks in $|\underset{\sim}{B}|$ seen at 1 AU coalesce form a broader peak. In addition, there is an enhancement in the power at wavelengths with the scale of the stream length, due to the depressions in B caused by the motion of fast plasma away from slow plasma in the trailing part of a stream. There is also a kinematic transfer to longer wavelengths of power in the fluctuations in the trailing part of the streams, due to the stretching that results as the fast plasma moves away from the slow plasma.

The radial variation of the spectrum of magnetic field strength fluctuations in the mixed flow system Figure 47 differs from that of the corotating system. Instead of a change to a more complex distribution of energy with frequency, the mixed flow system shows the same simple $f^{-5/3}$ dependence at 1.5 AU that was observed at 1 AU. The main change is a possible extension of the $f^{-5/3}$ dependence to lower frequency (periods $\sim$ 10 days) at larger distances. This behavior is consistent with the evolution of a turbulent flow. Invariance of the shape of the spectrum with distance, i.e., the existence of a "universal spectrum" for mixed flows and transient flows is very important from both a physical and a practical point of view.

C. Filtering and Entrainment

The concepts of filtering and entrainment were discussed in Sections 4B and 6B, respectively. Let us now consider them in relation to spectra of the speed and magnetic field strength and in relation to one another. Both filtering and entrainment consider the evolution of amplitudes or intensities at different wavelengths or frequencies as a function of distance, e.g., the ratio P_λ/P_L where P_λ is the amplitude or intensity at a small wavelength and P_L is that at a larger wavelength. The basic question is how this ratio changes with distance from the sun.

According to the concepts of "filtering", the ratio P_λ/P_L decreases because short wavelength disturbances "damp out" faster than long wavelength disturbances, i.e., the solar wind tends to as a "low-pass filter". The dominant scale of solar wind structures is larger at greater distances from the sun simply because the smaller structures disappear more rapidly than the

layer structures. As described by Holzer (1979) "...structures with wavelengths comparable to or greater than the transit length to 1 AU ...are damped very little at 1 AU, whereas structures with much shorter wavelength are strongly damped at 1 AU. Similarly, an observer at 20 AU would observe a structure with a 1 AU wavelength (T $\sim$ 3 days) to be strongly damped, and a structure with a 10 AU wavelength (T $\sim$ 27 days) to be weakly damped". Likewise, Hundhausen (1984) said "streams or waves of shorter wavelengths are preferentially "filtered-out" compared to streams or waves of longer wavelengths as the structures are more outward through the solar system". Referring to higher frequency speed fluctuations, Gosling et al. (1976) say ..."The large-amplitude speed fluctuations, which are present at the leading edge of a structure at 1 AU are gone by the time the stream reaches 4.65 AU. In the present example, as in the previous one, these short wavelength fluctuations disappear because they quickly steepen to form successive shock pairs that overtake one another". Thus, in the concept of filtering, the essential idea is "damping", the selective removal of certain frequencies as in a filter, rather than a transfer of energy from one scale to another.

In the concept of entrainment, the essential feature is a net transfer of magnetic energy from small scales to larger scales (see Section 6B). The ratio P_λ/P_L may decrease both because there is a decrease in P_λ and because of an increase in P_L. It is not necessary to invoke damping or dissipation of energy, such as the conversion of magnetic energy to heat by means of shocks, even for small-scale fluctuations, although the possibility of some damping is not excluded.

The essential difference between entrainment and filtering, as this author sees it, is illustrated schematically in Figure 49, which refers to a system with features of many different scales. In filtering, the spectrum steepens because energy is removed at high frequencies faster than at low frequencies. In entrainment, energy is transferred from high frequencies to low frequencies.

C. Turbulence

Although the ideas of filtering and entrainment are useful in discussing relatively simple flow configurations, e.g., those consisting of 2 or 3 flows,

or systems of corotating flows, they are less useful in discussing complicated flow systems containing many interacting non-stationary flows of many different scales and types. For example, in discussing systems of transients it would be impossible to model the flows with deterministic codes such as those which have been used to describe filtering and entrainment. Even if one could develop codes and computers to handle all the 3-D time dependent processes, one could never in practice obtain the necessary boundary conditions and initial conditions. Thus, one is forced to consider a statistical approach for certain flow systems, and the most natural MHD theory is that of MHD turbulence. Unfortunately, the theory of MHD turbulence is poorly developed, (e.g., Montgomery, 1983; and Matthaeus and Goldstein, 1983). Most of the work on MHD turbulence concerns 2-D stationary homogeneous incompressible turbulence, and it is based on scaling laws, dimensional arguments and idealized computer simulations. Thus, it should be applied to the 3-dimensional, inhomogeneous, compressible solar wind with great care. Nevertheless, it offers some valuable physical concepts and a precise mathematical language which are useful for discussing the observations.

A basic feature of the turbulence approach is the emphasis on spectra, i.e., the distribution of energy or amplitudes of the fluctuations in wave-number space and in frequency space, rather than on time series. A spectrum allows one to look at fluctuations on a wide range of scales in a single figure, and it exhibits regularities that are less evident in time series plots. For example, in discussing transient systems (Figure 43) we have seen that an extremely complex magnetic field strength profile in the time domain became a straight line in the frequency domain. Evidently there are interactions among flows of different sizes which act to maintain a "universal spectrum". Turbulence theory describes this spectrum and related phenomena in terms of dynamical interactions which involve a transfer of energy in k-space or frequency space.

Some of the basic concepts of MHD turbulence theory are 1) an energy source which generates the fluctuations; 2) a characteristic scale or frequency at which this energy is introduced into the system, a "stirring scale", which is at intermediate lengths, 3) a direct cascade of energy to higher frequencies, 4) dissipation of energy at high frequencies, and 5) an

inverse cascade of magnetic helicity to low frequencies. The correlation length provides an estimate of the energy source scale. In the solar wind near 1 AU this is comparable to the width of an interaction region. Dessler and Fejer (1963), Parker (1963) and Jokipii and Davis (1969) suggested that a Kelvin-Helmholz instability at a stream interface might produce waves and turbulence, but this process is probably not very important, at least near 1 AU (Burlaga et al., 1971). However, it is likely that corotating shock pairs can act as a source of turbulence in corotating interaction regions in the outer heliosphere, and this may become increasingly important at larger distances. The transfer of energy to high frequencies is a nonlinear effect related to the $(\underset{\sim}{V}\cdot\nabla)\,\underset{\sim}{V}$ term in Eq. 1. The dissipation at high frequencies is not understood in the case of the solar wind, although phenomenologically it is related to the viscosity and magnetic resistivity. The inverse cascade at low frequencies (Frisch et al., 1975) is an MHD effect related to magnetic helicity, and it depends on the magnetic curvature force in Equation (1) among other things. It results in the formation of larger scale structures as magnetic helicity generated at lengths near the stirring scale is transferred to larger scales. These concepts are reviewed by Montgomery (1983).

Finally, let us contrast turbulence with filtering and entrainment. An essential feature of turbulence is a universal spectrum with a slope that does not change with time or distance and which is insensitive to the details of the source or sink of energy. In filtering and entrainment the slope of the spectrum does change, becoming steeper or more complicated. In turbulence, energy is transferred to both high and low frequencies, whereas in entrainment it is transferred preferentially to low frequencies, and in filtering it is preferentially "damped out". Thus, the three concepts are distinct, but each has its place in heliospheric dynamics. Turbulence is important for understanding transient systems; entrainment is useful for describing evolution of magnetic fields as a result of the interaction of fast flows with slower flows; and filtering can describe the evolution of a set of non-interacting streams of various sizes with increasing distance from the sun.

9. Conclusion

Much has been learned about the structure and dynamics of the outer heliosphere during the last decade as a result observations from the Voyager and Pioneer spacecraft. The large scale of the observations forces one to consider the heliosphere from a new perspective, to think of new dynamical processes, and to introduce new concepts. The early studies of isolated gas dynamic flows must be replaced by MHD dynamics of interacting flows and flow systems. The simple deterministic models that have been dominant in early studies of the solar wind are now seen to have limited applicability, and statistical approaches are being developed. New concepts that have been introduced, such as inverse cascades, filtering, entrainment, etc., must be further explored and clarified, to make them more precise and quantitative. MHD turbulence is probably very important in solar wind dynamics, but the subject is poorly developed from a theoretical point of view. The statistical analysis of solar wind parameters has scarcely begun, but it is clearly necessary for an understanding of complex, large-scale flows. The multitude of possible interactions among shocks and flows of various types needs to be explored systematically with observations, models and analytical theory.

Voyagers 1 and 2 and Pioneers 10 and 11 are continuing to move through the outer heliosphere and gather data. The lengthy data reduction procedures require even more care in dealing with the low field strengths, densities and temperatures at large heliocentric distances, and the analysis of the complex flows and fields in the outer heliosphere becomes increasingly difficult. Thus one can expect continued growth of our knowledge of the heliosphere, but comprehensive understanding of the data will take some time. If this review stimulates the specialists in solar wind physics to think critically about the results presented and to remedy the deficiencies of current knowledge of the heliosphere, then it will have served its purpose. It is also hoped that this review will serve to encourage specialists in other fields to bring their talents to bear on heliospheric problems and to transfer results of heliospheric physics to their fields.

Acknowledgments.

References

Acuña, M. H., L. F. Burlaga, R. P. Lepping, and N. F. Ness, Initial results from the Voyagers 1, 2 magnetic field experiments, Contributions to the Fourth Solar Wind Conference, NASA/GSFC TM 79711, p. 1, in Solar Wind Four, p. 143, ed. by H. Rosenbauer, Report No. MPAE-W-100-81-31, 1981.

Akasofu, S. -I, Reply, Solar Wind Five, p. 484, ed. M. Neugebauer, NASA Conf. Pub. 2280, 1983.

Akasofu, S. -I and K. Hakamada, Solar wind disturbances in the outer heliosphere caused by successive solar flares from the same active region, Solar Wind Five, p. 475, ed. M. Neugebauer, NASA Conf. Pub. 2280, 1983.

Barnes, A., Solar System Plasma Physics, Vol. 1, edited by E. N. Parker, C. F. Kennel, and L. J. Lanzerotti, p. 251, North-Holland, Amsterdam, 1979a.

Barnes, A., Physics of the solar wind, Rev. Geophys. Space Res., 17, 596, 1979b.

Behannon, K. W., Heliocentric distance dependence of the interplanetary magnetic field, Rev. Geophys. Space Phys., 16, 125, 1978.

Behannon, K. W. and L. F. Burlaga, Alfvén waves and Alfvénic fluctuations in the solar wind, Solar Wind Four, p. 374, ed. H. Rosenbauer, Max-Planck Institute Report No. MPAE-W-100-81-31, 1981.

Behannon, K. W., M. H. Acuña, L. F. Burlaga, R. P. Lepping, N. F. Ness, and F. M. Neubauer, Magnetic field experiment for Voyagers 1 and 2, Space Sci. Rev., 21, 235, 1977.

Behannon, K. W., L. F. Burlaga, and A. J. Hundhausen, A comparison of interplanetary current sheet inclinations, J. Geophys. Res., 88, 7837, 1983.

Belcher, J. W. and L. Davis, Large-amplitude Alfvén waves in the interplanetary medium, 2, J. Geophys. Res., 76, 3534, 1971.

Bridge, H. S., J. W. Belcher, R. J. Butler, A. J. Lazarus, A. M. Mavretic, J. D. Sullivan, G. L. Siscoe, and V. M. Vasyliunas, The plasma experiment on the 1977 Voyager mission, Space Sci. Rev., 21, 259, 1977.

Burlaga, L. F., A reverse hydromagnetic shock in the solar wind, Cosmic Electrodynamics, 1, 233, 1970.

Burlaga, L. F., Hydromagnetic waves and discontinuities in the solar wind, Space Sci. Rev., 12, 600, 1971.

Burlaga, L. F., Shock phenomena in interplanetary space, NASA/GSFC X-692-72-395, 1972.

Burlaga, L. F. Interplanetary stream interfaces, J. Geophys. Res., 79, 3717, 1974.

Burlaga, L. F., Interplanetary streams and their interaction with earth, Space Sci. Rev., 17, 327, 1975.

Burlaga, L. F., Magnetic fields, plasmas and coronal holes: The inner solar system, Space Sci. Rev., 23, 201, 1979.

Burlaga, L. F., Heliospheric magnetic fields and plasmas, Rev. Geophysics and Space Physics, 21, 363, 1983a.

Burlaga, L. F., Corotating Pressure waves without fast streams in the solar wind, J. Geophys. Res., 88, 6085, 1983b.

Burlaga, L. F., Understanding the heliosphere and its energetic particles, NASA/GSFC TM 85085, Invited Paper, to appear in Proceedings of the 18th International Cosmic Ray Conference, Bangalore, 1983c.

Burlaga, L. F. and E. Barouch, Interplanetary stream magnetism: Kinematic effects, Astrophys. J., 203, 257, 1976.

Burlaga, L. F. and K. W. Behannon, Magnetic clouds between 2-4 AU, Solar Phys., 81, 181, 1982.

Burlaga, L. F. and M. L. Goldstein, Radial variations of large-scale magnetohydrodynamic fluctuations in the solar wind, submitted to J. Geophys. Res., 1984.

Burlaga, L. F. and J. King, Intense interplanetary mangetic fields observed by geocentric spacecraft during 1963-1975, J. Geophys. Res., 84, 6633, 1979.

Burlaga, L. F. and K. W. Ogilvie, Magnetic and thermal pressures in the solar wind, Solar Phys., 15, 61, 1970.

Burlaga, L. F. and K. W. Ogilvie, Solar wind temperature and speed, J. Geophys. Res., 78, 2028, 1973.

Burlaga, L. F., K. W. Ogilvie, D. H. Fairfield, M. D. Montgomery, and S. J. Bame, Energy transfer at colliding streams in the solar wind, Astrophys. J., 164, 237, 1971.

Burlaga, L., R. Lepping, R. Weber, T. Armstrong, C. Goodrich, J. Sullivan, D. Gurnett, P. Kellogg, E. Keppler, F. Mariani, F. Neubauer, H. Rosenbauer, and R. Schwenn, Interplanetary particles and fields, Nov. 22 to Dec. 6, 1977: Helios, Voyager observations between 0.6 and 1.6 AU, J. Geophys. Res., 85, 2227, 1980.

Burlaga, L. F., E. C. Sittler, F. Mariani, and R. Schwenn, Magnetic loop behind an interplanetary shock: Voyager, Helios and IMP-8 observations, J. Geophys. Res., 86, 6673, 1981.

Burlaga, L. F., L. Klein, N. R. Sheeley, Jr., D. J. Michels, R. A. Howard, M.. J. Koomen, R. Schwenn, and H. Rosenbauer, A magnetic cloud and a coronal mass ejection, Geophys. Res. Lett., 9, 1317, 1982a.

Burlaga, L. F., R. P. Lepping, K. W. Behannon, L. W. Klein, and F. M. Neubauer, Large scale variations in the IMF: Voyager 1 and 2 observations between 1-5 AU, J. Geophys. Res., 87, 4345, 1982b.

Burlaga, L. F., R. Schwenn, and H. Rosenbauer, Dynamical evolution of interplanetary magnetic fields and flows between 0.3 AU and 8.5 AU: Entrainment, Geophys. Res. Lett., 10, 413, 1983.

Burlaga, L. F., F. B. McDonald, M. A. I. Van Hollebeke, R. Schwenn, and H. Rosenbauer, Modulation of cosmic rays by interplanetary transients: Helios 1 observations from 1977-1980, Bulletin of the American Physical Society 28, 742, 1983b.

Burlaga, L. F., L. W. Klein, R. P. Lepping, and K. W. Behannon, Large-scale interplanetary magnetic fields: Voyager 1 and 2 observations between 1 AU and 9.5 AU, submitted to J. Geophys. Res., 1984a.

Burlaga, L. F,., V. Pizzo, A. Lazarus, and P. Gazis, Stream dynamics between 1 AU and 2 AU: A comparison of observations and theory, J. Geophys. Res., in press, 1984b.

Burlaga, L. F., F. B. McDonald, R. Schwenn, and A. Lazarus, Interplanetary flow systems associated with cosmic ray modulation in 1977-1980, Bulletin of the American Physical Society, 27, 571, 1982, and J. Geophys. Res., in press, 1984c.

Chao, J. K., V. Formisano, and P. C. Hedgecock, Shock pair observations, solar wind, NASA Spec. Publ., 308, 435, 1972.

Colburn, D. S. and C. P. Sonnett, Discontinuities in the solar wind, Space Sci. Rev., 5, 439, 1966.

Coleman, P. J., Jr., E. J. Smith, L. Davis, Jr., and D. E. Jones, The radial dependence of the interplanetary magnetic field: 1.0-1.5 AU, J. Geophys. Res., 74, 2826, 1969.

Collard, H. R. and J. H. Wolfe, Radial gradient of the solar wind velocity from 1 to 5 AU in Solar Wind Three, ed. by C. T. Russell, University of California Press, 1974.

Collard, H. R., J. D. Mihalov, and J. H. Wolfe, Radial variation of the solar wind speed between 1 and 15 AU, J. Geophys. Res., 87, 2203, 1982.

Cuperman, S., Plasma fluid aspects of the solar wind, Space Sci. Rev., 26, 277, 1980.

Dessler, A. J. and J. A. Fejer, Interpretation of Kp index and M-region geomagnetic storms, Planet. Space Sci., 11, 505, 1963.

Dryer, M. Interplanetary shock waves - Recent developments, Space Sci. Rev., 17, 277, 1975.

Dryer, M. (ed.), The August 1972 events: A project of SCOSTEP's study of traveling interplanetary phenomena, Space Sci. Rev., 19, 499, 1976.

Dryer, M. and R. S. Steinolfson, MHD solution of interplanetary disturbances generated by simulated velocity perturbations, J. Geophys. Res., 81, 5413, 1976.

Dryer, M., C. Candelaria, Z. Smith, R. Steinolfson, E. J. Smith, J. H. Wolfe, J. D. Mihalov, and P. Rosenau, Dynamic MHD modeling of the solar wind disturbances during the August 1972 events, J. Geophys. Res., 83, 532, 1978a.

Dryer, M., Z. K. Smith, E. J. Smith, J. D. Mihalov, J. H. Wolfe, R. S. Steinolfson, and S. T. Wu, Dynamic MHD modeling of solar wind corotating stream interaction regions observed by Pioneer 10 and 11, J. Geophys. Res., 83, 4347, 1978b.

Formisano, V. and J. K. Chao, On the generation of shock pairs in the solar wind, Cosmic Plasma Physics, ed., K. Schindler, p. 103, Plenum, New York, 1972.

Frisch, U., A. Pouquet, J. Léorat, and A. Mazure, Possibility of an inverse cascade of magnetic helicity in magnetohydrodynamic turbulence, J. Fluid Mech., 68, 769, 1975.

Gazis, P. R., Solar wind evolution, Thesis, Massachusetts Institute of Technology, 1983.

Gazis, P. R. and A. Lazarus, Voyager observatons of the solar wind temperature: 1-10 AU, Geophys. Res. Lett., 9, 431, 1982.

Gazis, P. R. and A. Lazarus, The radial evolution of the solar wind, 1-10 AU, Solar Wind Five, NASA Conf. Pub. 2280, ed. M. Neugebauer, 1983.

Gold, T., Magnetic storms, Space Sci. Rev., 1, 100, 1962.

Goldstein, H., On the field configuration in magnetic clouds, Solar Wind Five, ed. M. Neugebauer, p. 731, NASA Conference Pub. 2280, 1983.

Goldstein, B. E. and J. R. Jokipii, Effects of stream-associted fluctuatins upon the radial evolution of average solar wind parameters, J. Geophys. Res., 82, 1095, 1977.

Goldstein, M., L. Burlaga, and W. Matthaeus, Power spectral signatures of interplanetary corotating and transient flows, J. Geophys. Res., 89, 1984.

Gosling, J. T., Solar wind stream evolution, Solar Wind Four, edited by H. Rosenbauer, p. 107, Report No. MPAE-W-100-81-31, p. 107, 1981.

Gosling, J. T., A. J. Hundhausen, and S. J. Bame, Solar wind evolution at large heliocentric distances: Experimental demonstration and the test of a model, J. Geophys. Res., 81, 2111, 1976.

Gosling, J. T., J. R. Asbridge, S. J. Bame, and W. C. Feldman, Solar wind stream interfaces, J. Geophys. Res., 83, 1401, 1978.

Hakamada, K. and S. -I. Akasofu, Simulation of three-dimensional solar wind disturbances and resulting geomagnetic storms, Space Sci. Rev., 31, 3, 1982.

Holzer, T. E., The solar wind and related astrophysical phenomena, in Solar System Plasma Physics, Vol. 1, E. N. Parker, C. F. Kennel, and L. J. Lanzerotti, eds., North-Holland, 1979.

Hundhausen, A. J., Coronal Expansion and Solar Wind, Springer-Verlag, New York, 1972.

Hundhausen, A. J., Evolution of large-scale solar wind structures beyond 1 AU, J. Geophys. Res., 78, 2035, 1973a.

Hundhausen, A. J., Nonlinear model of high-speed solar wind streams, J. Geophys. Res., 78, 1528, 1973b

Hundhausen, A. J., An interplanetary view of coronal holes, in Coronal Holes and High Speed Wind Streams, p. 225, J. B. Zirker, Ed., Colorado Associated University Press, 1977.

Hundhausen, A. J., Solar activity and the solar wind, Rev. Geophys. Space Phys., 17, 2034, 1979.

Hundhausen, A. J., Some macroscopic properties of shock waves in the solar wind, 1984.

Hundhausen, A. J. and J. T. Gosling, Solar wind structure at large heliocentric distances, An interpretation of Pioneer 10 observations, J. Geophys. Res., 81, 1436, 1976.

Intriligator, D. S., The August 1972 solar-terrestrial events: Solar wind plasma observations, Space Sci. Rev., 19, 629, 1976.

Intriligator, D. S., The large scale and long term evolution of the solar wind speed distribution on high speed streams, in Study of Traveling Interplanetary Phenomena, edited. M. Shea, D. F. Smart, and S. T. Wu, D. Reidel, Hingham, Mass., 1977.

Intriligator, D. S., Interplanetary transient phenomena originating at the sun, in Solar and Interplanetary Dynamics, M. Dryer and E. Tandberg-Hansen (eds), p. 357, D. Reidel, 1980.

Ivanov, K. G. and A. F. Harchiladze, Dynamics of hydromagnetic clouds from powerful solar flares, preprint, 1983.

Jokipii, R., Radial variaton of solar wind parameters, Geophys. Res. Lett., 3, 141, 1976.

Jokipii, R. and L. Davis, Jr., Long wavelength turbulence and the heating of the solar wind, Astrophys. J., 156, 1101, 1969.

Kayser, S., Persistence of shocks to large distancesin the solar wind, preprint, 1984.

King, J. H., Solar cycle variations in IMF intensity, J. Geophys. Res., 84, 5938, 1979.

King, J. H., On the enhancement of the IMF magnitude during 1978-1979, J. Geophys. Res., 86, 4828, 1981.

Klein, L. W. and L. F. Burlaga, Interplanetary magnetic clouds at 1 AU, J. Geophys. Res., 87, 613, 1982.

Kohlhase, C. E. and P. A. Penzo, Voyager mission description, Space Sci. Rev., 21, 77, 1977.

Matthaeus, W. H. and M. Goldstein, Measurement of rugged invariants of magnetohydrodynamic turbulence in the solar wind, J. Geophys. Res., 87, 6011, 1982a.

Matthaeus, W. H., and M. L. Goldstein, Stationarity of magnetohydrodynamic fluctuations in the solar wind, J. Geophys. Res., 87, 10347, 1982b.

Matthaeus, W. H. and M. Goldstein, Magnetohydrodynamic turbulence in the solar wind, Solar Wind Five, p. 73, ed. M. Neugebauer, NASA Conf. Pub. 2280, 1983.

Matthaeus, W. H. and D. Montgomery, Selective decay hypothesis at high mechanical and magnetic Reynolds numbers, Ann. N.Y. Acad. Sci., 357, 203, 1980.

Matthaeus, W. H., M. L. Goldstein, and C. Smith, Evaluation of magnetic helicity in homogeneous turbulence, Phys. Rev. Letters, 48, 1256, 1982.

Matsuda, T. and T. Sakurai, Dynamics of the azimuthally dependent solar wind, Cosmic Electrodynamics, 3, 97, 1972.

McDonald, F. B., N. Lal, J. H. Trainor, M. A. I. Van Hollebeke, and W. R. Webber, The solar modulation of galactic cosmic rays in the outer heliosphere, Ap. J. (Letters), 249, L71, 1981a.

McDonald, F. B., J. H. Trainor, J. D. Mihalov, J. H. Wolfe, and W. R. Webber, Radially propagating shock waves in the outer heliosphere: The evidence from Pioneer 10 energetic particle and plasma observations, Ap. J. (Letters), 246, L165, 1981b.

McDonald, F. B., L. F. Burlaga, J. H. Trainor, M. A. I. Van Hollebeke, and T. von Rosenvinge, Observations of the long term cosmic ray modulation between 1 AU and 25 AU, Bull. of the American Physical Society, 17, 571, 1982.

Meyer, P., E. N. Parker, and J. A. Simpson, Solar cosmic rays of February 1956 and their propagation through interplanetary, Space Phys. Rev., 104, 768, 1956.

Mihalov, J. D. and J. H. Wolfe, Pioneer-10 observations of the solar wind proton temperature heliocentric gradient, Solar Phys., 60, 399, 1978.

Mihalov, J. D. and J. H. Wolfe, Pioneer 10 studies of interplanetary shocks at large heliocentric distances, Geophys. Res. Lett., 6, 491, 1979.

Montgomery, D., Theory of hydromagnetic turbulence, in Solar Wind Five, p. 107, ed. M. Neugebauer, NASA Conf. Pub. 2280, 1983.

Morrison, P., Solar-connected variations of the cosmic rays, Phys. Rev., 95, 641, 1954.

Nerney, S. F., and S. T. Suess, Corrections to the azimuthal IMF due to meriodional flow in the solar wind, Ap. J., 200, 503, 1975.

Ness, N. F., K. W. Behannon, R. P. Lepping, and K. H. Schatten, Use of two magnetometers for magnetic field measurements on a spacecraft, J. Geophys. Res., 76, 3564, 1971.

Neubauer, F. M., Optimization of multimagnetometer systems on a spacecraft, J. Geophys. Res., 80, 3235, 1975.

Parker, E. N., The gross dynamics of a hydromagnetic gas cloud, Astrophys. J Supp., 25, 51, 1957.

Parker, E. N., Dynamics of the interplanetary gas and magnetic fields, Astrophys. J., 128, 664, 1958.

Parker, E. N., Sudden expansion of the corona following a large solar flare and the attendant cosmic ray effects, Ap. J., 133, 1014, 1961.

Parker, E. N., Interplanetary Dynamical Processes, Interscience, New York, 1963.

Parker, E. N., Dynamical theory of the solar wind, Space Sci. Rev., 4, 666, 1965.

Pizzo, V., An evaluation of corotating solar wind stream models, Solar Wind Four, p. 153, ed. by H. Rosenbauer, Report No. MPAE-W-100-81-31, 1981.

Pizzo, V., A three-dimensional model of corotating streams in the solar wind. 3. Magnetohydrodynamic streams, J. Geophys. Res., 87, 4374, 1982.

Pizzo, V., Quasi-steady solar wind dynamics, Solar Wind Five, ed. Marcia Neugebauer, p. 675, NASA Conference Pub. 2280, 1983a.

Pizzo, V., Successive solar flares from the same active region: Comments, in Solar Wind Five, ed. Marcia Neugebauer, p. 481, NASA Conference Pub. 2280, 1983b.

Pizzo, V., Interplanetary shocks on the large scale--A retrospective on the last decade's theoretical efforts, preprint, 1984.

Rosenberg, R. L., M. G. Kivelson, P. J. Coleman, Jr., and E. J. Smith, The radial dependences of the interplanetary magnetic field between 1.0 and 5.0 AU: Pioneer 10, J. Geophys. Res., 83, 4165, 1978.

Sheeley, N. and J. W. Harvey Coronal holes, solar wind streams, and geomagnetic disturbances during 1978 and 1979, Solar Phys., 70, 237, 1981.

Simon, M. and W. I. Axford, Shock waves in the interplanetary medium, Planet. Space Sci., 14, 901, 1966.

Sittler, Jr., E. C. and J. D. Scudder, An empirical polytrope law for solar wind thermal electrons between 0.45 and 4.76 AU: Voyager 2 and Mariner 10, J. Geophys. Res., 85, 5131, 1980.

Slavin, J. A., E. J. Smith, and B. T. Thomas, Large scale temporal and radial gradients in the IMF: Helios 1, 2, ISEE-3, and Pioneer 10, 11, Geophys. Res. Lett., in press, 1984.

Smith, E. J., Radial gradients in the interplanetary magnetic field between 1.0 and 4.3 AU: Pioneer 10, in Solar Wind Three, ed. C. T. Russell, University of California Press, Los Angeles, 1974.

Smith, E. J., Interplanetary magnetic fields, Rev. Geophys. Space Phys., 17, 610, 1979.

Smith, E. J., Solar wind magnetic field observations, in Solar Wind Four, p. 96, ed. by H. R. Rosenbauer, Report No. MPAE-W-100-81-31, 1981.

Smith, E. J., Observations of interplanetary shocks: Recent progress, Space Sci. Rev., 34, 101, 1983.

Smith, E. J. and A. Barnes, Spatial dependences of the solar wind, 1-10 AU, p. 521, in Solar Wind Five, ed. M. Neugebauer, NASA CP 2280, 1983.

Smith, E. J., and J. H. Wolfe, Observations of interaction regions and corotating shocks between one and five AU: Pioneers 10 and 11, Geophys. Res. Lett., 3, 137, 1976.

Smith, E. J. and J. H. Wolfe, Pioneer 10, 11 observations of evolving solar wind streams and shocks beyond 1 AU, in Study of Traveling Interplanetary Phenomena, ed. by M. A. Shea, D. F. Smart, and S. T. Wu, pp. 227-257, D. Reidel, Hingham, Mass., 1977.

Smith, E. J. and J. H. Wolfe, Fields and plasmas in the outer solar system, Space Sci. Rev., 23, 217, 1979.

Smith, E. J., L. Davis, Jr., P. J. Coleman, Jr., D. S. Colburn, P. Dyal, and D. E. Jones, August 1972 solar-terrestrial events observations of interplanetary shocks at 2.2 AU, J. Geophys. Res., 82, 1077, 1977.

Smith, Z. K., M. Dryer, R. W. Fillius, E. J. Smith, and J. H. Wolfe, Compression of Jupiter's magnetosphere by the solar wind: Reexamination via MHD simulation of evolving corotating interaction regions, J. Geophys. Res., 86, 6773, 1981.

Smith, E. J., L. Davis, Jr., P. J. Coleman, Jr., D. S. Colburn, P. Dyal, and D. E. Jones, August 1972 solar-terrestrial events: Observations of interplanetary shocks at 2.2 AU, J. Geophys. Res., 82, 1077, 1977.

Sonnett, C. P. and D. S. Colburn, The SI^+ - SI^- pair and interplanetary forward-reverse shock ensembles, Planet. Space Sci., 13, 675, 1965.

Steinolfson, R. S., M. Dryer, Y. Nakagawa, Numerical MHD simulation of interplanetary shock pairs, J. Geophys. Res., 80, 1223, 1974.

Steinolfson, R. S., M. Dryer, and Y. Nakagawa, Interplanetary shock pair disturbances: Comparison of theory with space probe data, J. Geophys. Res., 80, 1989, 1975.

Suess, S. T., Models of coronal hole flows, Space Sci. Rev., 23, 159, 1979.

Suess, S. T. and S. F. Nerney, Meridional flow and the validity of the two-dimensional approximation in stellar wind modeling, Astrophys. J., 184, 17, 1973.

Suess, S. T. and S. F. Nerney, The global solar wind and predictions for Pioneers 10 and 11, Geophys. Res. Lett., 2, 75, 1975.

Thomas, B. T. and E. J. Smith, The Parker spiral configuration of the interplanetary magnetic field between 1 and 8.5 AU, J. Geophys. Res., 85, 6861, 1980.

von Neumann, J., Progress report on the theory of shock waves, National Defense Research Committee, Division 8, Office of Scientific Research and Development, No. 1140, 1943.

Whang, Y. C., Magnetohydrodynamics of corotating interplanetary structures, J. Geophys. Res., 85, 2285, 1980.

Whang, Y. C., The forward-reverse shock pair at large heliocentric distances, to appear in J. Geophys. Res., 1984.

Whang, Y. C. and L. F. Burlaga, Coalescence of two pressure waves associated with stream interactions, in press, 1984.

Whang, Y. C. and T. H. Chien, Magnetohydrodynamic interaction of high-speed streams, J. Geophys. Res., 86, 3263, 1981.

Figure Captions

Figure 1. Trajectories of Voyager 1 and 2 projected into the ecliptic plane.

Figure 2. Inertial heliographic (IHG) coordinate system. Note that the origin is at the sun, the Z_{IHG}-axis is along the sun's spin axis, and the $X_{IHG} - Y_{IHG}$ plane contains the solar equator.

Figure 3. Heliographic (HG) coordinate system. The origin is at the location of the observer, $\hat{X}_{HG}$ points radially away from the sun, and $\hat{Y}_{HG}$ is parallel to the solar equatorial plane. The direction of a vector $\underset{\sim}{B}$ in this coordinate system is given by the angles δ and λ defined as shown.

Figure 4. Radial variation of the strength of the interplanetary magnetic field observed by Voyager 2. Each bar represents a 25 day average and the associated error in the mean. The curve is Parker's theoretical curve with the constant A = 4.75 found from a least squares fit to the data.

Figure 5. This shows 26 day averages of 1) the magnetic field strength observed at 1 AU normalized by 6.75 nT (light curve) and the magnetic field strength observed at Voyagers 1 and 2 normalized by a value given by the curve in Figure 4, as a function of time. The Voyager averages have been shifted back in time by an amount corresponding to the radial propagation time from 1 AU to the average position of Voyager in the averaging interval. No significant radial gradient is seen.

Figure 6. Daily averages of the magnetic field strength and direction observed by Voyager 2 between 1 AU and 5 AU. The curves are Parker's theoretical curves for a spiral field. Note the large fluctuations about the nominal spiral model.

Figure 7. Magnitudes of daily averages of the components of $\underset{\sim}{B}$. Here, RTN corresponds to XYZ, in Figure 3. Solid lines are best fits, assuming a power law dependence on R. Dashed lines represent the spiral model predictions. $B_N = 0$ in the spiral model, so the fluctuations in B_N are waves which are superimposed on the mean field. Dots are daily averages.

Figure 8. Sector pattern observed by Voyager 1. Each sign indicates dominant polarity on one day: + outward, - inward, • mixed.

Figure 9. Relation between the magnetic polarities observed by Voyagers 1 and 2 projected to the sun and the white-light polarization brightness contours which indicate the extent of polar coronal holes. In the top panel, both coronal holes extend to near the solar equator, and one expects a nearly horizontal sector boundary. Voyagers 1 and 2 observed mixed polarities, consistent with such a boundary. In the bottom panel, "lobes" extend across the equator, and one expects the footpoints of the sector boundary surface to line near the dashed curve. The Voyager observations are consistent with this.

Figure 10. Left. Daily average of the magnetic field strength normalized with respect to the spiral field fit in Figure 4. Right. Daily averagees of the bulk speed. The approximate sector pattern in Figure 8 is reproduced here.

Figure 11. This shows the times at which Voyager 2 observed forward and reverse shocks, interfaces, and magnetic clouds (C). Cross-hatched regions indicate "corotating" interaction regions. They do not recur periodically, indicating the importance of temporal variations even for corotating flows. Shaded areas indicate data gaps.

Figure 12. A sketch of magnetic field lines in a non-uniform stationary flow, from Parker (1963).

Figure 13. The bottom panels show IMP-8 hour averages of the bulk speed and magnetic field strength at 1 AU. The other panels are the results of an MHD model with 1 AU data as inputs. The well-known formation and motion of a forward shock (FS) and a reverse shock (RS) is illustrated. Note that the shocks move apart at a constant rate.

Figure 14. A corotating stream. Curves are theoretical predictions of a MHD model based on input data from 1 AU. Dots are Voyager 1 observations.

Figure 15. Time profiles of solar wind speed and density at 1 AU, generated by a gas dynamic model with pure speed pulses at the inner boundary at T = 0 of duration 15, 50 and 150 hours, respectively. Streams of shorter duration "damp-out" faster than streams of longer duration. This effect is referred to as "filtering" (Holzer, 1979).

Figure 16. Observations of the "filtering-out of large-amplitude short-wavelength disturbances", from Gosling et al. (1976). The speed disturbances were seen at the front of a fast stream by IMP-7 at 1 AU, but they were not seen by Pioneer 10 at 4.65 AU.

Figure 17. Sketch illustrating the decay of a stream and the corresponding growth of a pressure wave. It is likely that successive streams or pressure waves will interact with one another before a secondary flow can develop.

Figure 18. Corotating pressure waves without fast streams. The pressure profiles on the left show regions of high and low pressure which evolve in time in a way analagous to that of simple compression and rarefaction waves in gas dynamicss. The panels on the right show that these waves are not driven locally by a fast stream. They represent new dynamical structures which are of fundamental importance in the outer heliosphere.

Figure 19. The field strength normalized by the Parker field model versus the density normalized by an R^{-2} law at 6 distance intervals. At large distances, B tends to be proportional to the density, showing that the organization of the outer heliosphere is different from that at the inner heliosphere. The linear relation is consistent with the dominance of large pressure waves in the outer heliosphere.

Figure 20. The time interval between the detection of a forward shock and its associated reverse shock versus distance from the sun. The shock separation increases with distance.

Figure 21. Sketch of the configuration of the outer heliosphere for stationary flows. Streams dominate the dynamics near the sun and pressure waves are dominant near 10 AU. Beyond 10 AU pressure waves may interact with one another, and beyond 25 AU this interaction is very extensive.

Figure 22. A magnetic cloud observed by Voyager 2.

Figure 23. This shows the proton momentum flux, the total (magnetic plus thermal) pressure, and the ratio β of the ion thermal pressure to the magnetic pressure for the magnetic cloud in Figure 22.

Figure 24. The extent of a magnetic cloud, determined from multispacecraft observations by spacecraft in the ecliptic plane.

Figure 25. Four magnetic clouds observed by Voyagers 1 and 2, (see text). The clouds are larger farther from the sun, suggesting that clouds expand.

Figure 26. Possible magnetic field configurations in a magnetic cloud. Configuration a) is not consistent with observations.

Figure 27. Speed profile observed by Voyager 1 near 8.5 AU (top); the corresponding speed profile observed by Helios 1 between 0.3 AU and 1 AU shifted to allow for radial propagation at a speed of 500 km/sec (middle); and Helios speed profile "corotated" to Voyager 1 using the observed speeds (bottom). There is a loss of small scale structure with increasing distance from the sun. This may be due in part to the "entrainment" of slow flows by faster flows, as suggested by the multivalued function in the lower panel.

Figure 28. Magnetic field lines between 1 AU and 10 AU based on a kinematic mapping of Voyager observations at ∿ 2 AU. Heavy lines indicate strong fields, and dashed lines weak fields. Two interaction regions, ∿ 180° apart, are seen near the sun, but they tend to coalesce at large distances because one is being convected faster than the other.

Figure 29. Coalescence of two interaction regions (pressure waves) observed at 1 AU to form a single larger interaction region at 2 AU as a slow stream is "entrained" by a fast stream.

Figure 30. This shows the theoretical curves for 1.44 AU (the position of Voyager 1) for the flow in Figure 29. Voyager observations are shown by dots. The two separate interaction regions (pressure waves) are beginning to coalesce at 1.44 AU.

Figure 31. A fast corotating stream overtaking a shock wave (F1). A forward-reverse shock pair (F2-RS) forms ahead of the fast stream. The two forward shocks F1 and F2 will coalesce beyond 3 AU and the reverse shock RS will intersect a third shock F3 between 2 AU and 3 AU producing a new high field region. Three high field regions observed at 1 AU coalesce to form a single high field region near 3 AU.

Figure 32. The results of a MHD model of the flow in Figure 31 (solid curves) plotted at 1.61 AU where they can be compared with the Voyager 1 data (dots). Note the single large pressure wave that is being formed as the corotating interaction region interacts with the flow behind F2.

Figure 33. A fast stream with a shock pair overtaking a shock pair without a fast stream. The points are Voyager observations, and the curves are "fits".

Figure 34. Schematic of the interaction of the shocks in Figure 34. The forward shock moves away from its corresponding reverse shock. The forward shock FA from one pair interacts with the reverse shock RB from the other pair just beyond 6 AU. A contact surface CS is formed by the interaction. This is a fundamental process in the outer heliosphere.

Figure 35. Two pressure waves, each bounded by a shock pair, were observed at Voyager in association with the streams shown in Figure 34. This shows theoretical results which indicate that each pressure wave expands, and after $\sim$ 7 days they begin to interact forming a "merged pressure wave".

Figure 36. Observation of the coalescence of two pressure waves. Helios 1 inside of 1 AU observed 2 pressure waves in association with 2 corotating streams (left panels). Voyager 1 observed a merged pressure wave near 8.5 AU consisting of the two original interaction regions (now broad and bounded by shocks) and a new interaction region (cross-hatched) where the 2 interaction regions "overlap".

Figure 37. The left panel shows a kinematical picture of the magnetic field lines for two corotating flows from opposite hemispheres of the sun. Interaction regions are denoted by the solid curves and rarefaction regions by the dashed curves. A dynamical model predicts the formation of a shock pair which bounds the interaction region (shaded area in the right panel). streams are identical.

Figure 38. Interaction of 2 pressure waves from twin streams, from Dryer and Steinolfson (1976). The time t is the elapsed period since the initiation of velocity pulses at 0.3 AU. An interaction between R_1 and F_2 occurs between 25.4 and 28.3 days.

Figure 39. Interactions of shock pairs corresponding to nearly identical recurrent streams (Pizzo, 1983). The flow is assumed to be periodic, as shown by the repetition of F1. The coalescence of separate pressure waves can be seen in the panel on the right.

Figure 40. A system of corotating flows. Note the repetitive pattern in the field strength $|\underset{\sim}{B}|$, density N and proton thermal speed V_p.

Figure 41. Power spectra of the magnetic field for the flow system in Figure 40. The upper curve is the power in the components of $\underset{\sim}{B}$ (the trace of the power spectral matrix), and the lower curve is the power in $|\underset{\sim}{B}|$. The circles and triangles show the two signs of magnetic helicity.

Figure 42. A system of mixed flows observed by Voyager 2.

Figure 43. Power spectra for the magnetic field in the mixed flow system shown in Figure 42.

Figure 44. The formation and evolution of a "shell" (shaded area) consisting of a system of transient flows moving through a stationary solar wind.

Figure 45. Solar wind disturbances caused by six successive flares during a period of 1[illegible] days, according to Akasofu and Hakamada (1983).

Figure 46. Radial evolution of the speed profiles for a system of mixed flows (left) and a system of corotating flows (right).

Figure 47. Radial evolution of the magnetic field strength for a system of mixed flows (left) and a system of corotating flows (right).

Figure 48. Power spectra of the magnetic field strength for the time series shown in Figure 47. The mixed flow system has a simple power law spectrum at both distances indicated, consistent with the evolution of MHD turbulence. The evolution of the spectrum at the right is consistent with the entrainment of slow moving interaction regions by faster interaction regions.

Figure 49. Sketch illustrating the differences between filtering, entrainment and turbulence. In "filtering", streams are "damped out". Small streams damp faster than large streams, leaving more power at long wavelengths at large distances from the sun. In entrainment, magnetic energy is transferred from small scales to larger scales as separate small interaction regions coalesce to form larger interaction regions. In "turbulence" there is a cascade of energy in such a way as to preserve the shape of the spectrum.

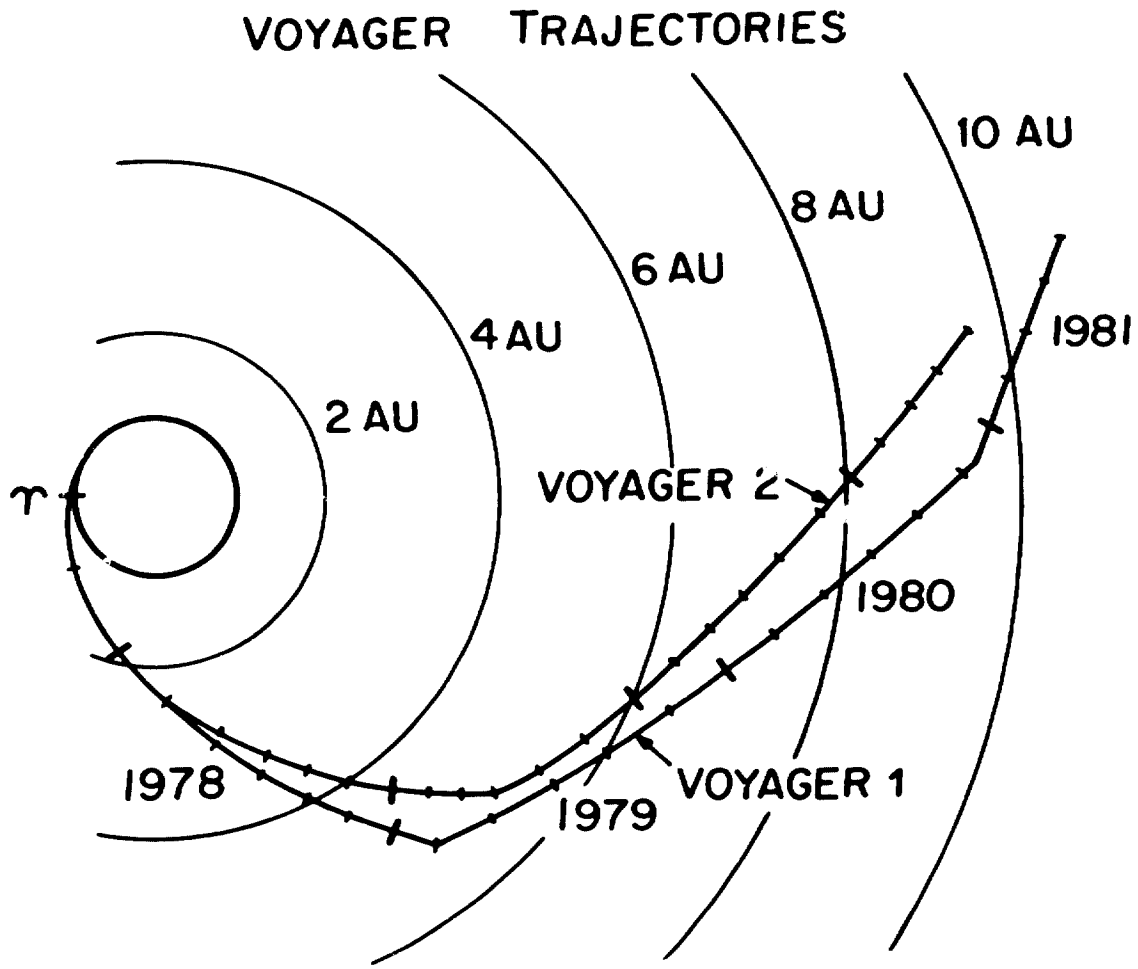
VOYAGER TRAJECTORIES
10 AU
8 AU
6 AU
4 AU
2 AU
1981
1980
1979
1978
VOYAGER 2
VOYAGER 1

Figure 1

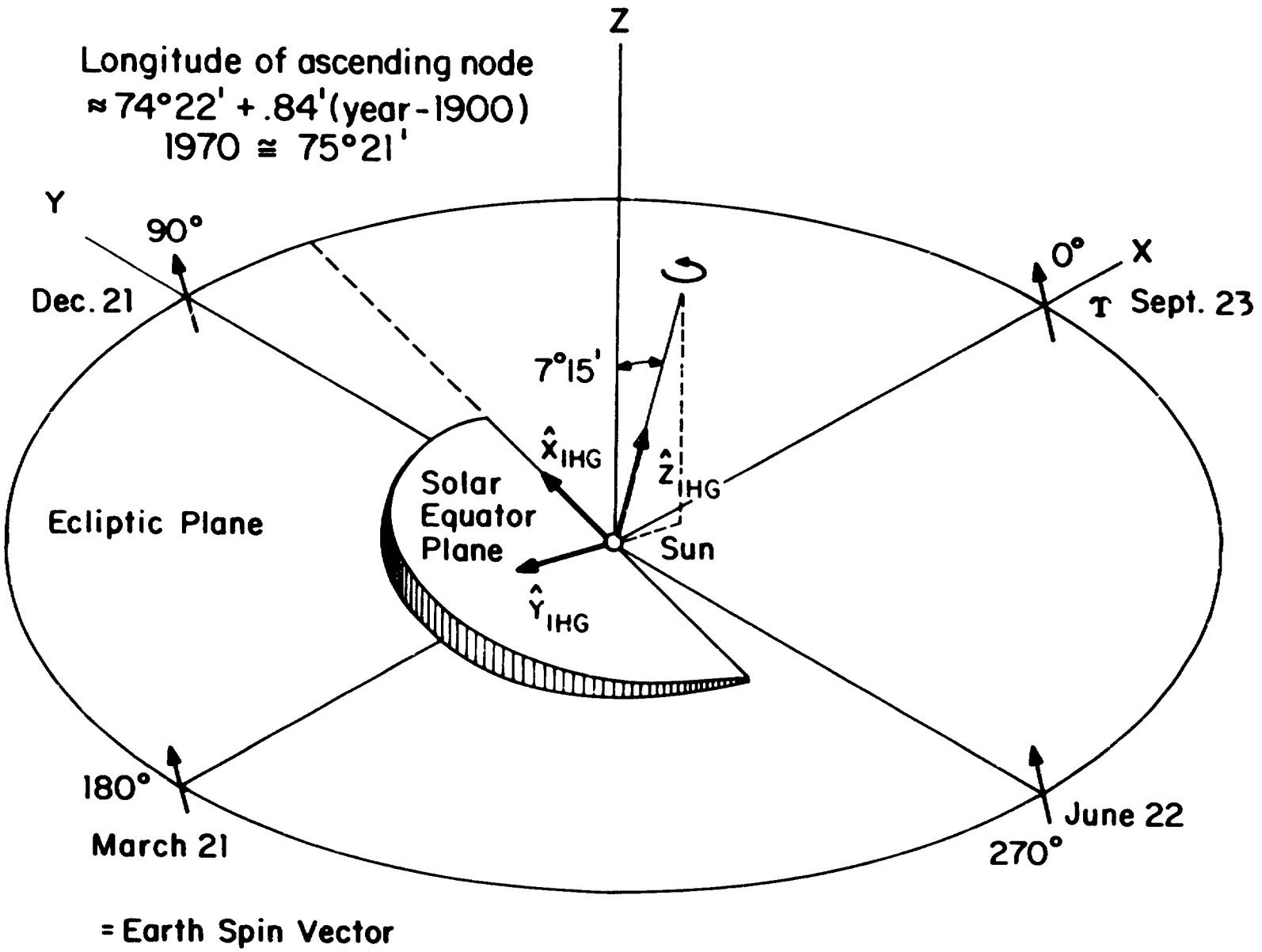

Figure 2

HG Coordinates

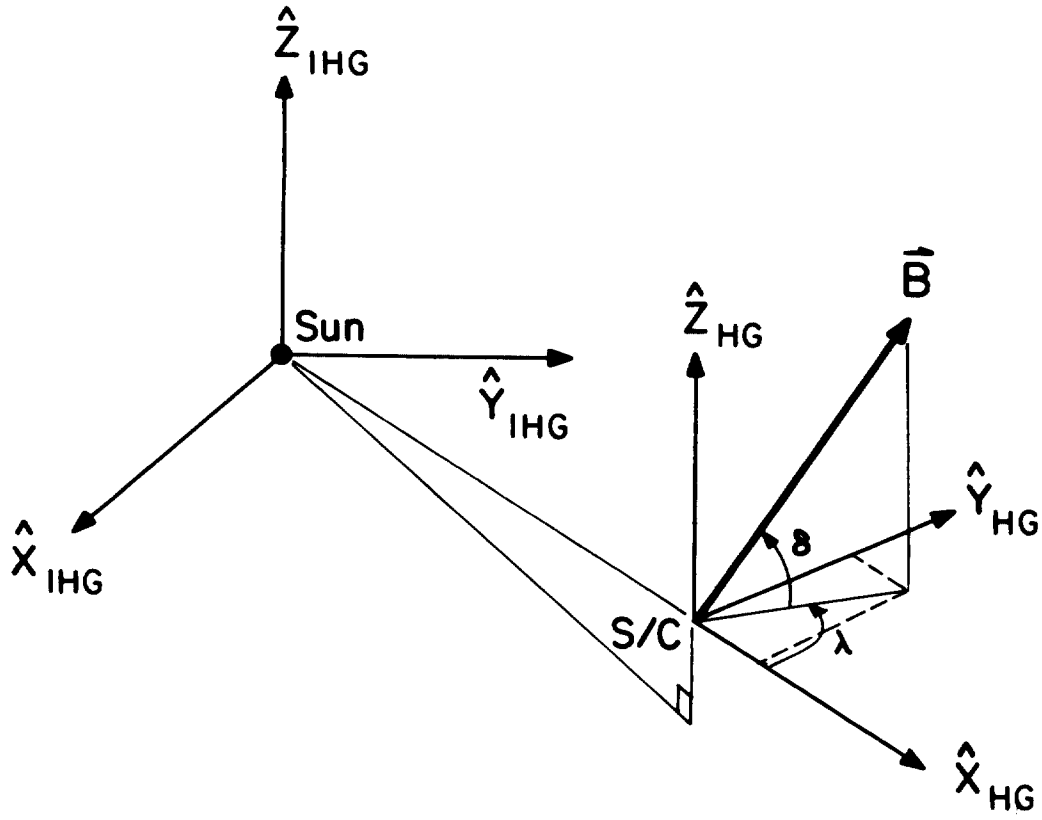

Figure 3

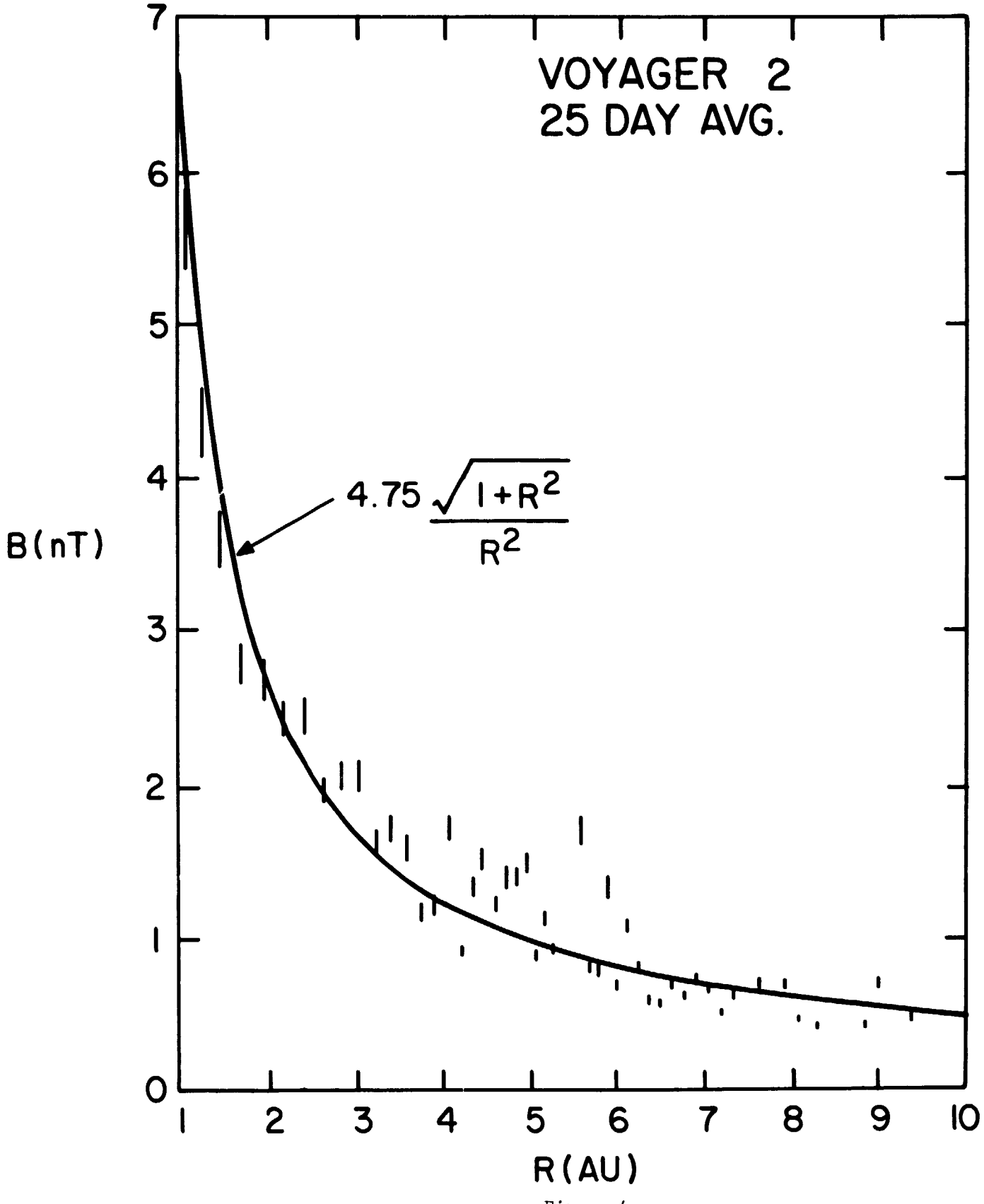
VOYAGER 2
25 DAY AVG.
$4.75\frac{\sqrt{1+R^2}}{R^2}$
B(nT)
R(AU)
0
1
2
3
4
5
6
7
8
9
10

Figure 4

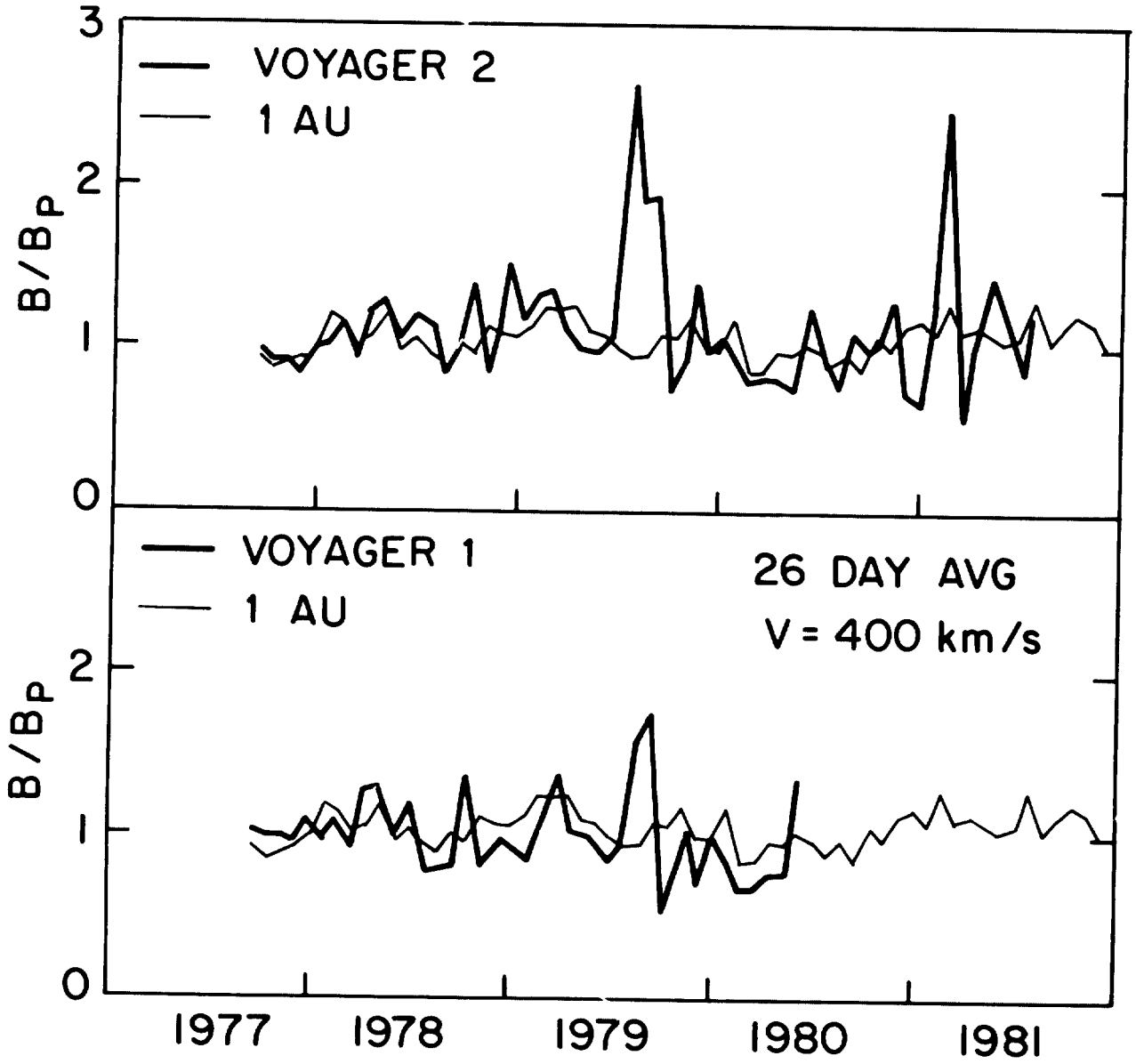

Figure 5

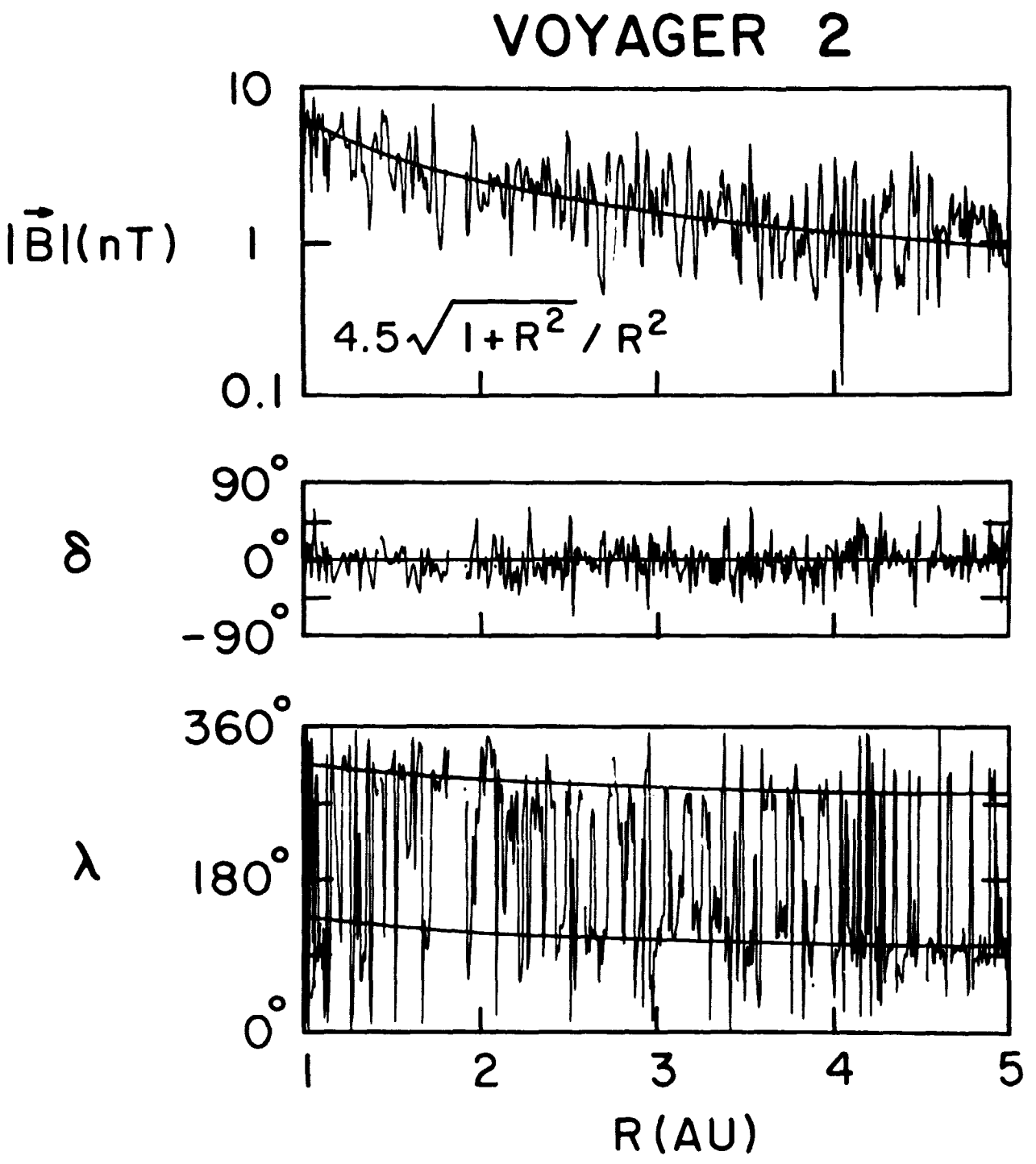

Figure 6

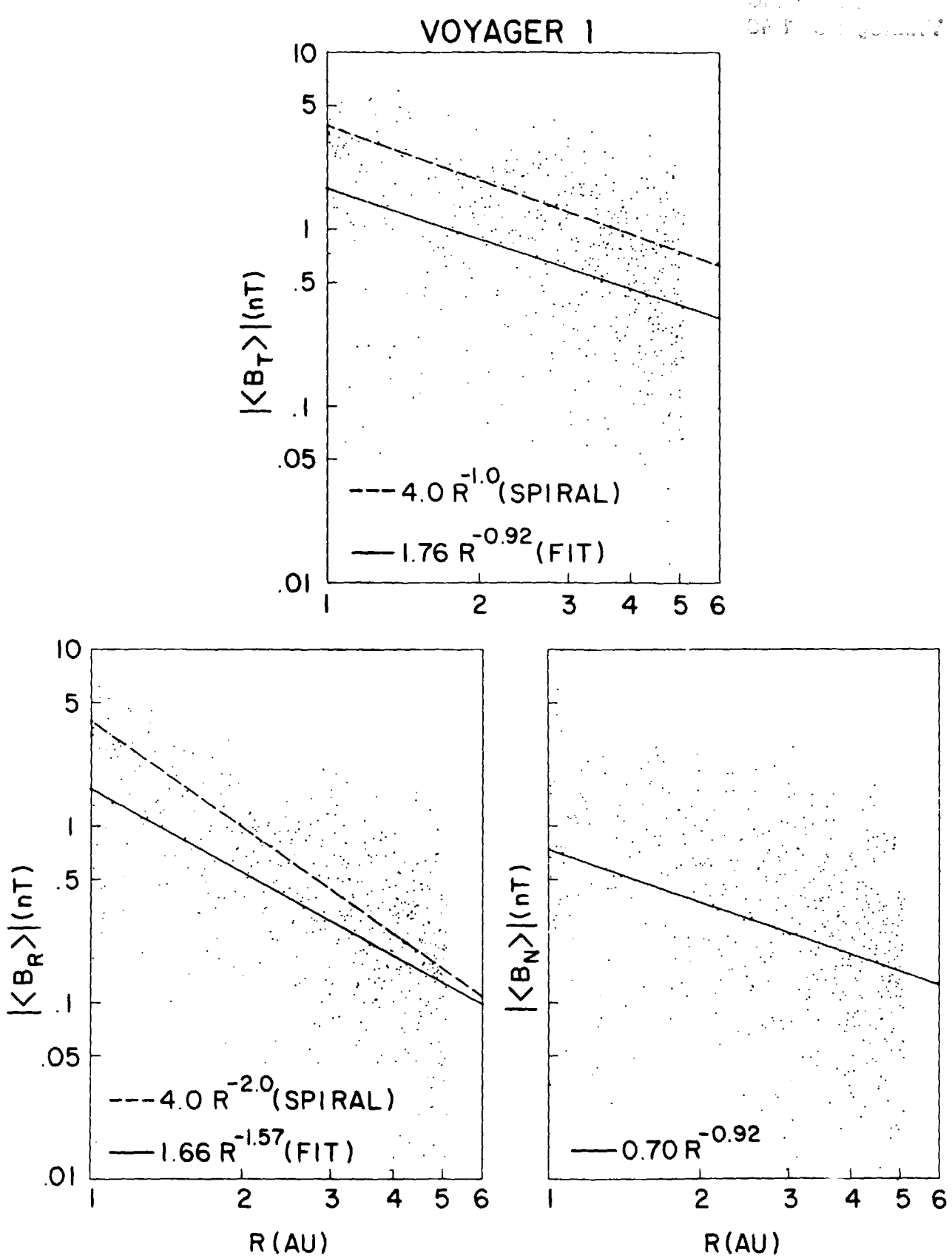
VOYAGER 1
10
5
1
.5
.1
.05
.01
|<B_T>|(nT)
---4.0 R^-1.0 (SPIRAL)
—1.76 R^-0.92 (FIT)
1
2
3
4
5
6
|<B_R>|(nT)
---4.0 R^-2.0 (SPIRAL)
—1.66 R^-1.57 (FIT)
R(AU)
|<B_N>|(nT)
—0.70 R^-0.92
R(AU)

Figure 7

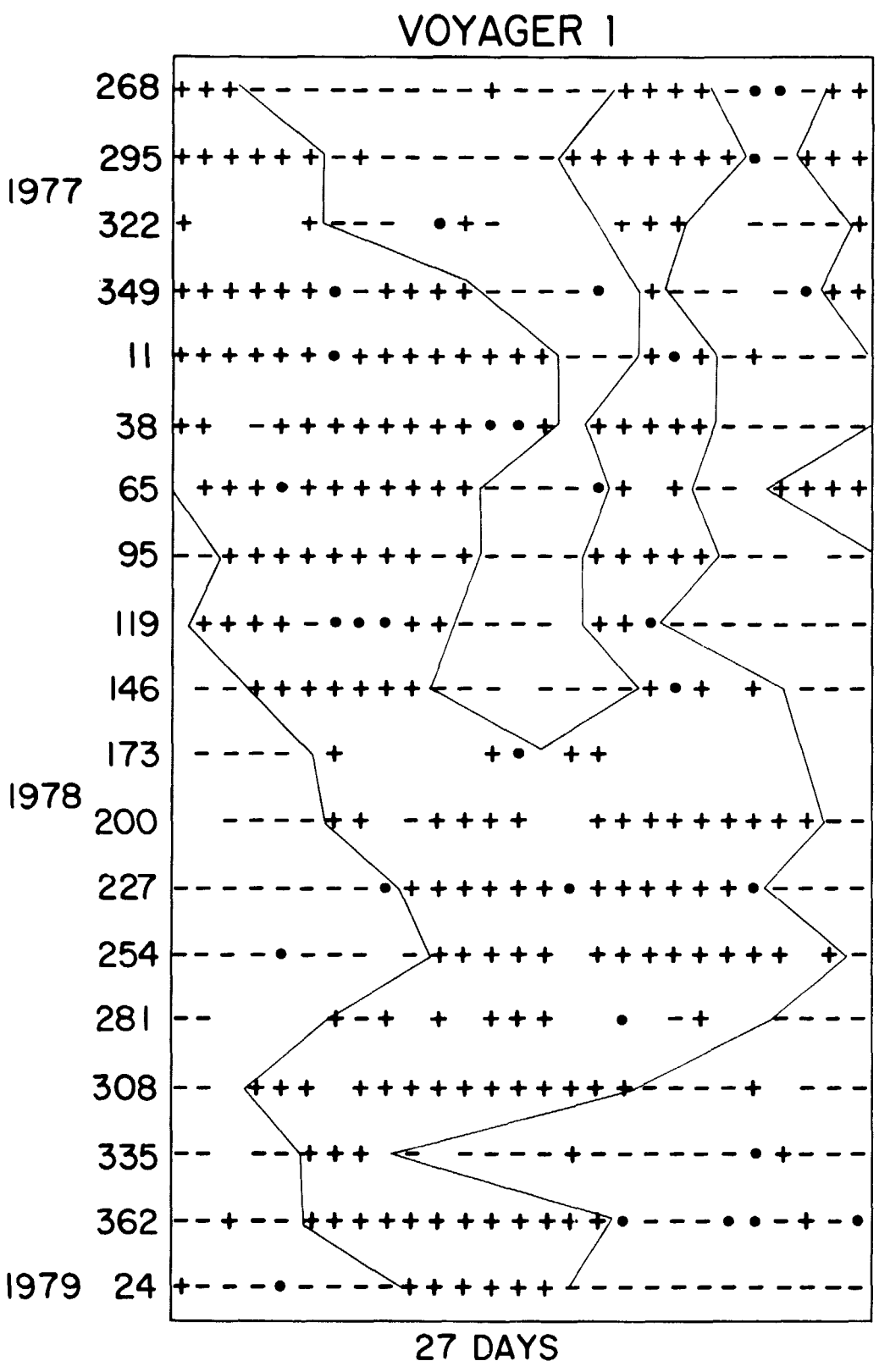

Figure 8

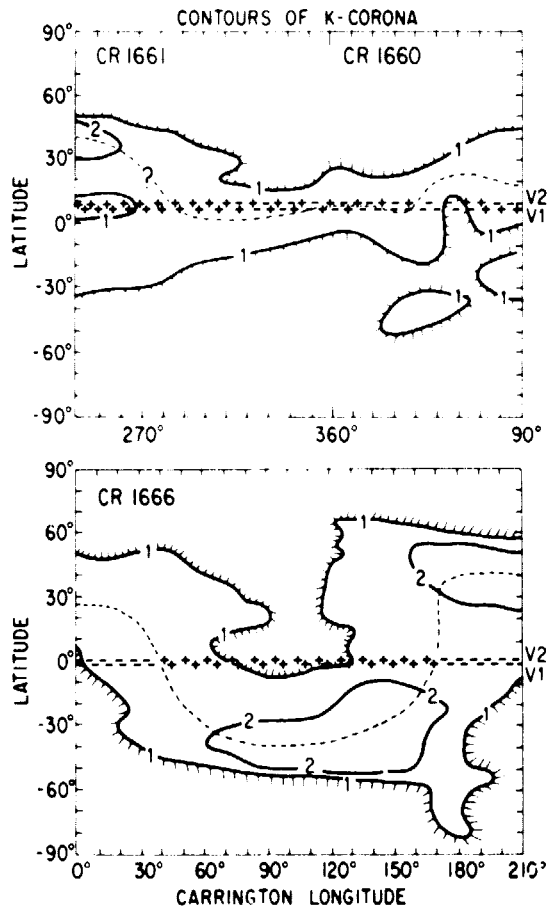

Figure 9

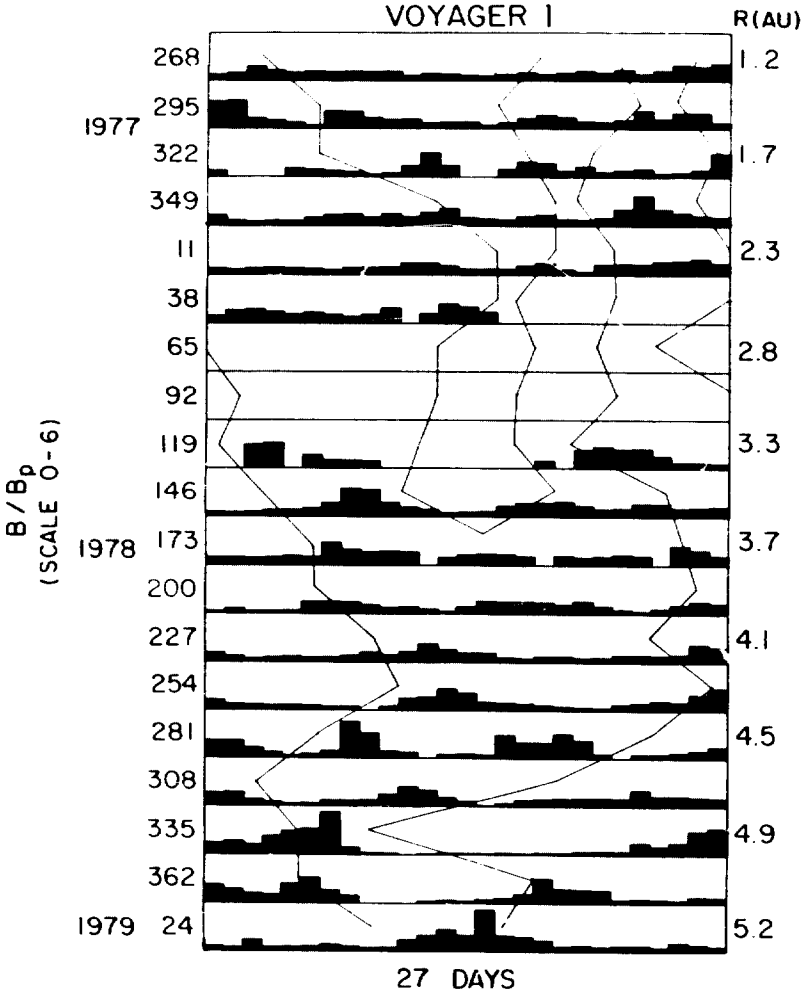

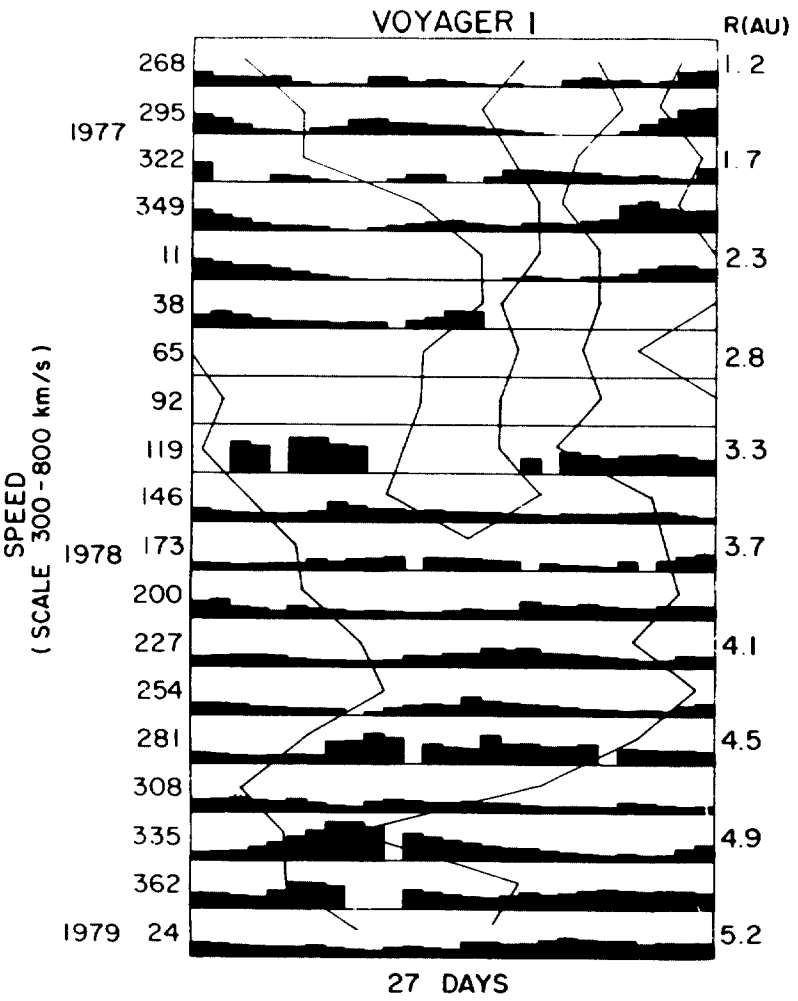

Figure 10

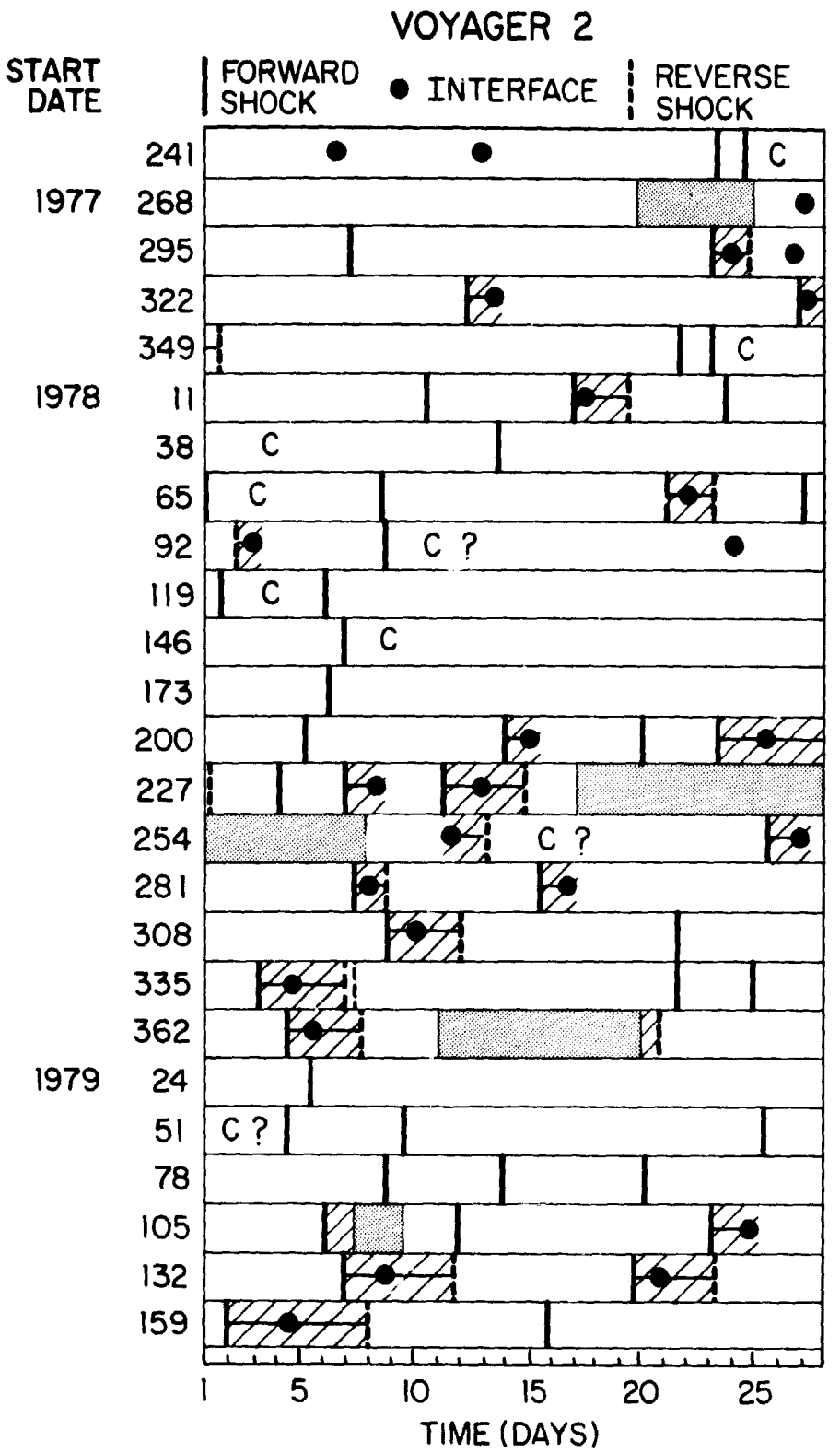

Figure 11

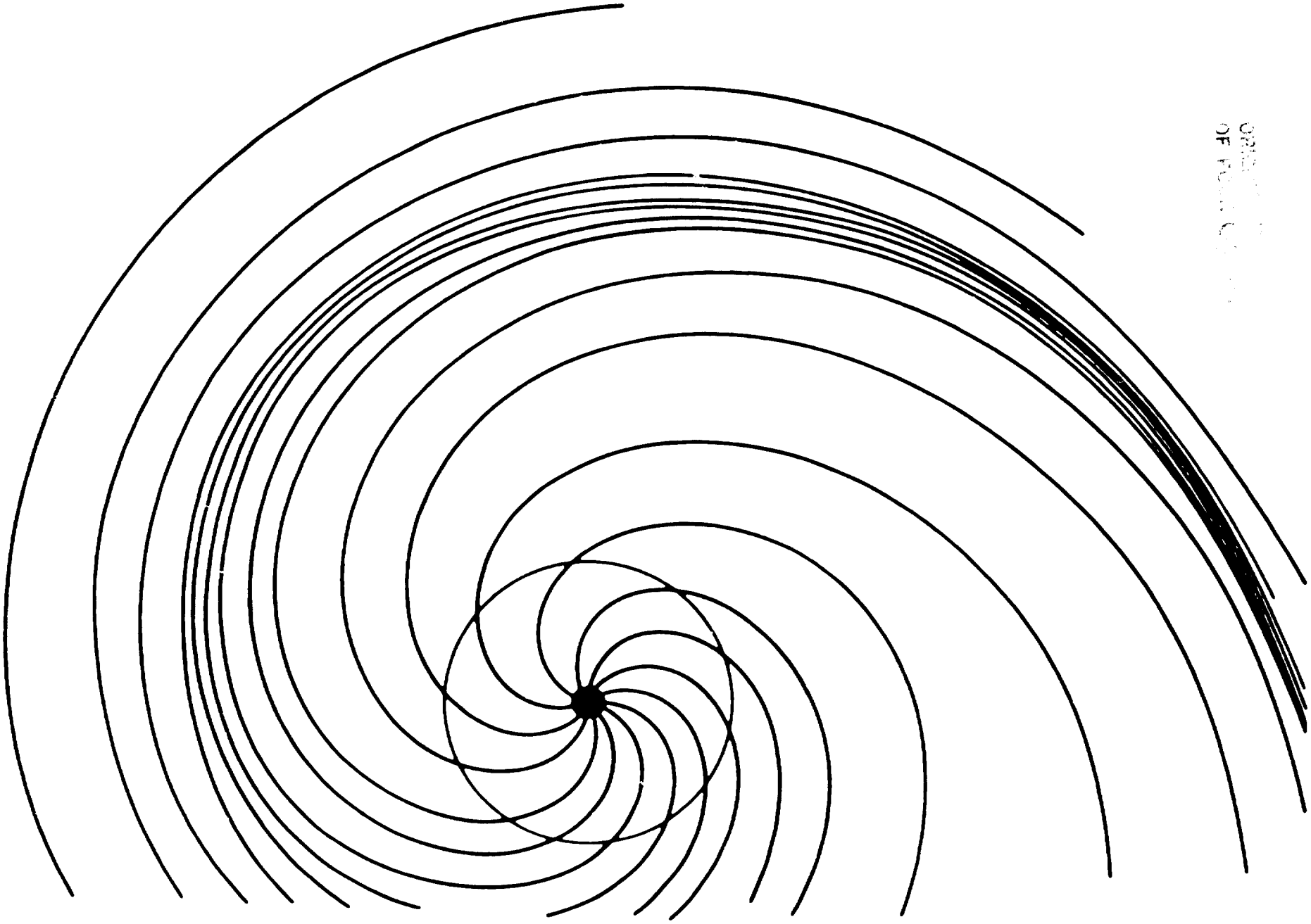

Figure 12

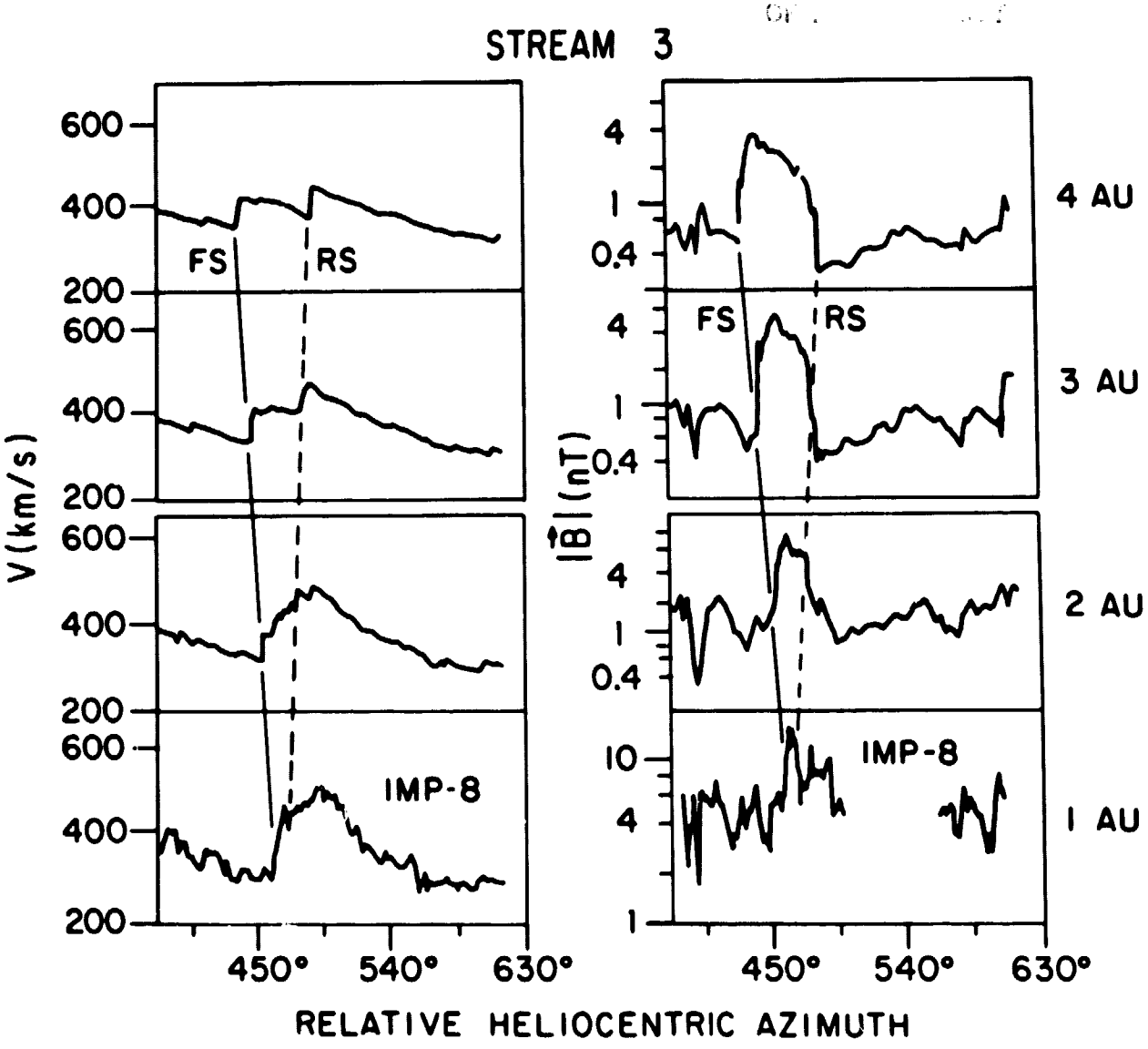
STREAM 3
V (km/s)
600
400
200
FS
RS
IMP-8
|B| (nT)
4
1
0.4
10
4
1
4 AU
3 AU
2 AU
1 AU
450°
540°
630°
RELATIVE HELIOCENTRIC AZIMUTH

Figure 13

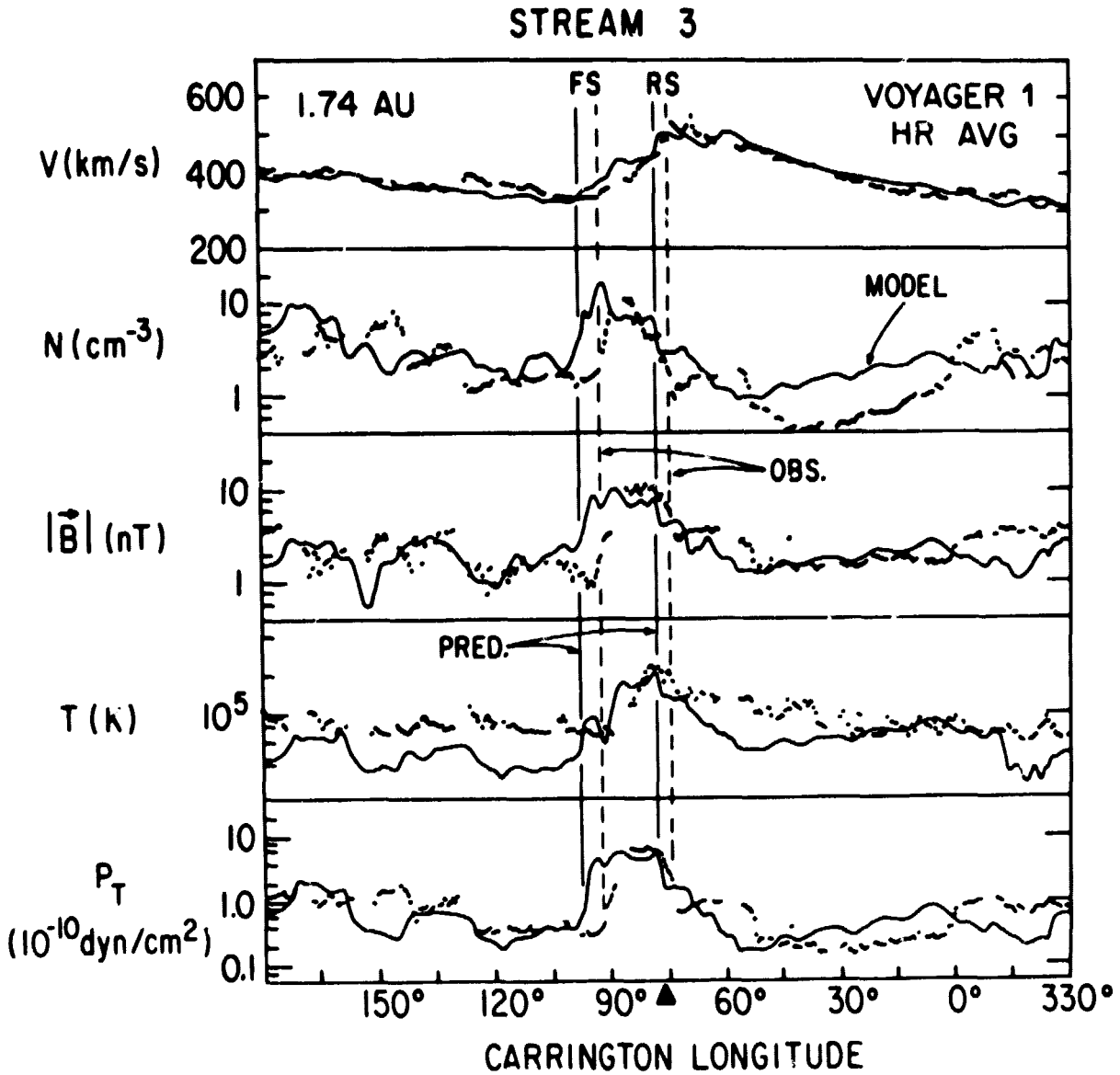

Figure 14

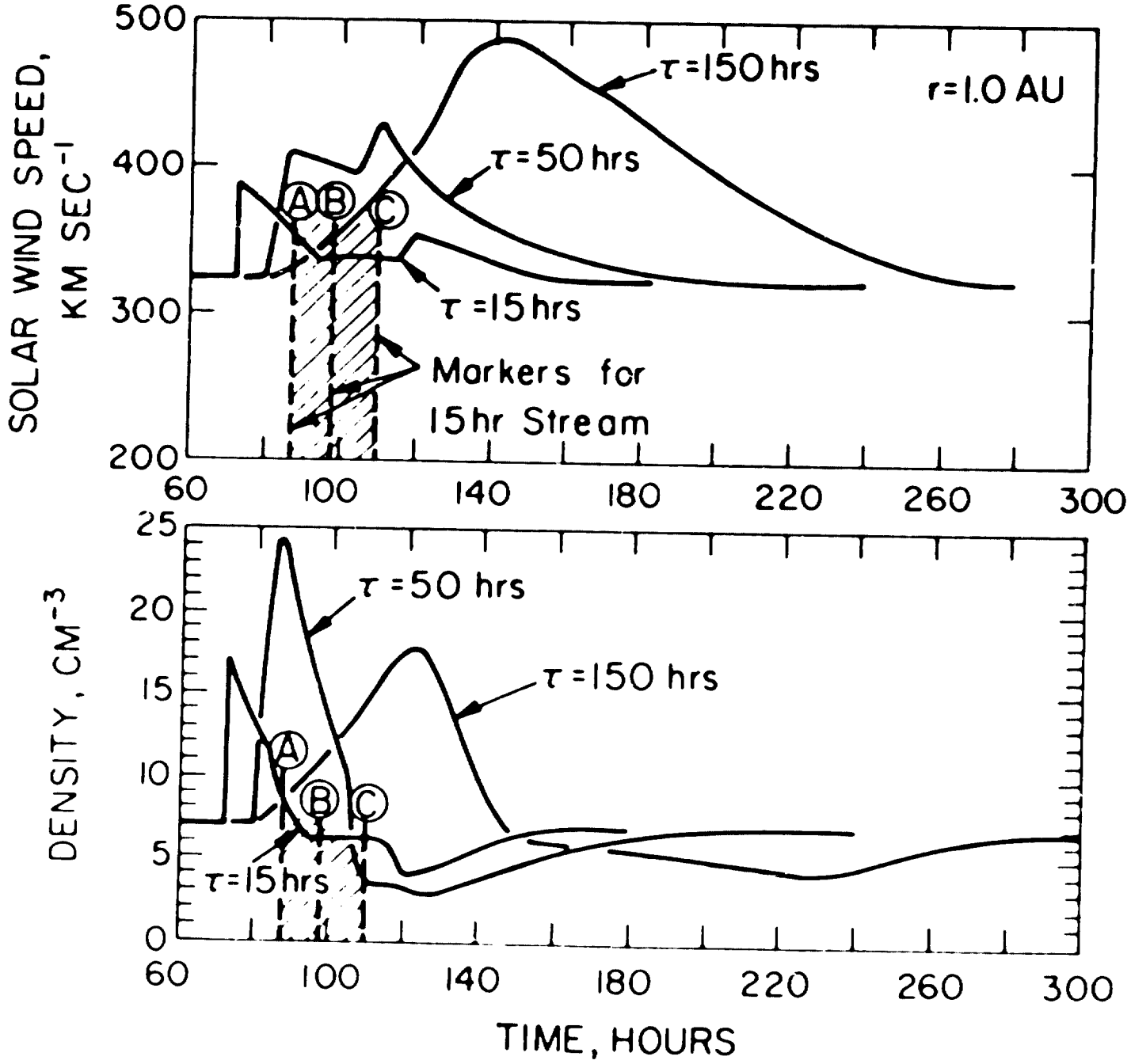
SOLAR WIND SPEED, KM SEC^{-1}
500
400
300
200
τ=150 hrs
r=1.0 AU
τ=50 hrs
A
B
C
τ =15 hrs
Markers for
15 hr Stream
60
100
140
180
220
260
300
DENSITY, CM^{-3}
25
20
15
10
5
0
τ =50 hrs
τ =150 hrs
A
B
C
τ=15 hrs
60
100
140
180
220
260
300
TIME, HOURS

Figure 15

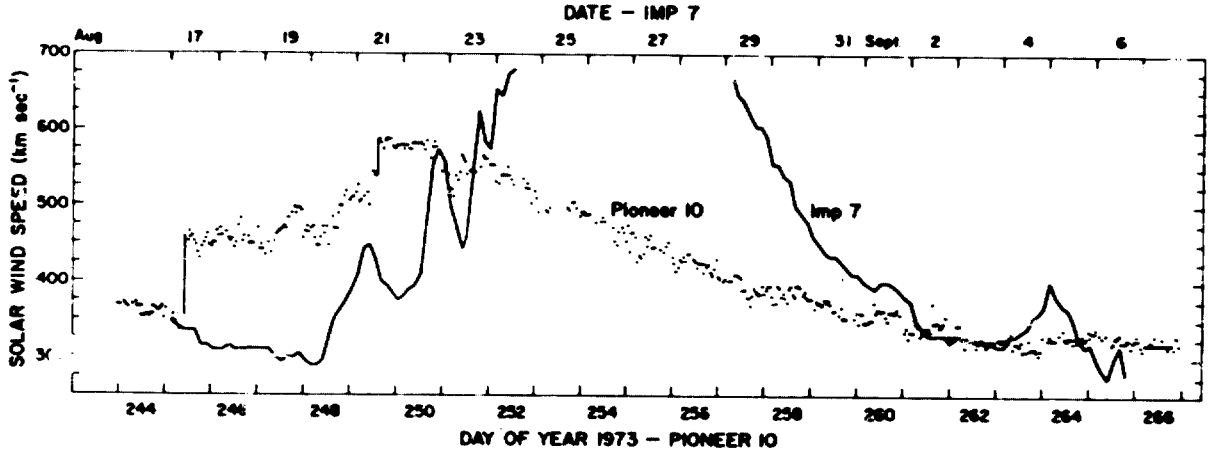
DATE – IMP 7
Aug
17
19
21
23
25
27
29
31
Sept
2
4
6
700
600
500
400
SOLAR WIND SPEED (km sec⁻¹)
Pioneer 10
Imp 7
244
246
248
250
252
254
256
258
260
262
264
266
DAY OF YEAR 1973 – PIONEER 10

Figure 16

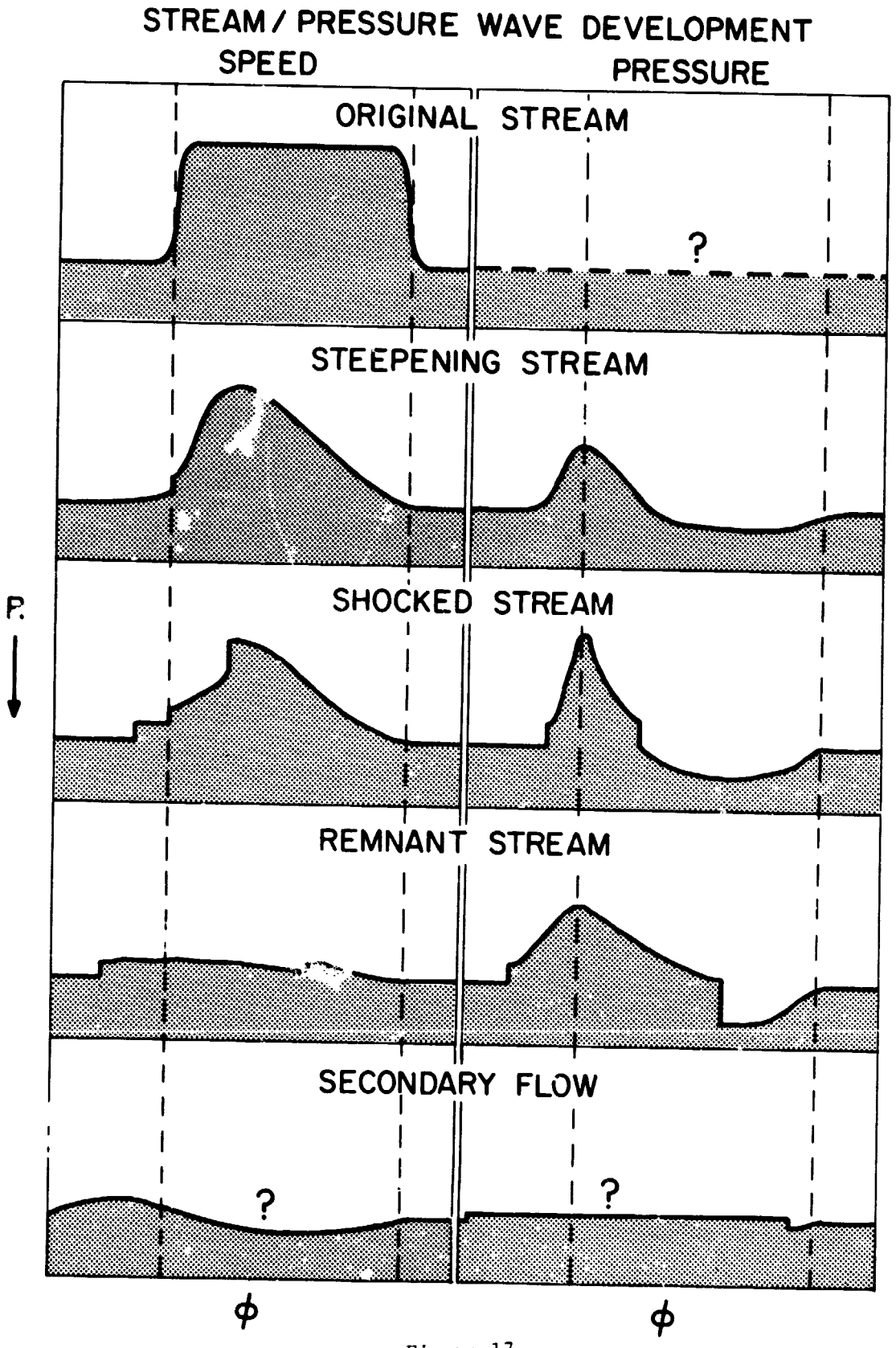

Figure 17

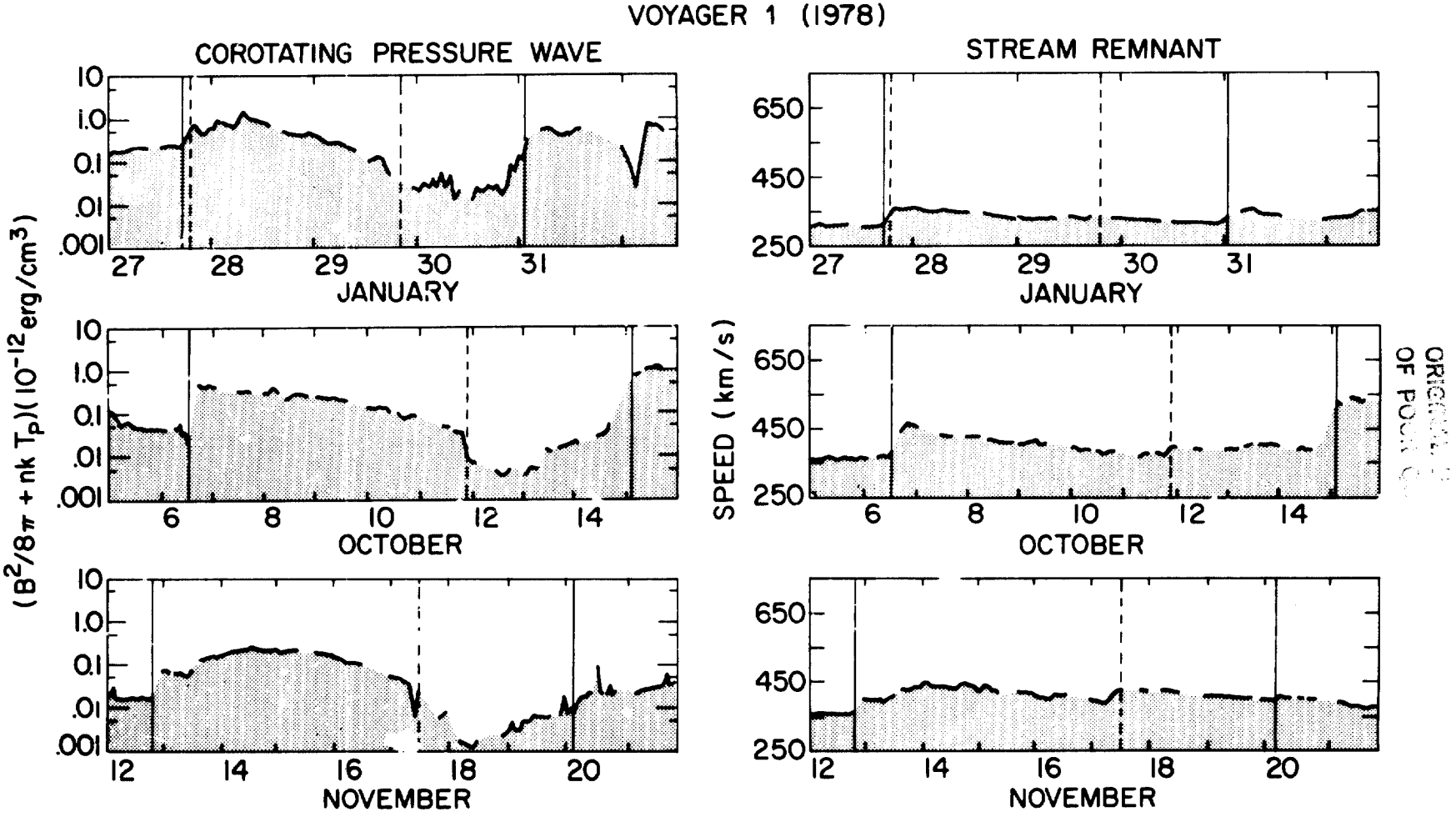
VOYAGER 1 (1978)
COROTATING PRESSURE WAVE
STREAM REMNANT
$(B^2/8\pi + nk\,T_p)(10^{-12}erg/cm^3)$
SPEED (km/s)
10
1.0
0.1
.01
.001
650
450
250
27
28
29
30
31
JANUARY
6
8
10
12
14
OCTOBER
12
14
16
18
20
NOVEMBER

Figure 18

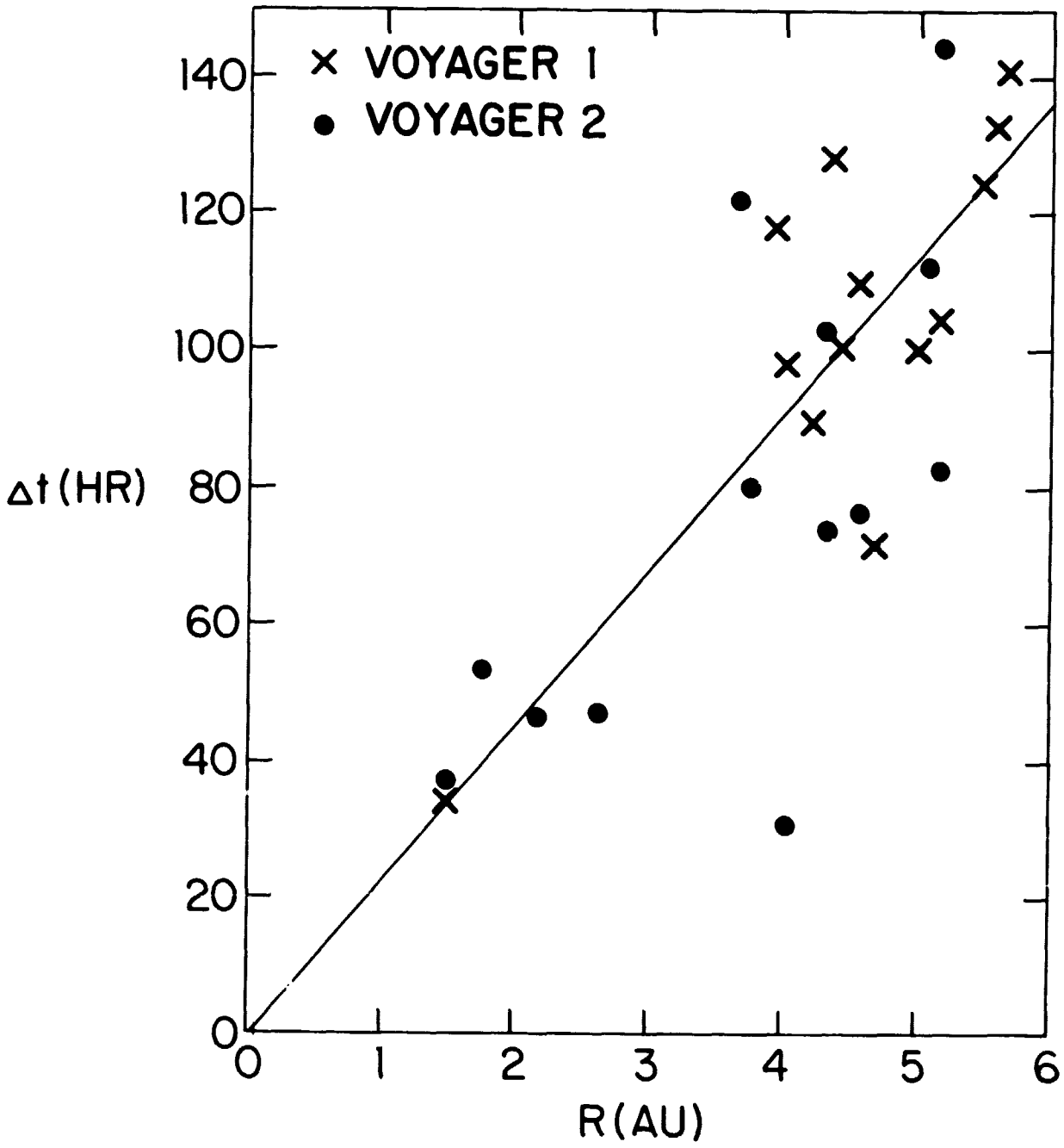

Figure 19

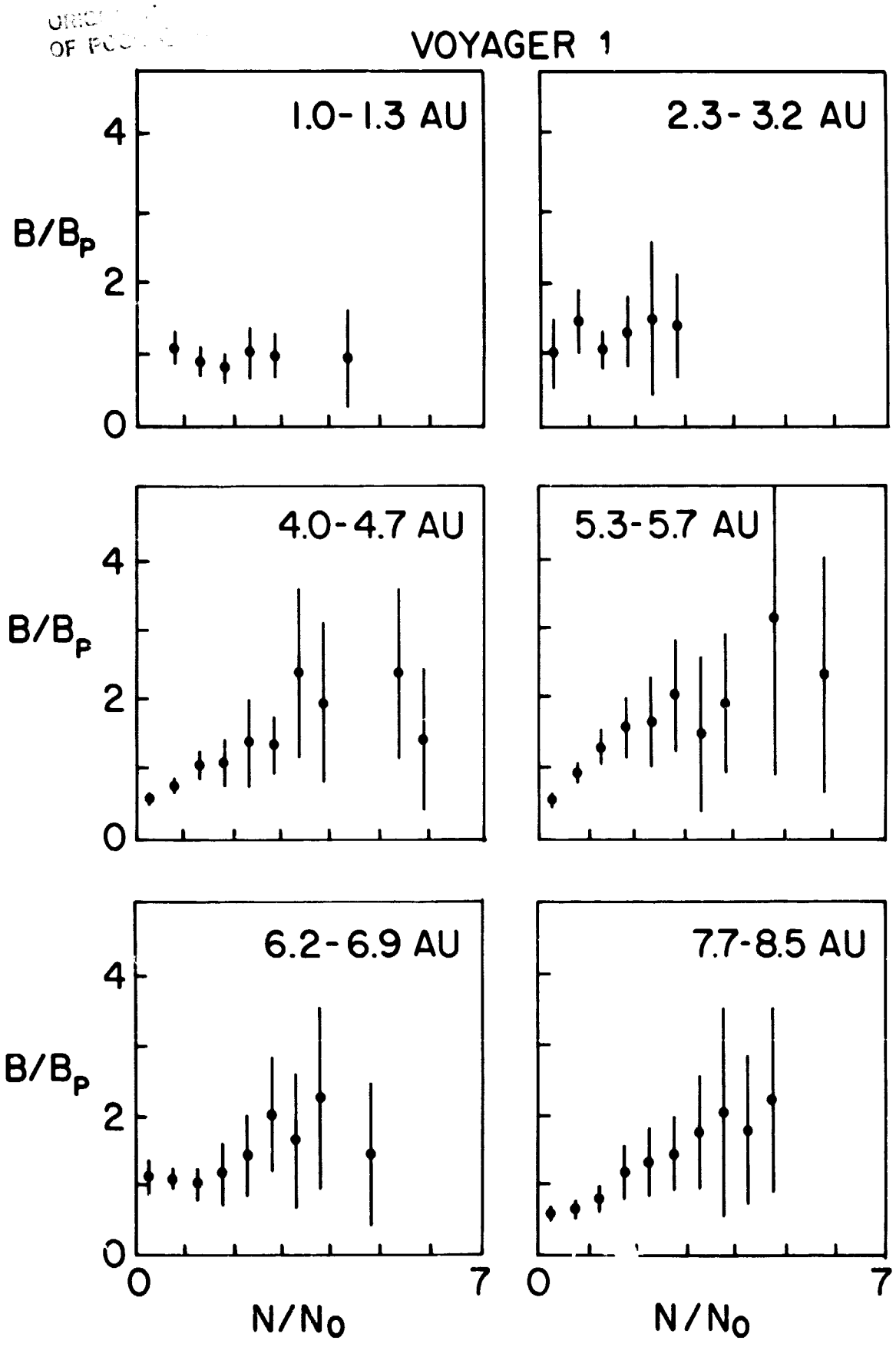

Figure 20

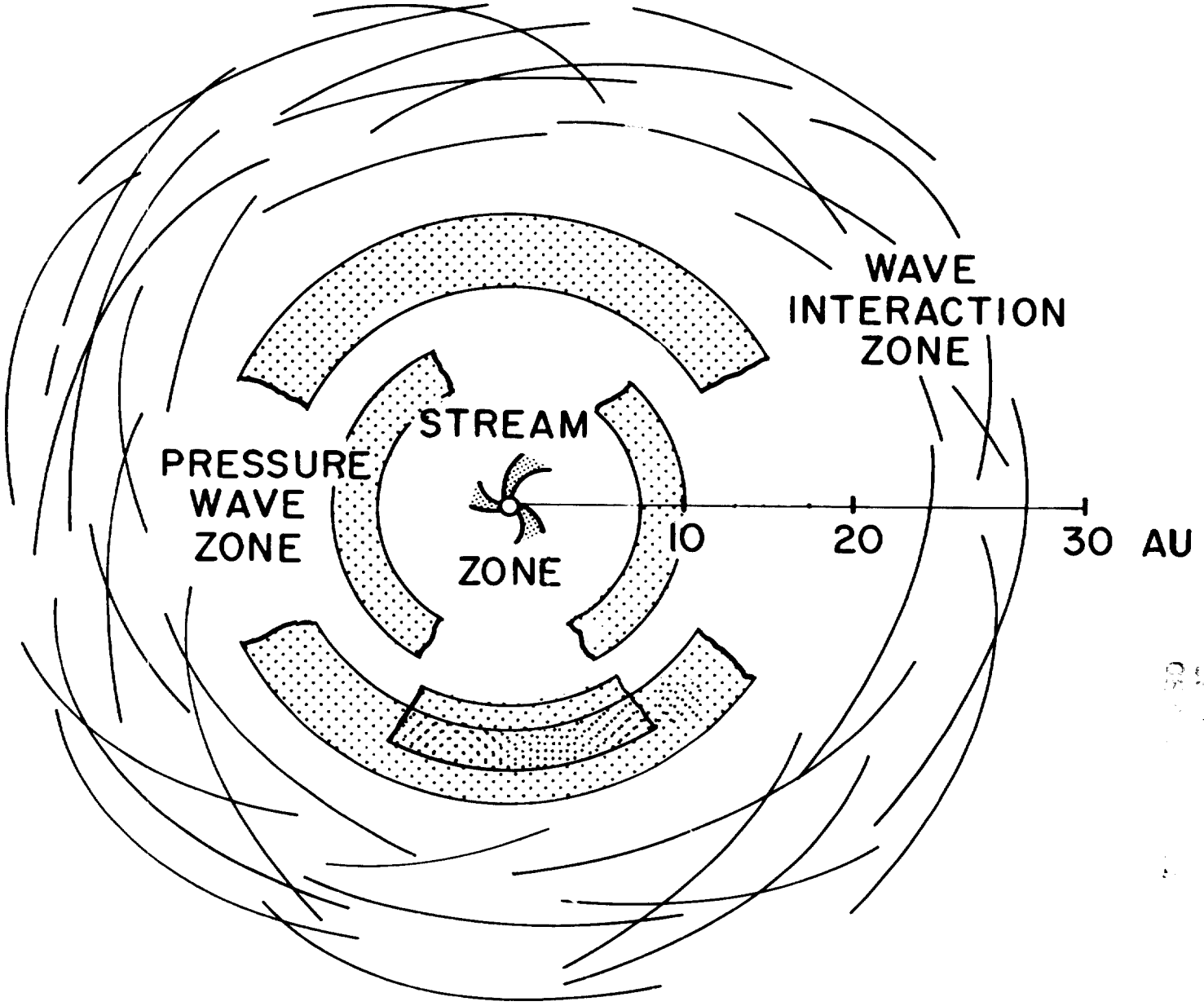
WAVE
INTERACTION
ZONE
STREAM
PRESSURE
WAVE
ZONE
ZONE
10
20
30 AU

Figure 21

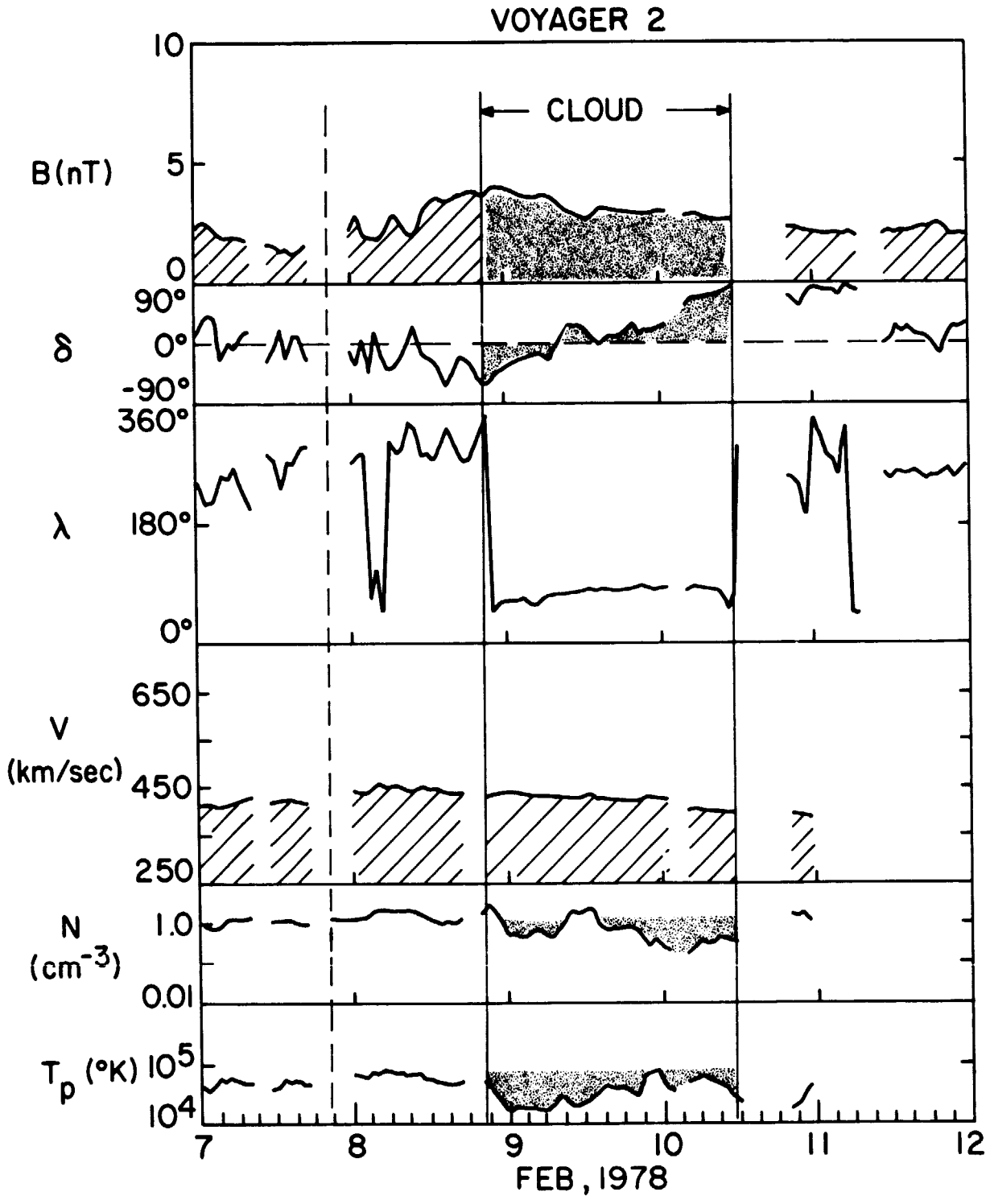

Figure 22

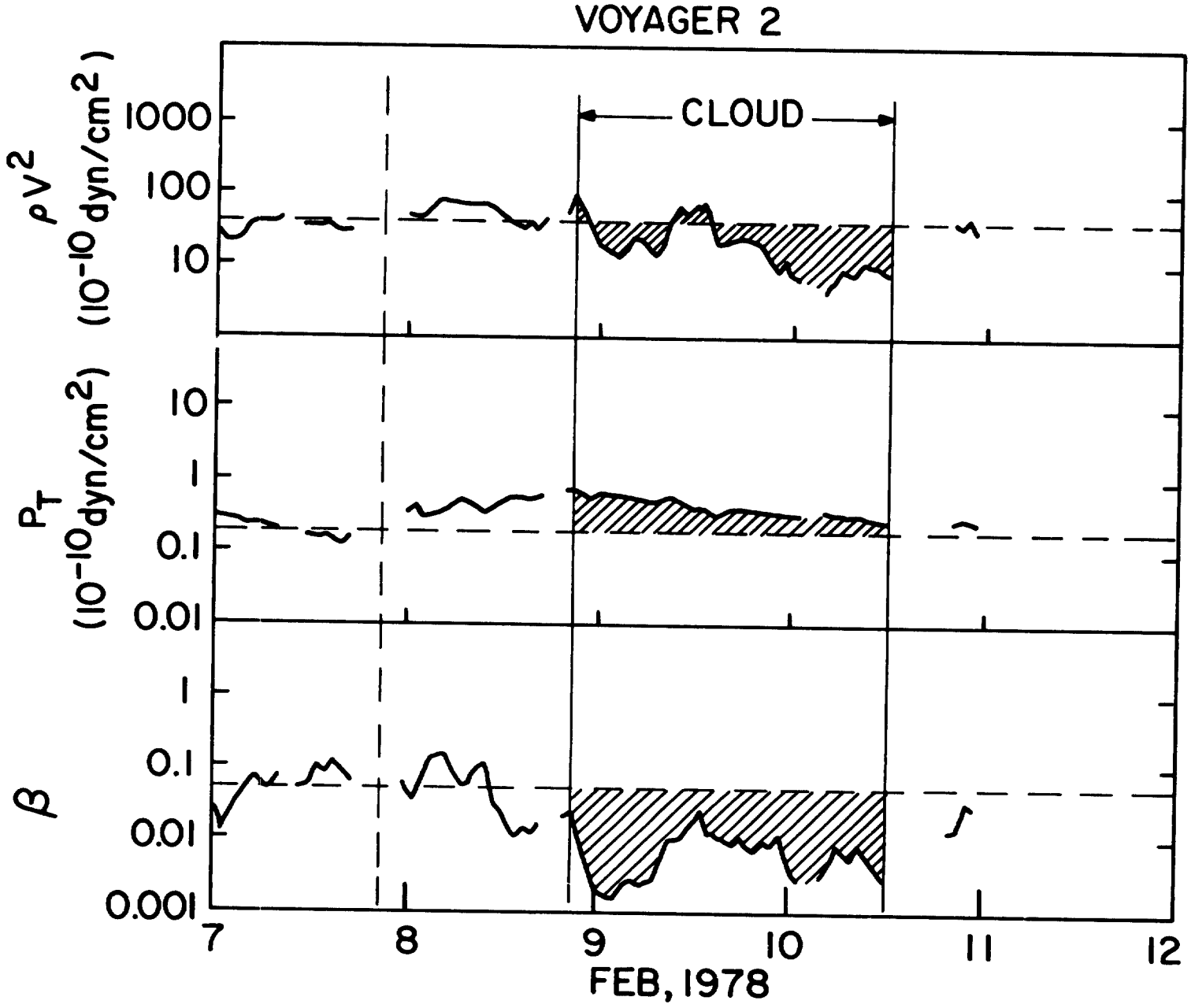
VOYAGER 2
CLOUD
ρV^2 (10^{-10} dyn/cm^2)
1000
100
10
P_T (10^{-10} dyn/cm^2)
10
1
0.1
0.01
β
1
0.1
0.01
0.001
7
8
9
10
11
12
FEB, 1978

Figure 23

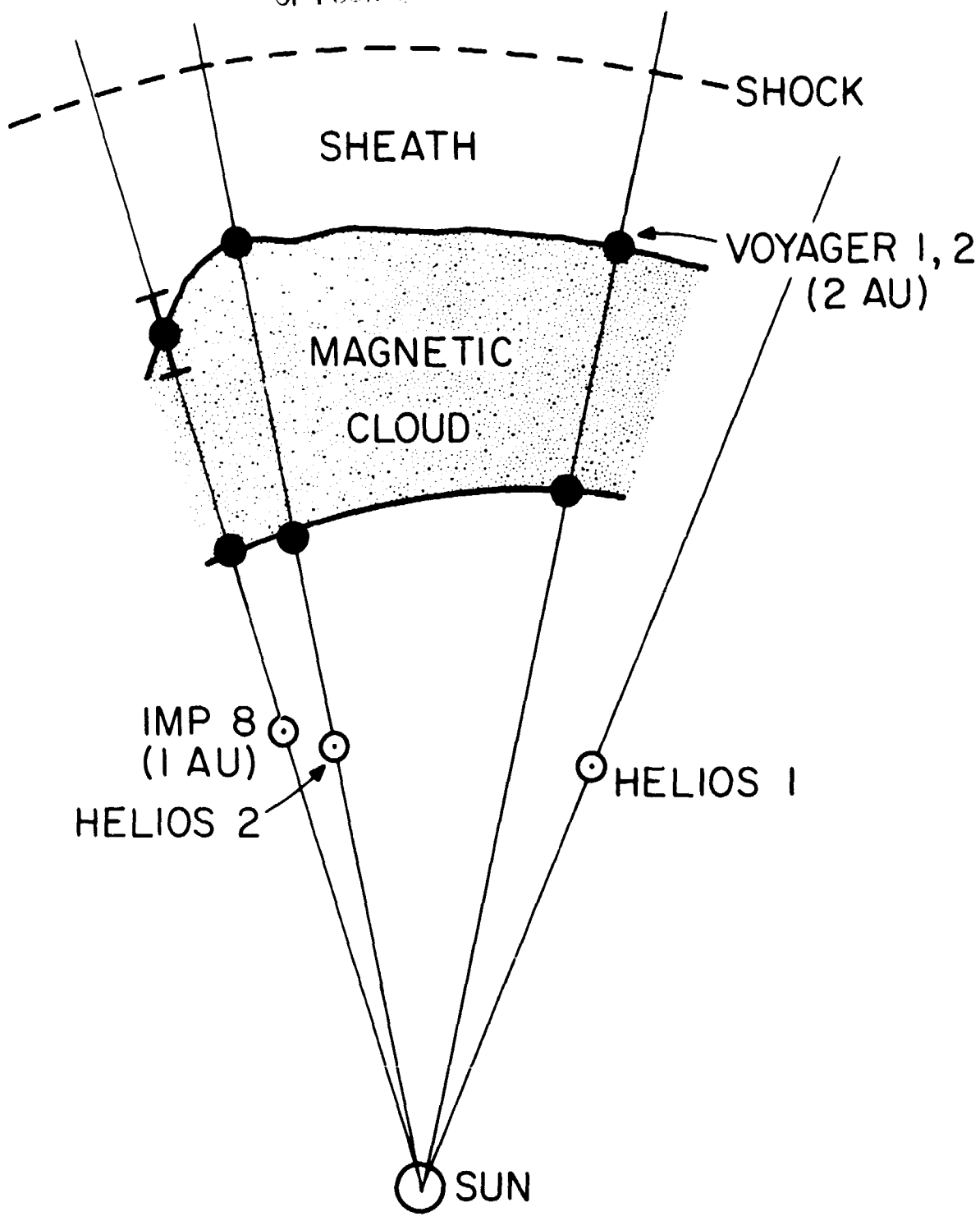

JAN 6, HR 22, 1978
EQUATORIAL PLANE

Figure 24

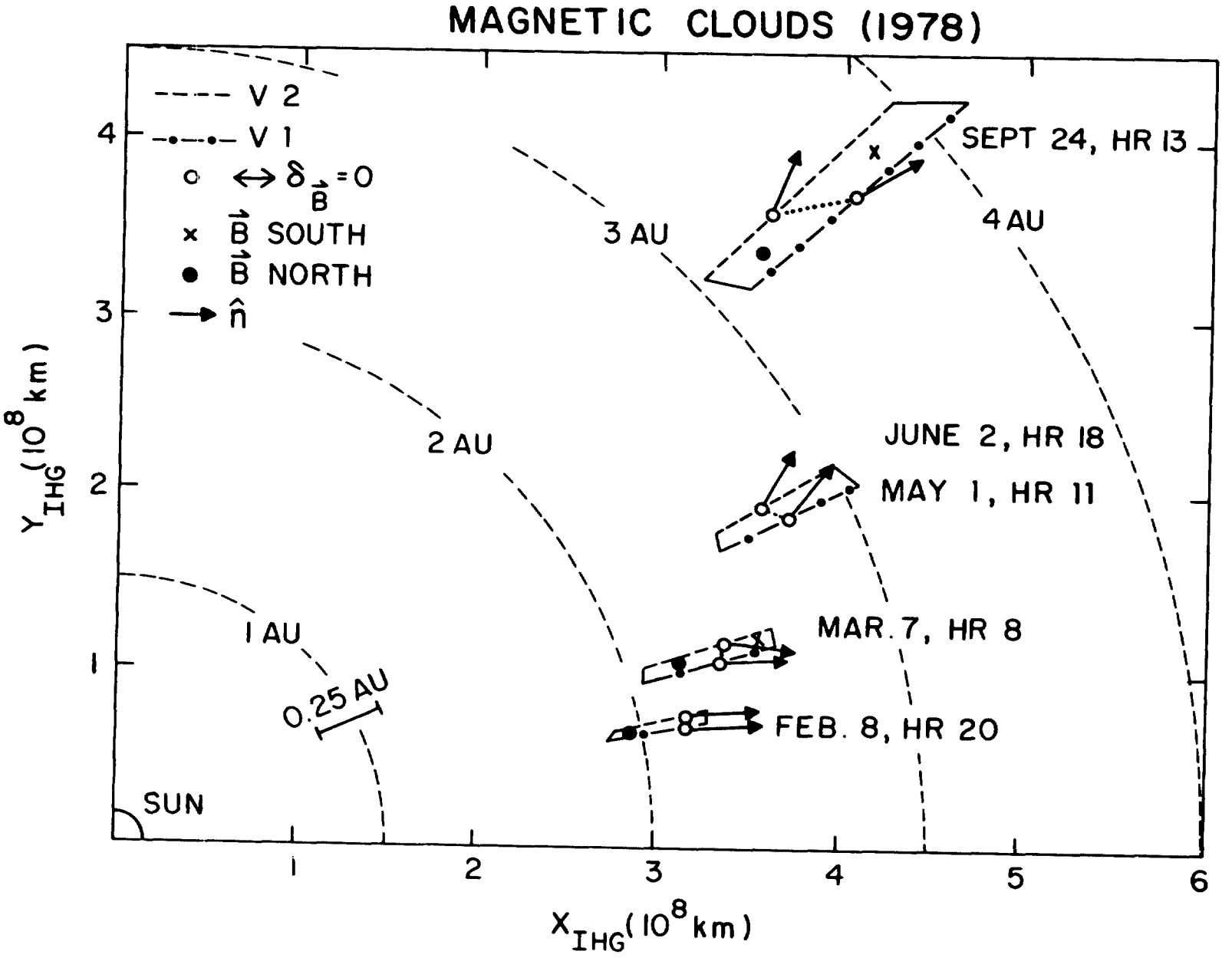
MAGNETIC CLOUDS (1978)
V 2
V 1
$\leftrightarrow \delta_{\vec{B}} = 0$
$\vec{B}$ SOUTH
$\vec{B}$ NORTH
$\hat{n}$
SEPT 24, HR 13
3 AU
4 AU
JUNE 2, HR 18
MAY 1, HR 11
2 AU
MAR. 7, HR 8
FEB. 8, HR 20
1 AU
0.25 AU
SUN
$Y_{IHG}(10^8 km)$
$X_{IHG}(10^8 km)$
1
2
3
4
5
6

Figure 25

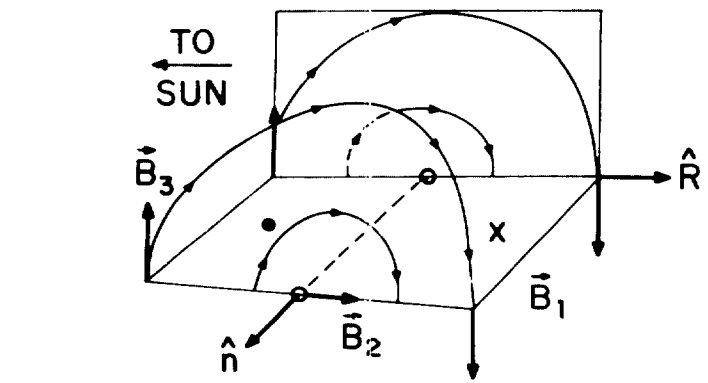

a)

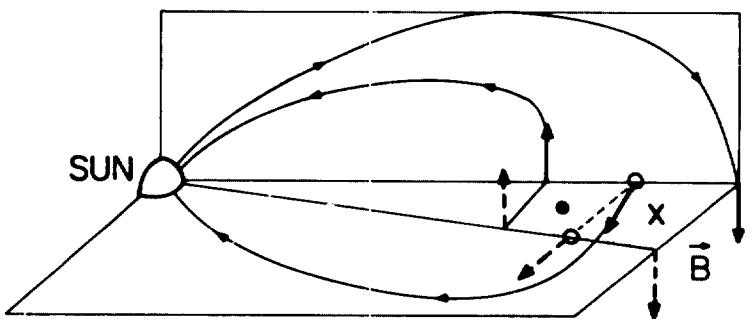

b)

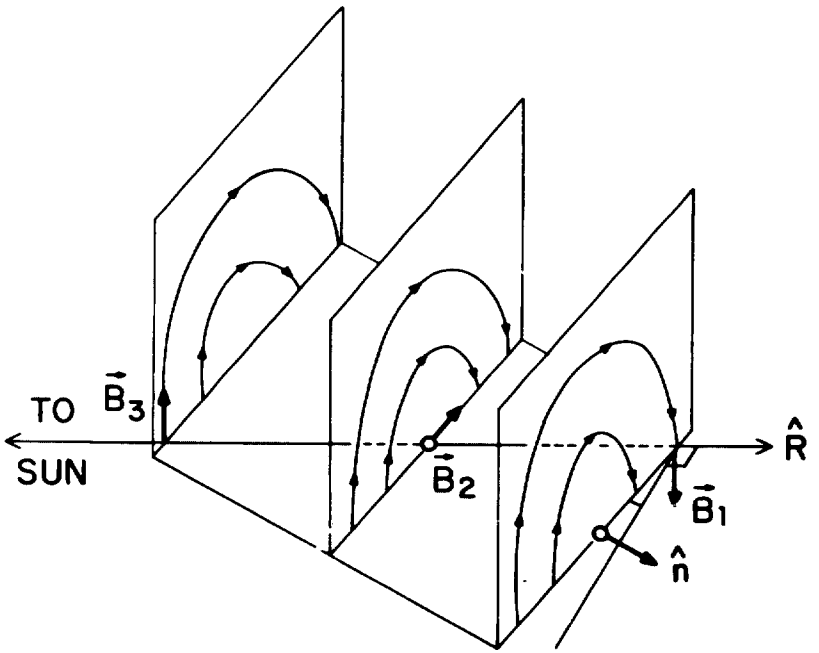

c)

Figure 26

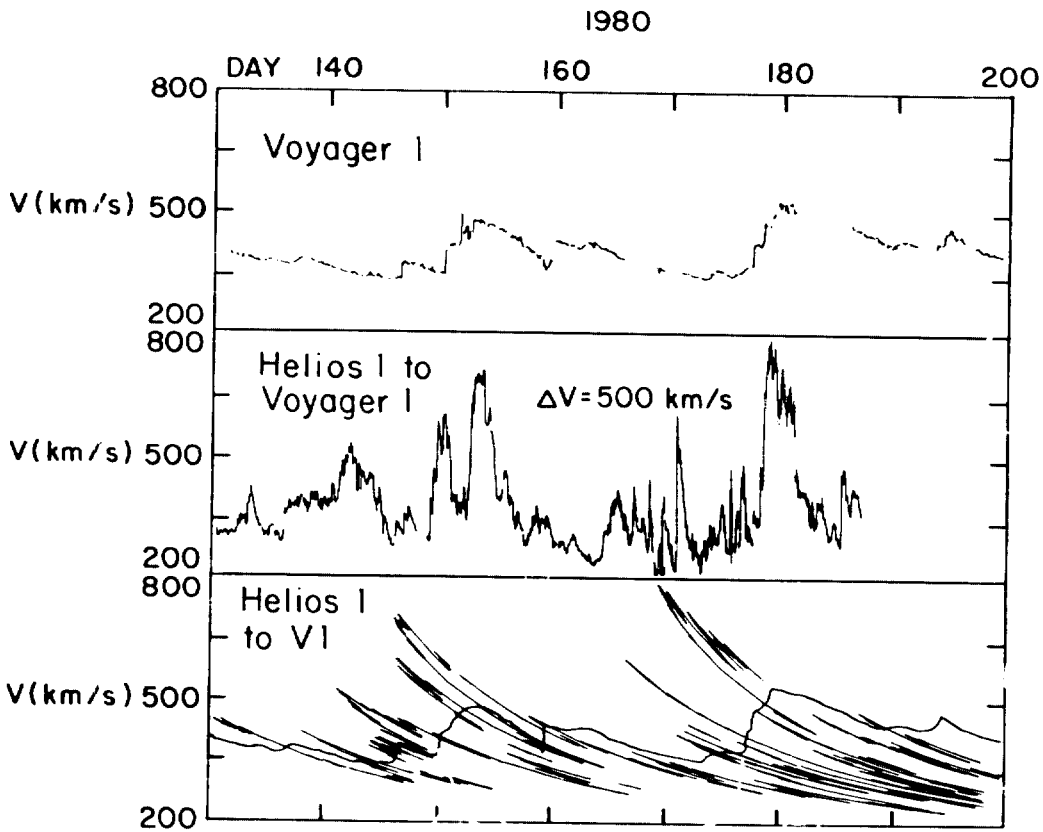

Figure 27

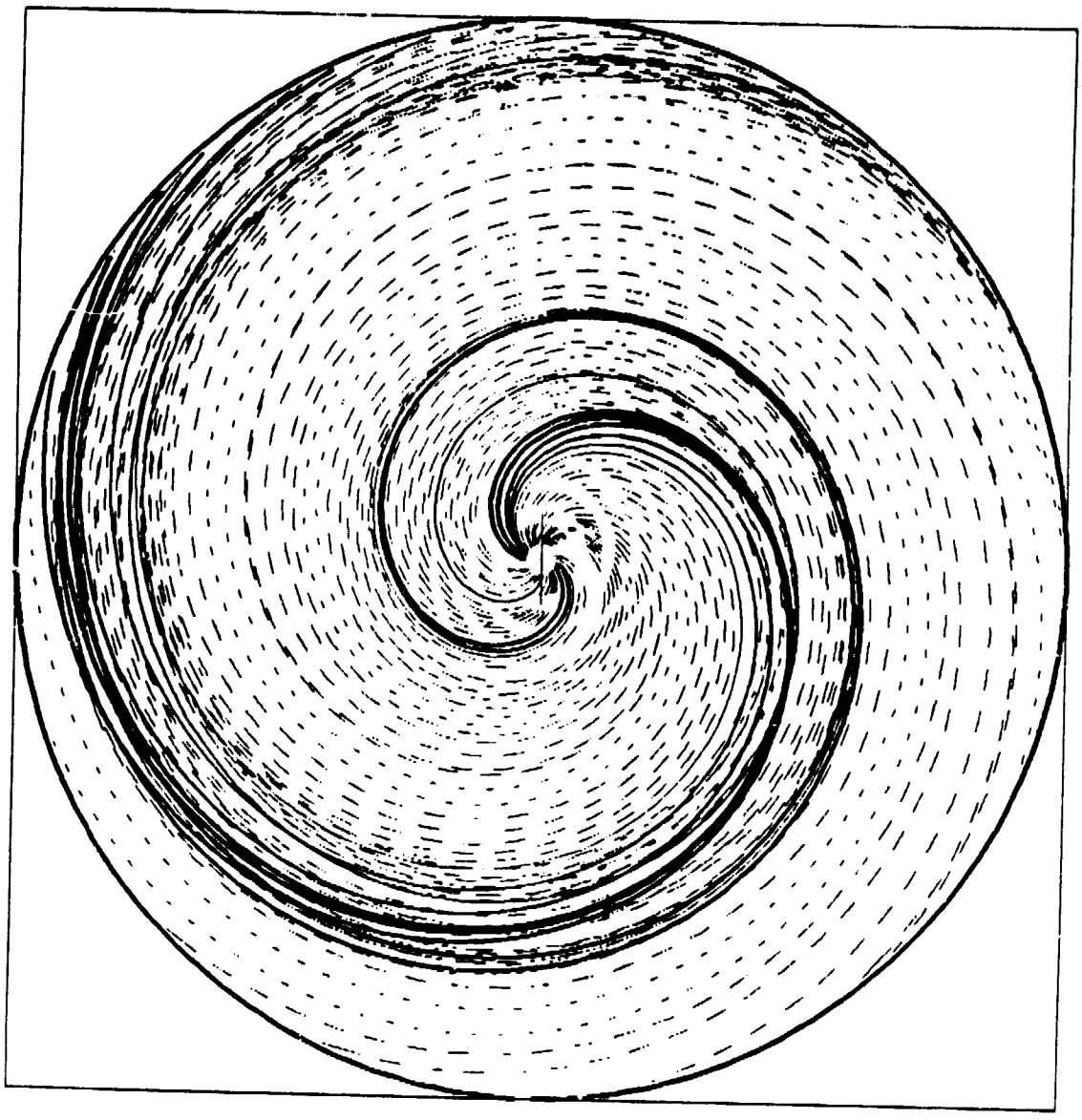

Figure 28

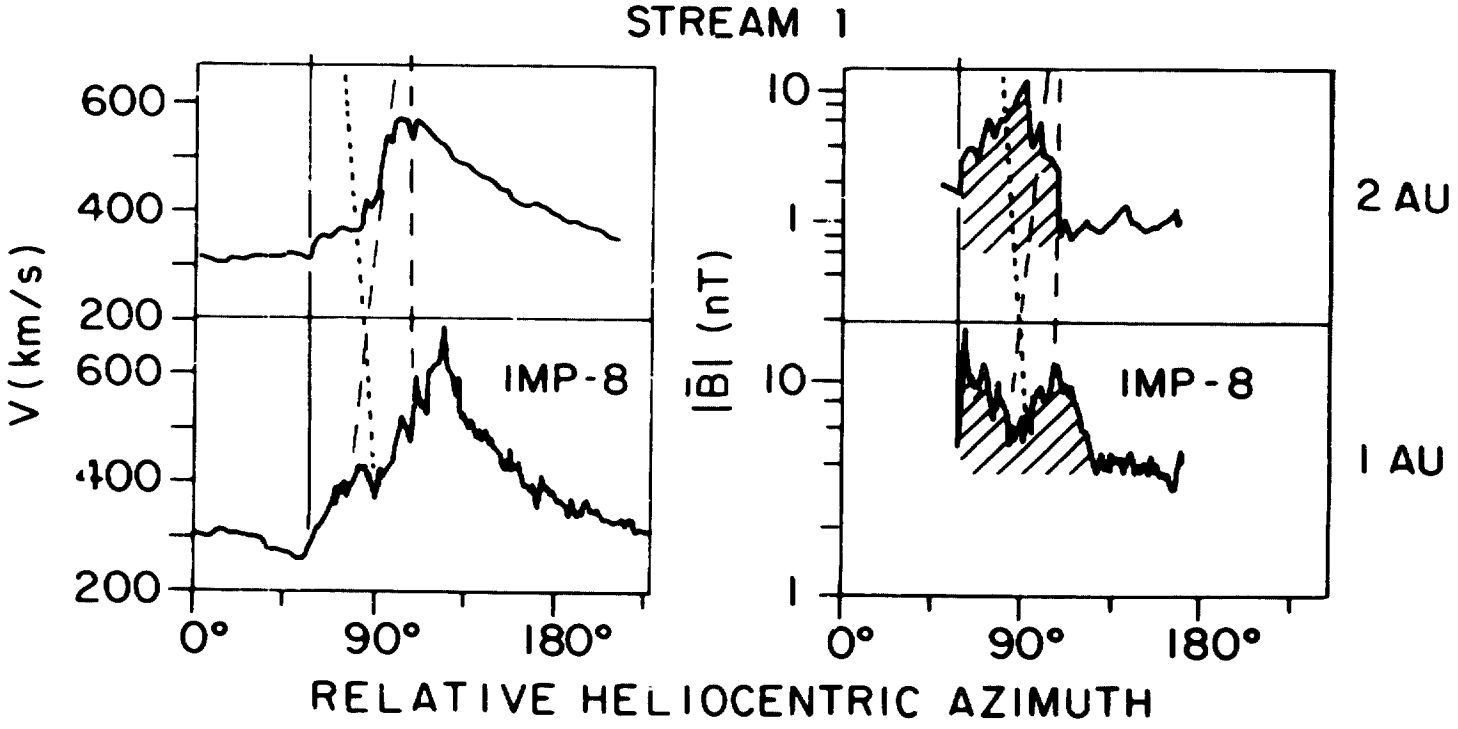
STREAM 1
600
400
200
V (km/s)
600
400
200
IMP-8
0°
90°
180°
10
1
|B| (nT)
10
1
IMP-8
2 AU
1 AU
0°
90°
180°
RELATIVE HELIOCENTRIC AZIMUTH

Figure 29

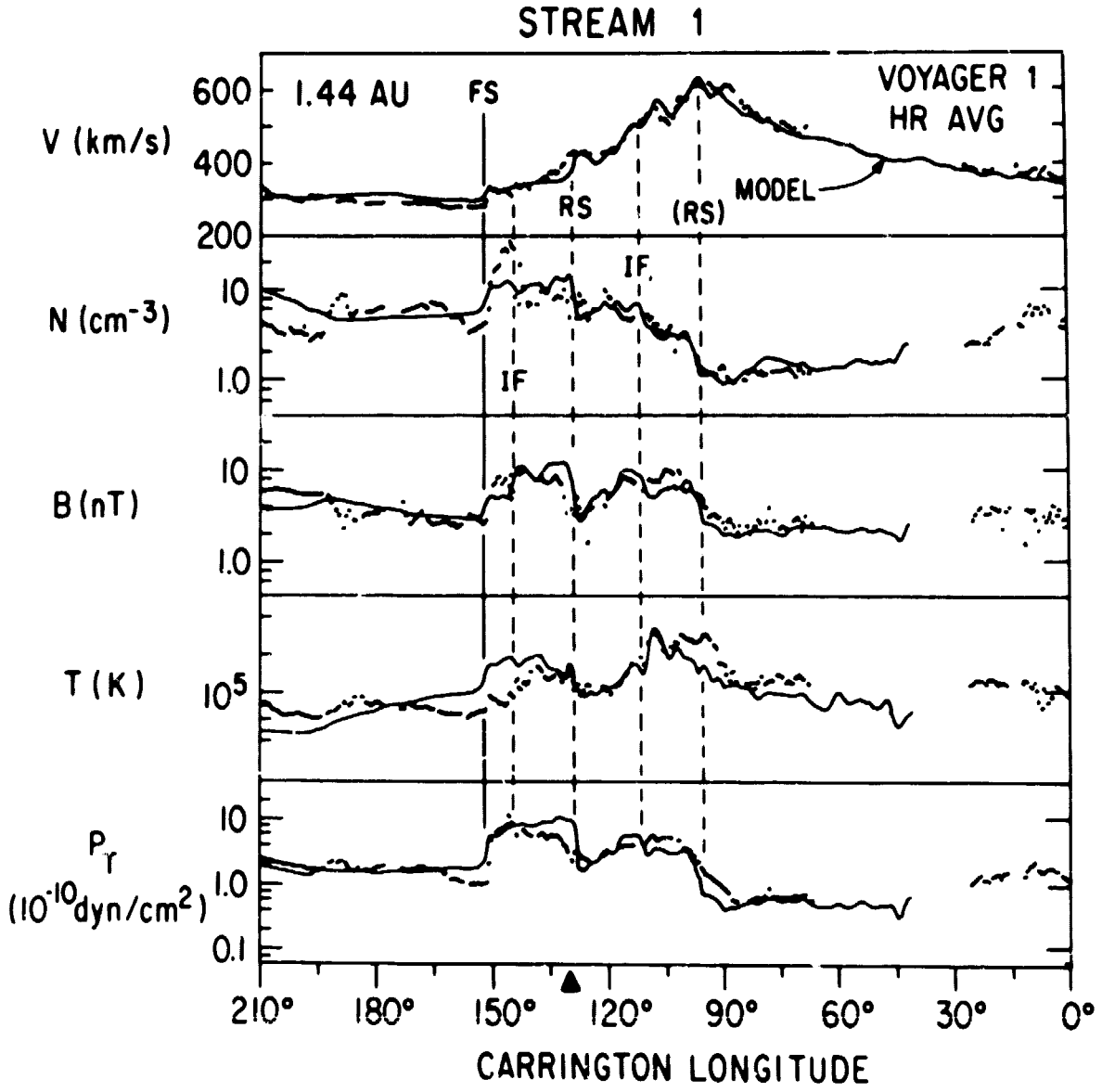

Figure 30

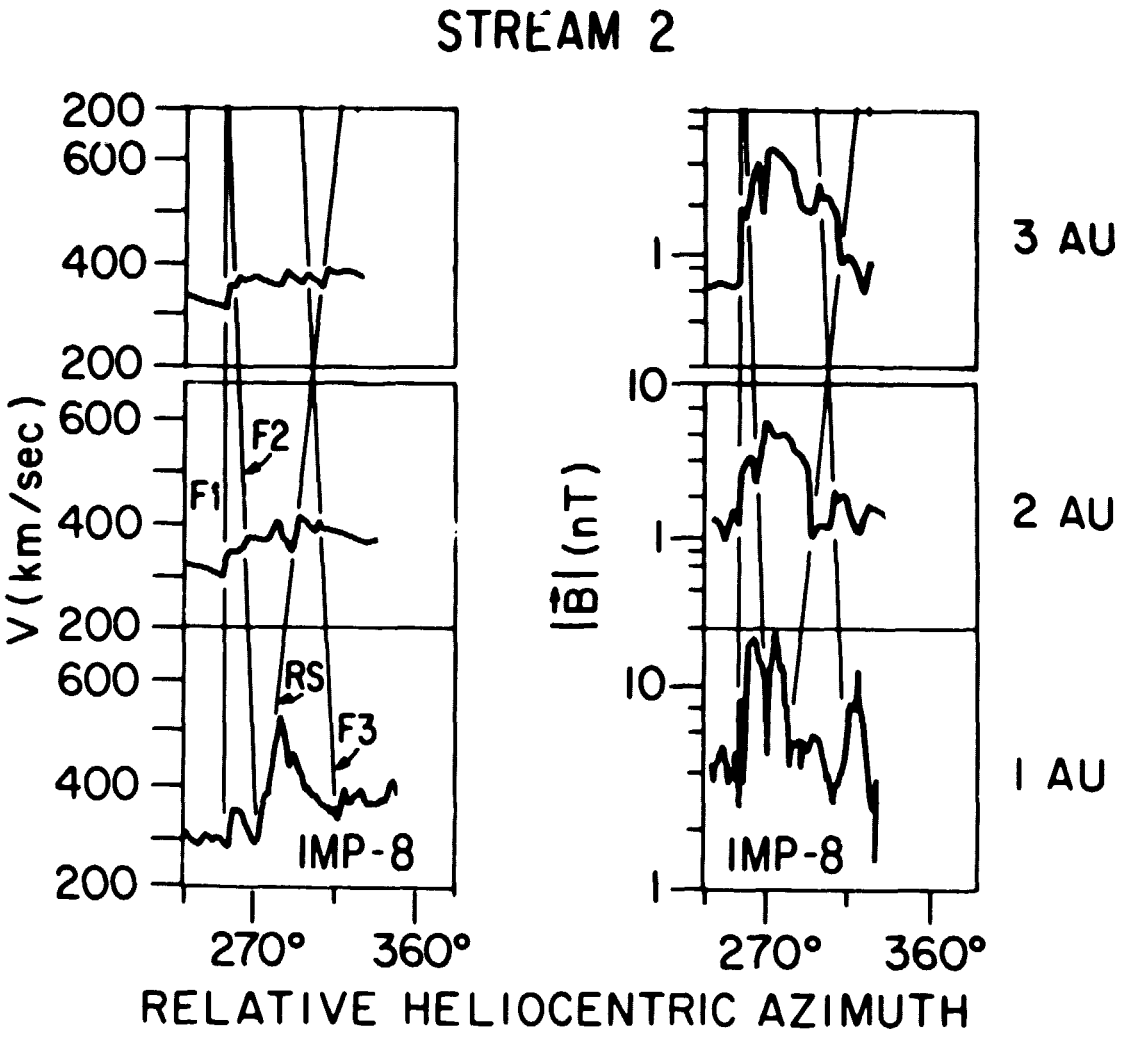

Figure 31

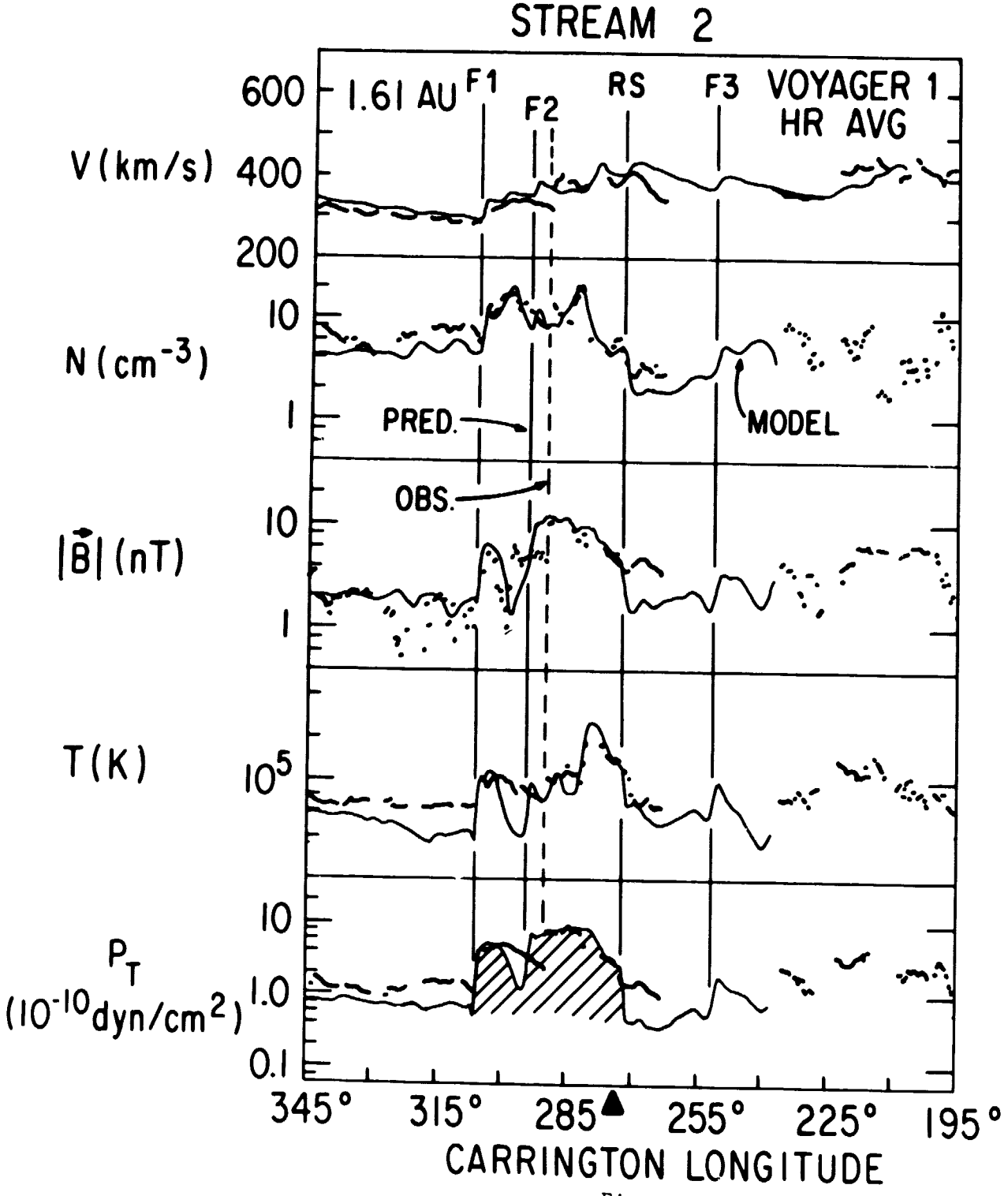

Figure 32

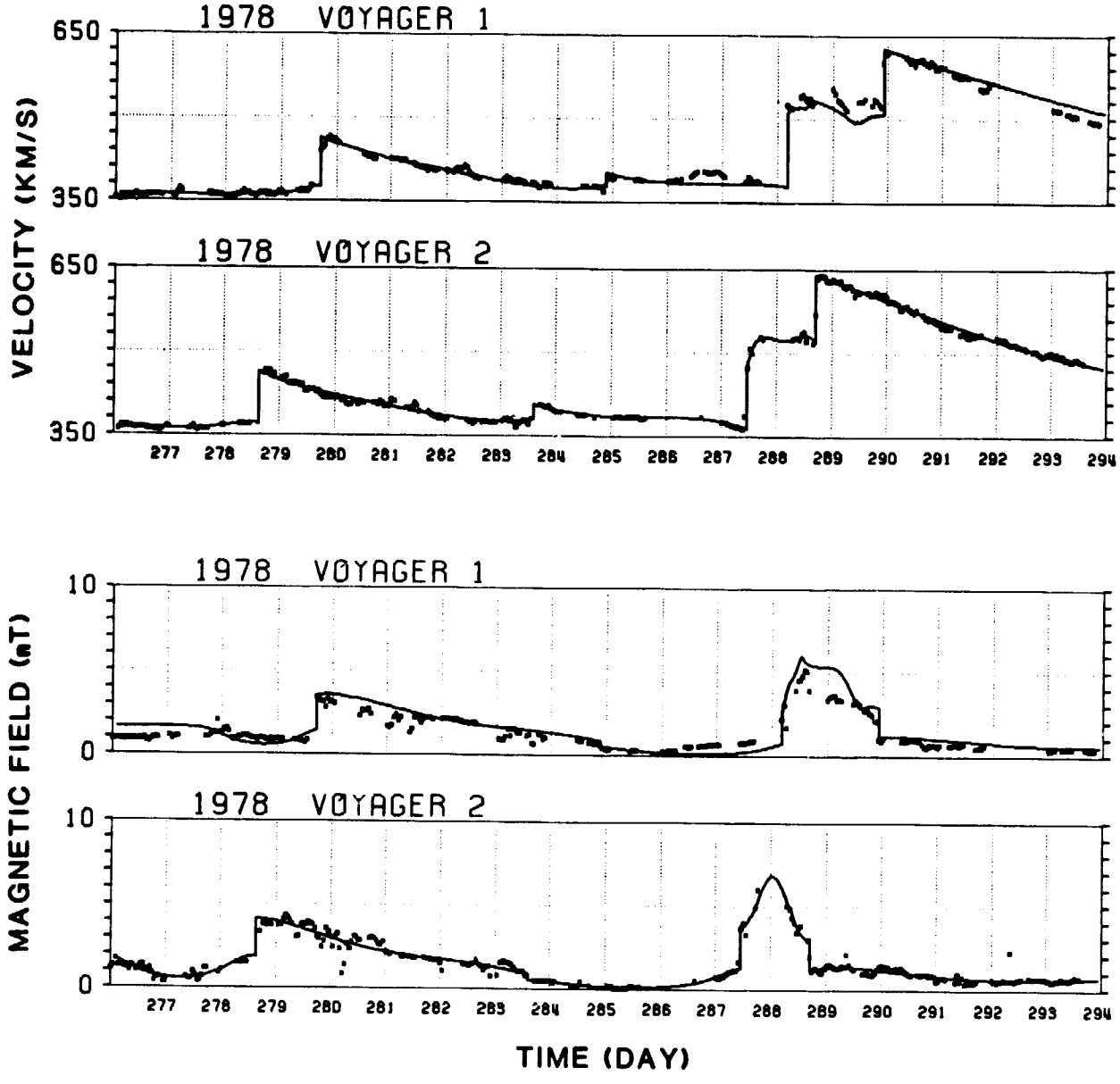

Figure 33

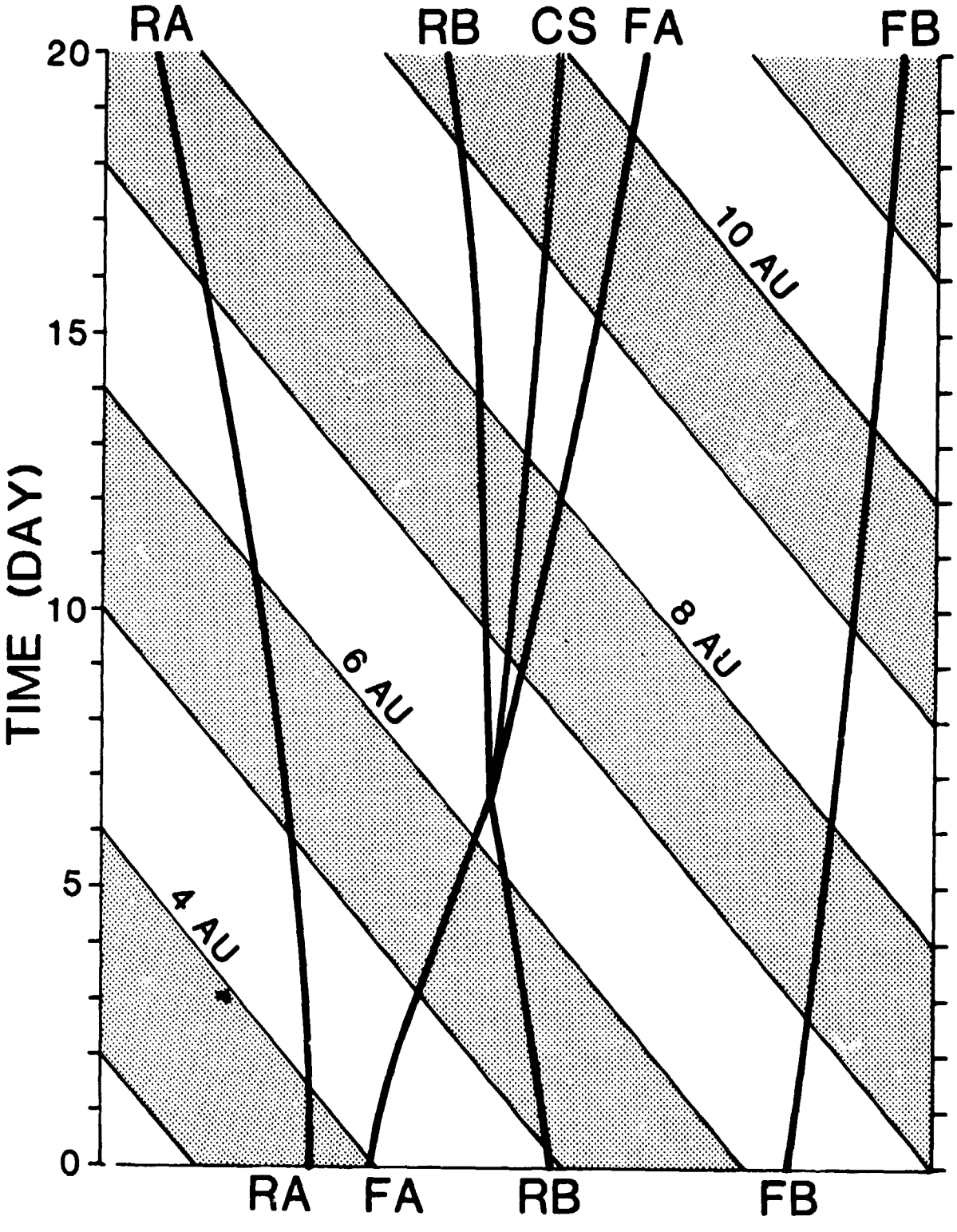

Figure 34

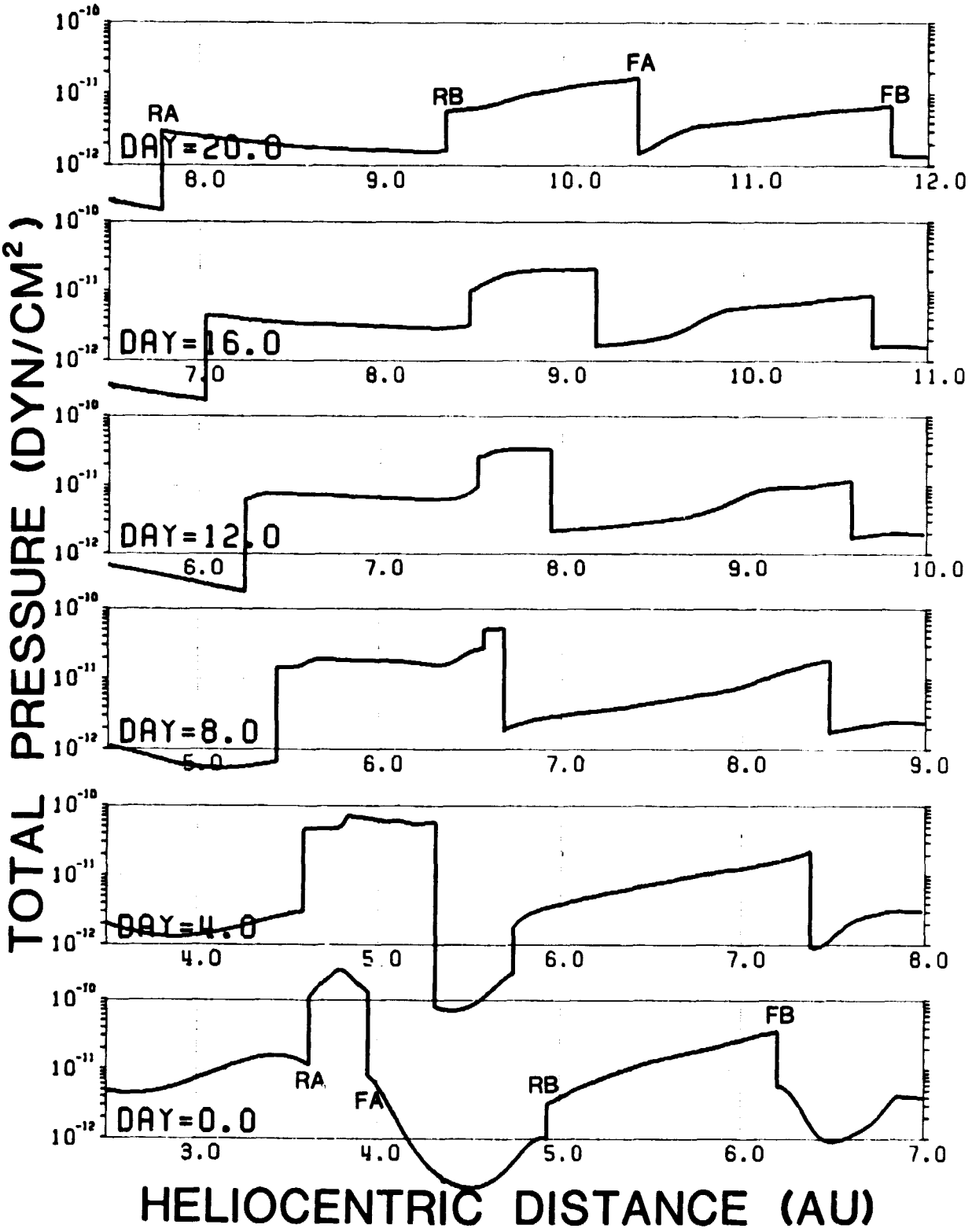

Figure 35

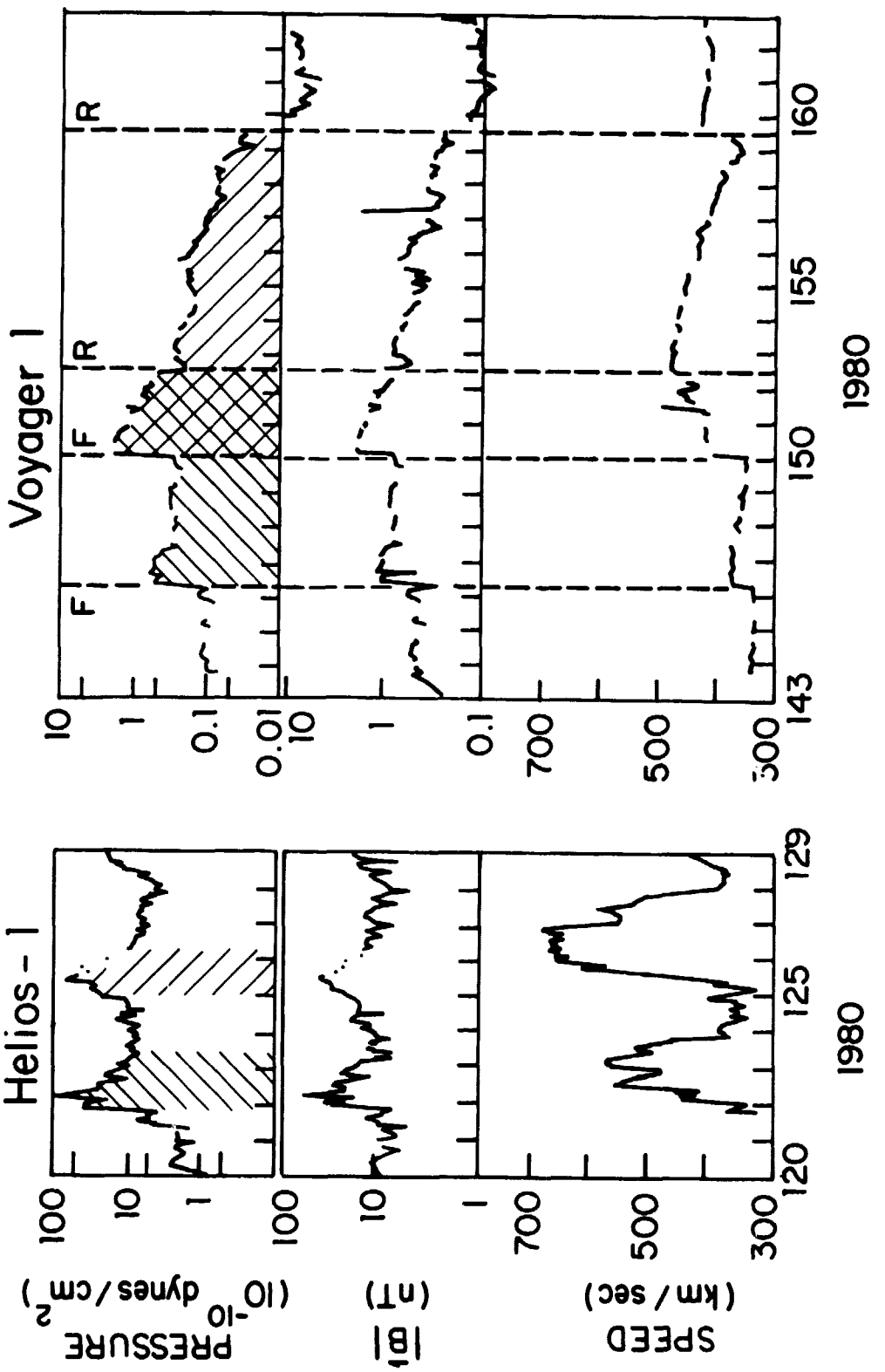

Figure 36

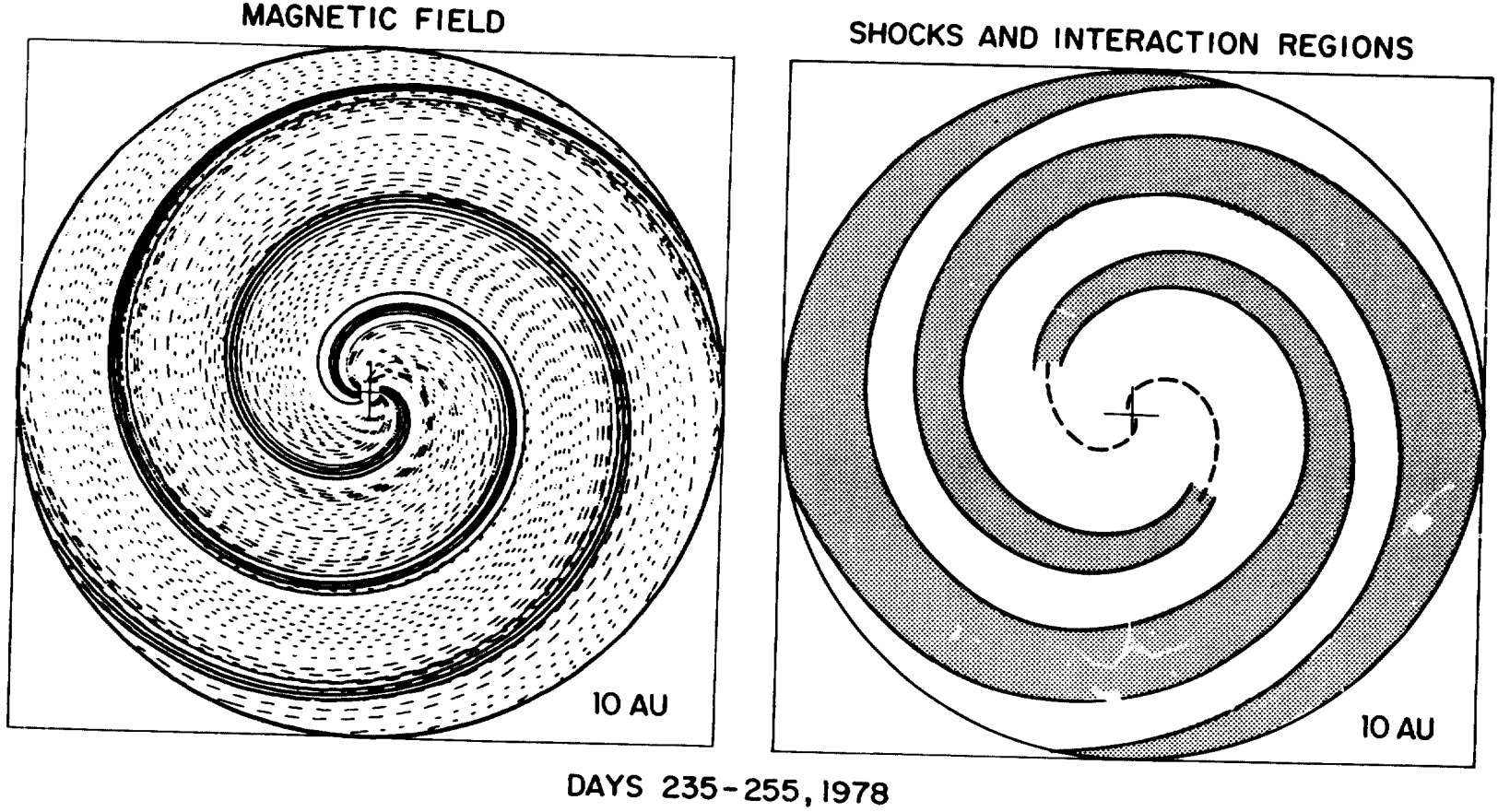

Figure 37

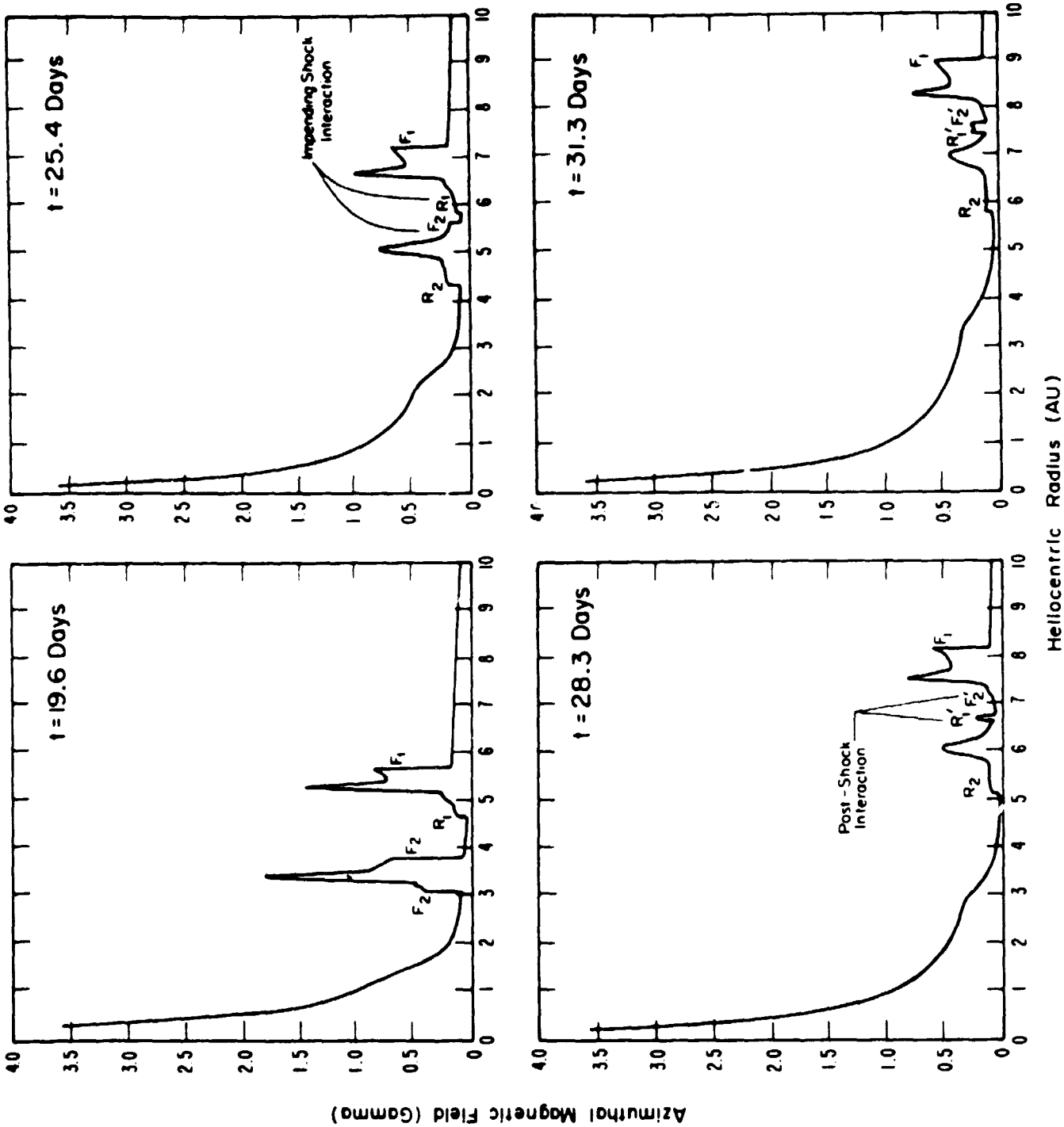

Figure 38

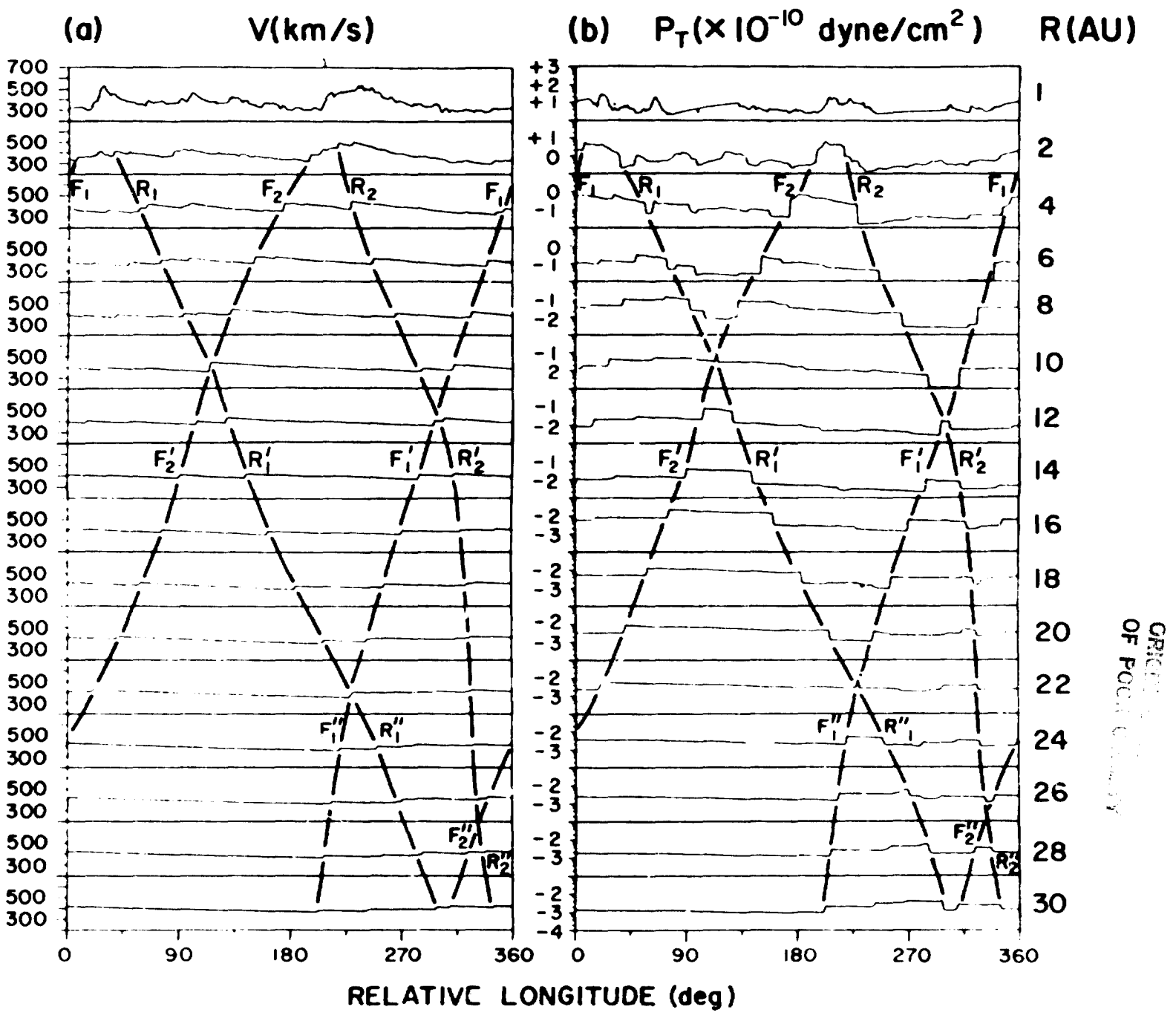
(a) V(km/s)
(b) P_T(×10^{-10} dyne/cm^2)
R(AU)
RELATIVE LONGITUDE (deg)
0
90
180
270
360
F_1 R_1 F_2 R_2 F_1
F_2' R_1' F_1' R_2'
F_1'' R_1''
F_2'' R_2''

Figure 39

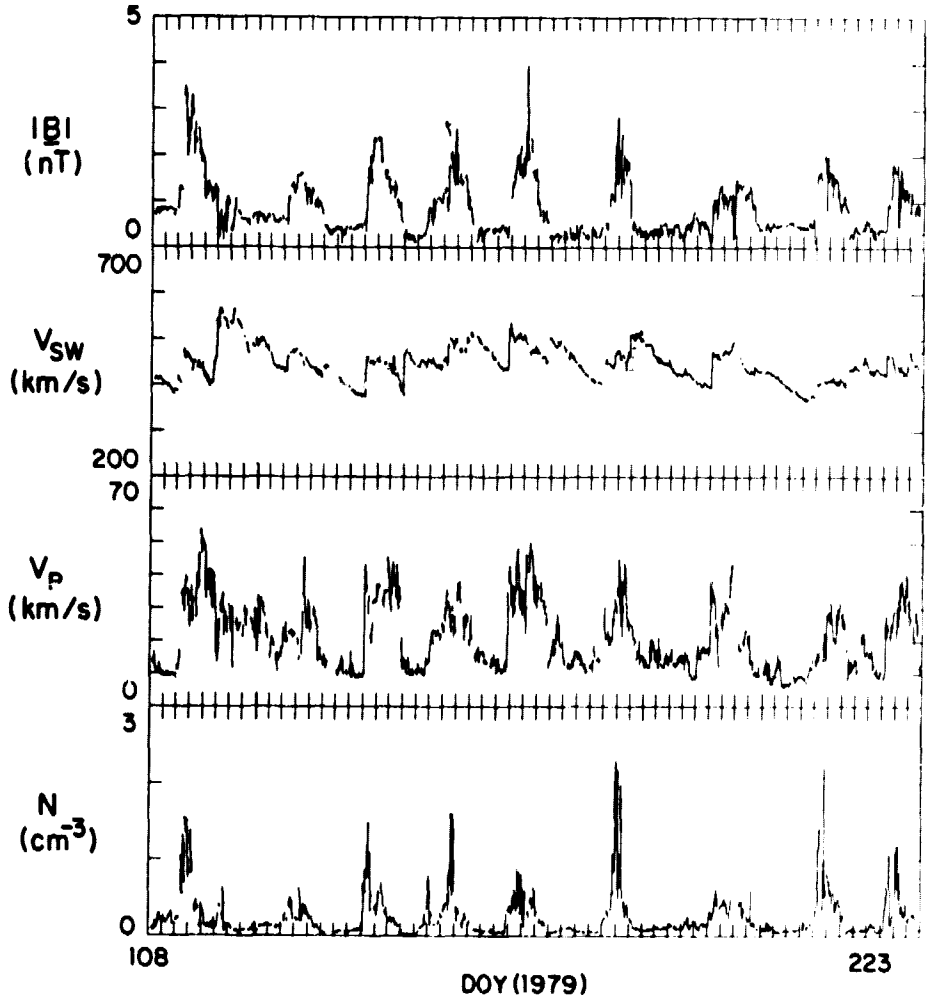

Figure 40

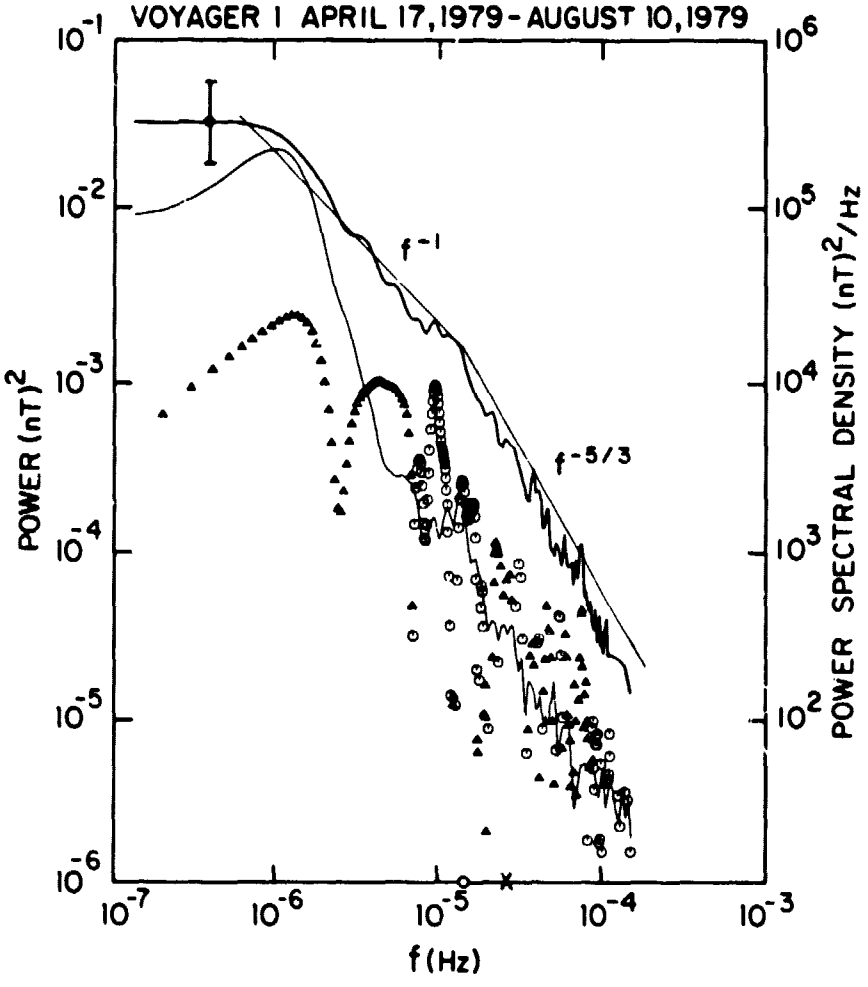

Figure 41

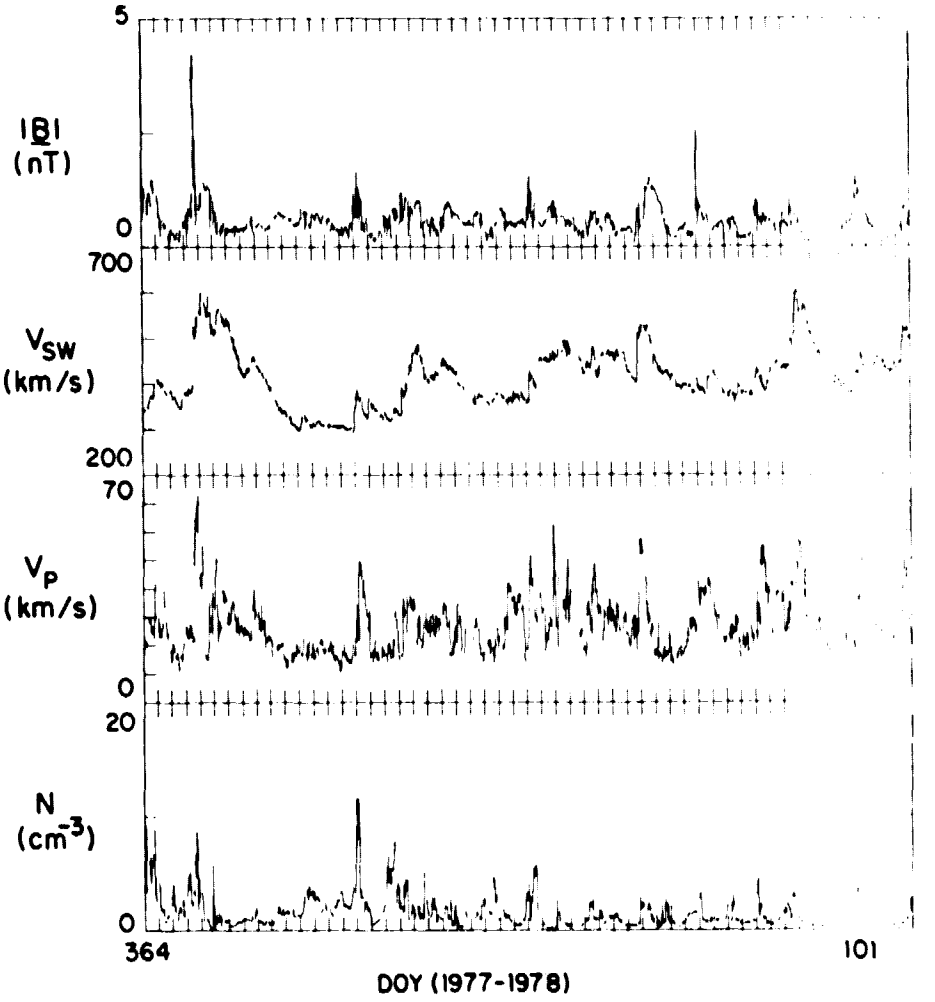

Figure 42

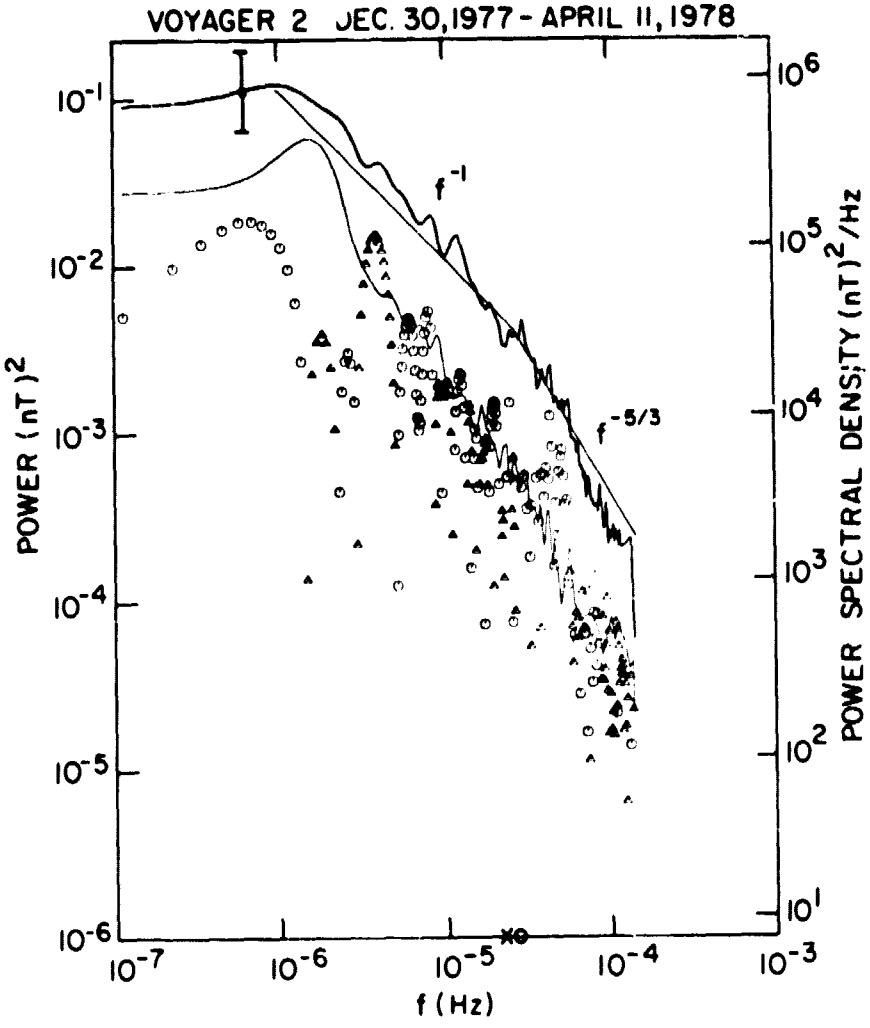

Figure 43

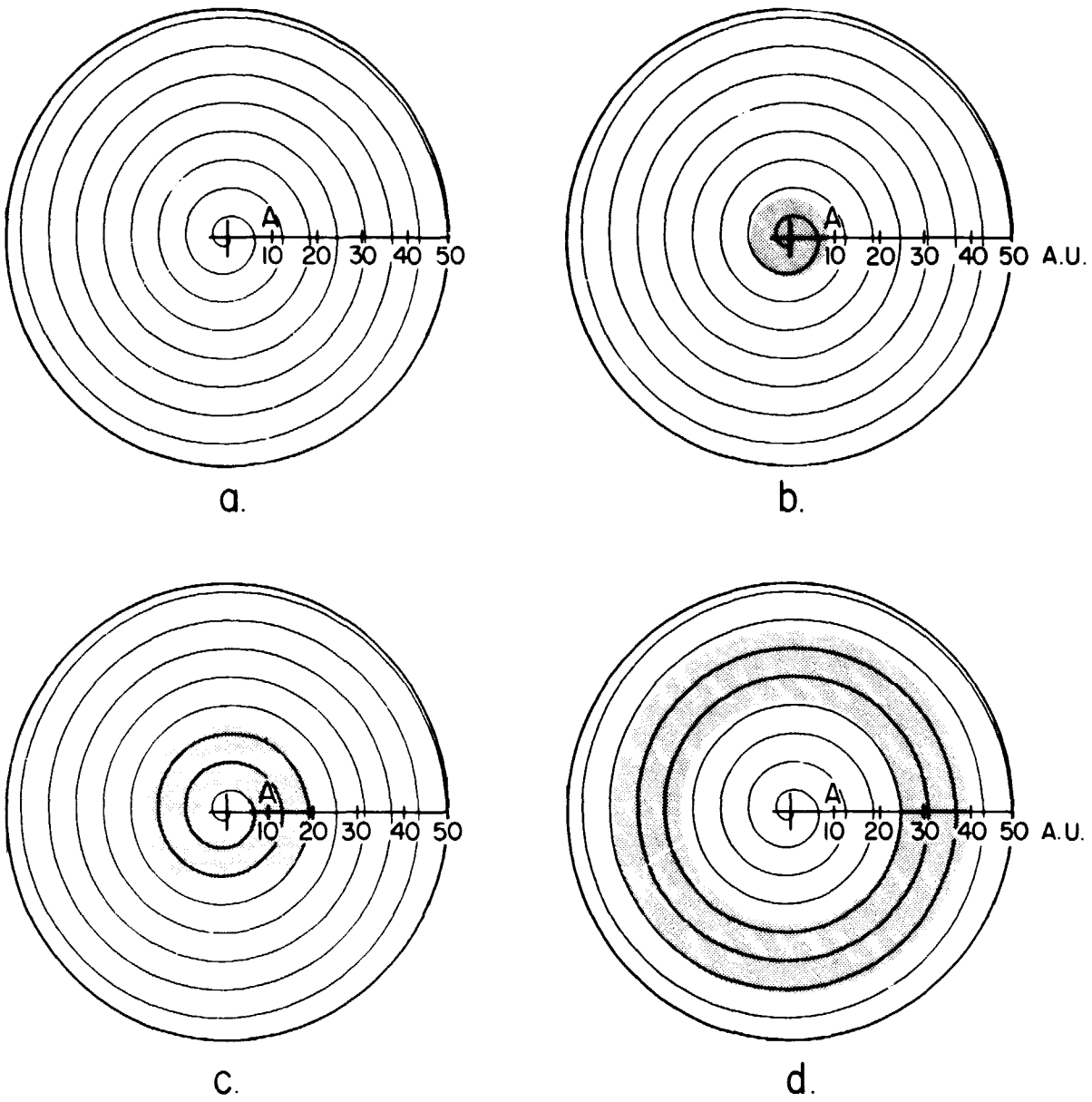

Figure 44

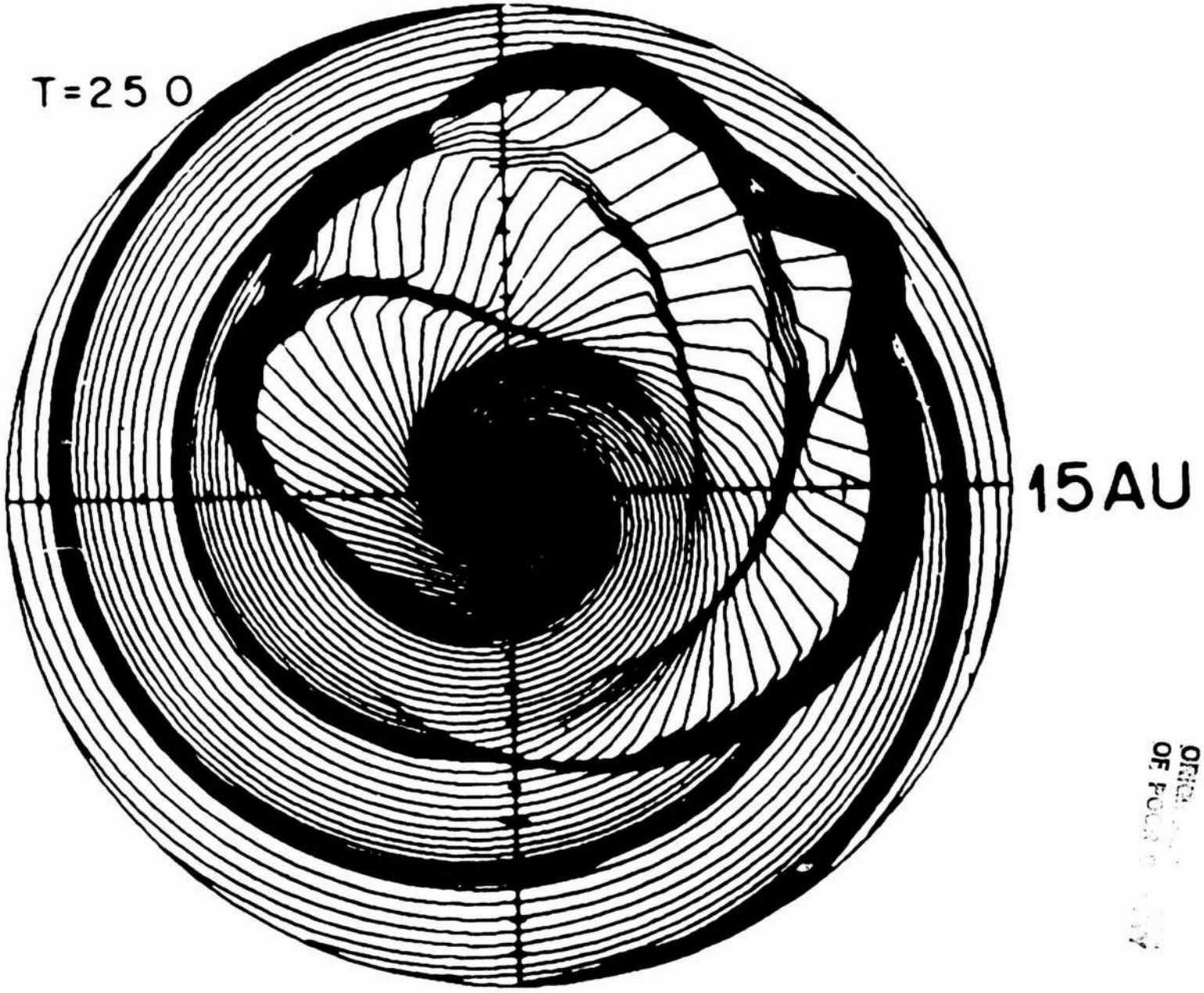

Figure 45

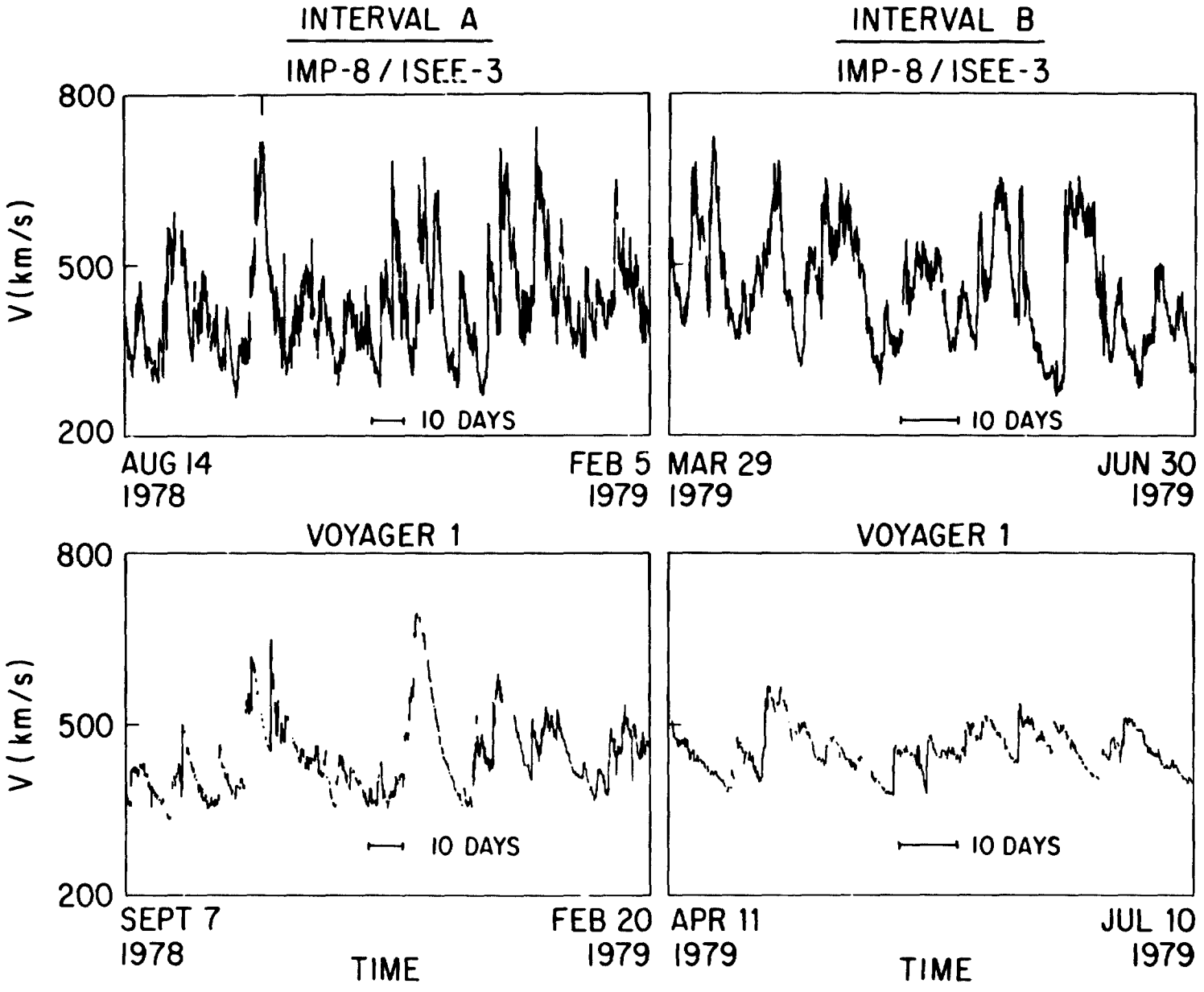

Figure 46

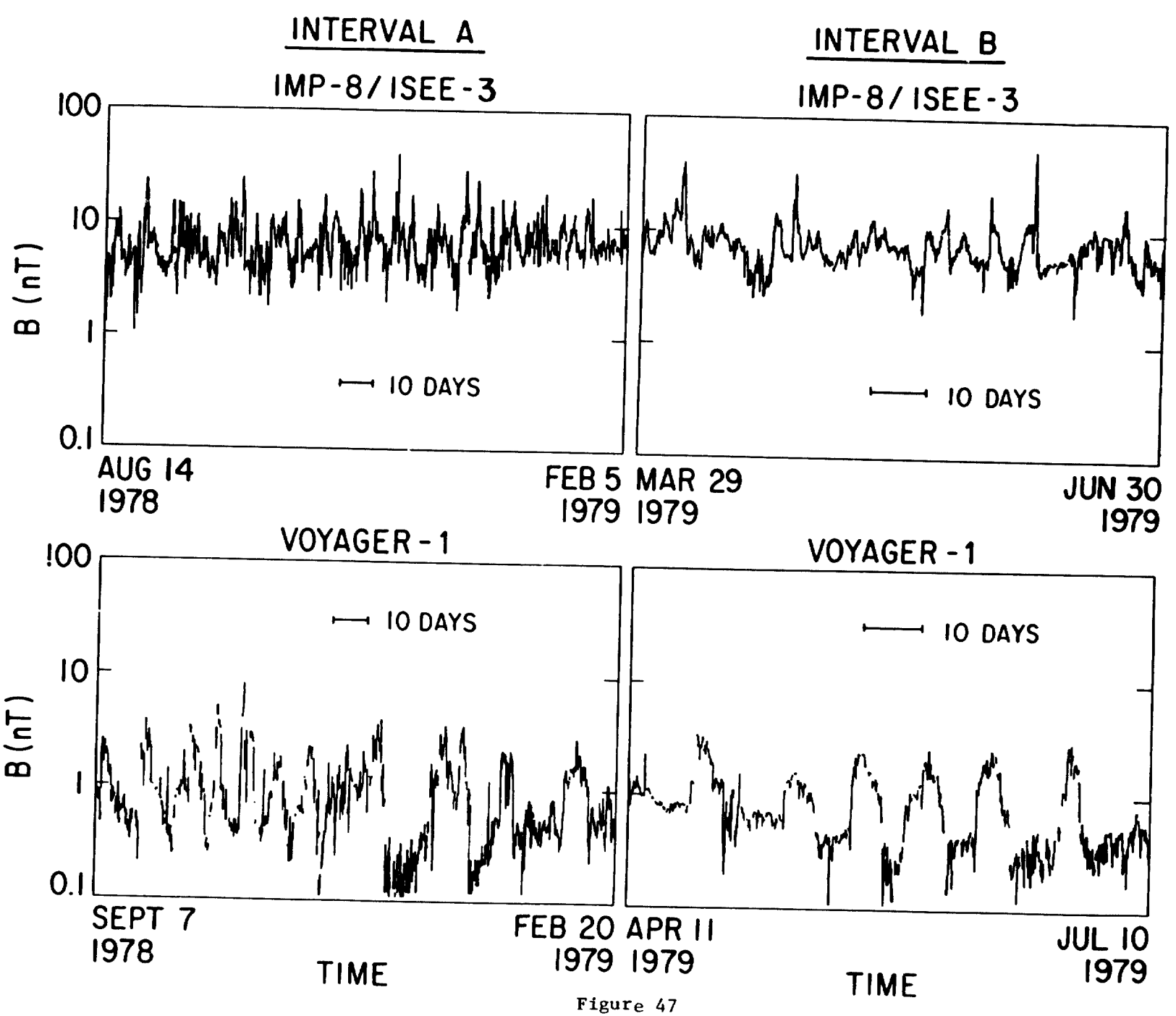

Figure 47

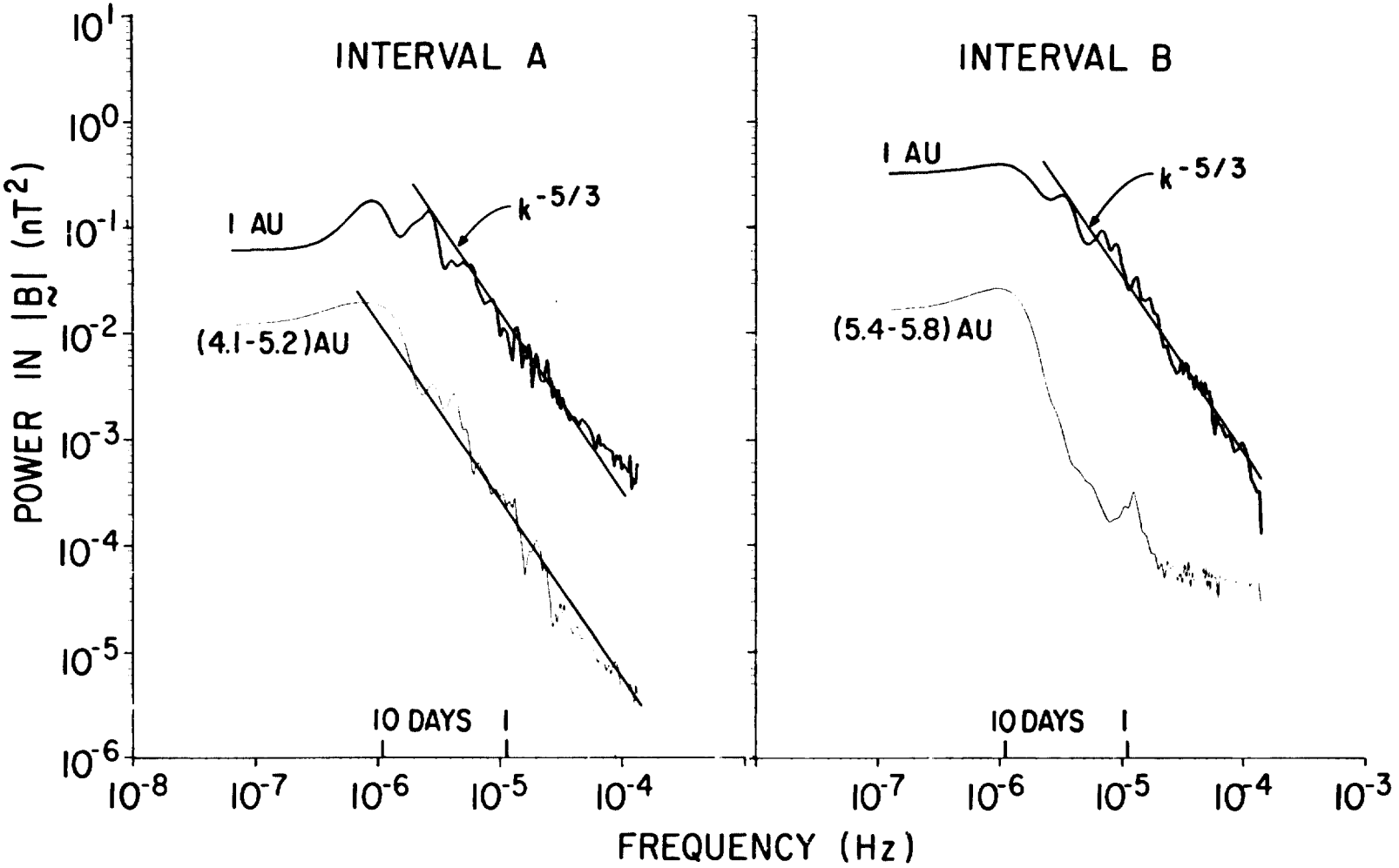
INTERVAL A
INTERVAL B
1 AU
k -5/3
(4.1-5.2)AU
(5.4-5.8)AU
10 DAYS
POWER IN |B|² (nT²)
FREQUENCY (Hz)

Figure 48

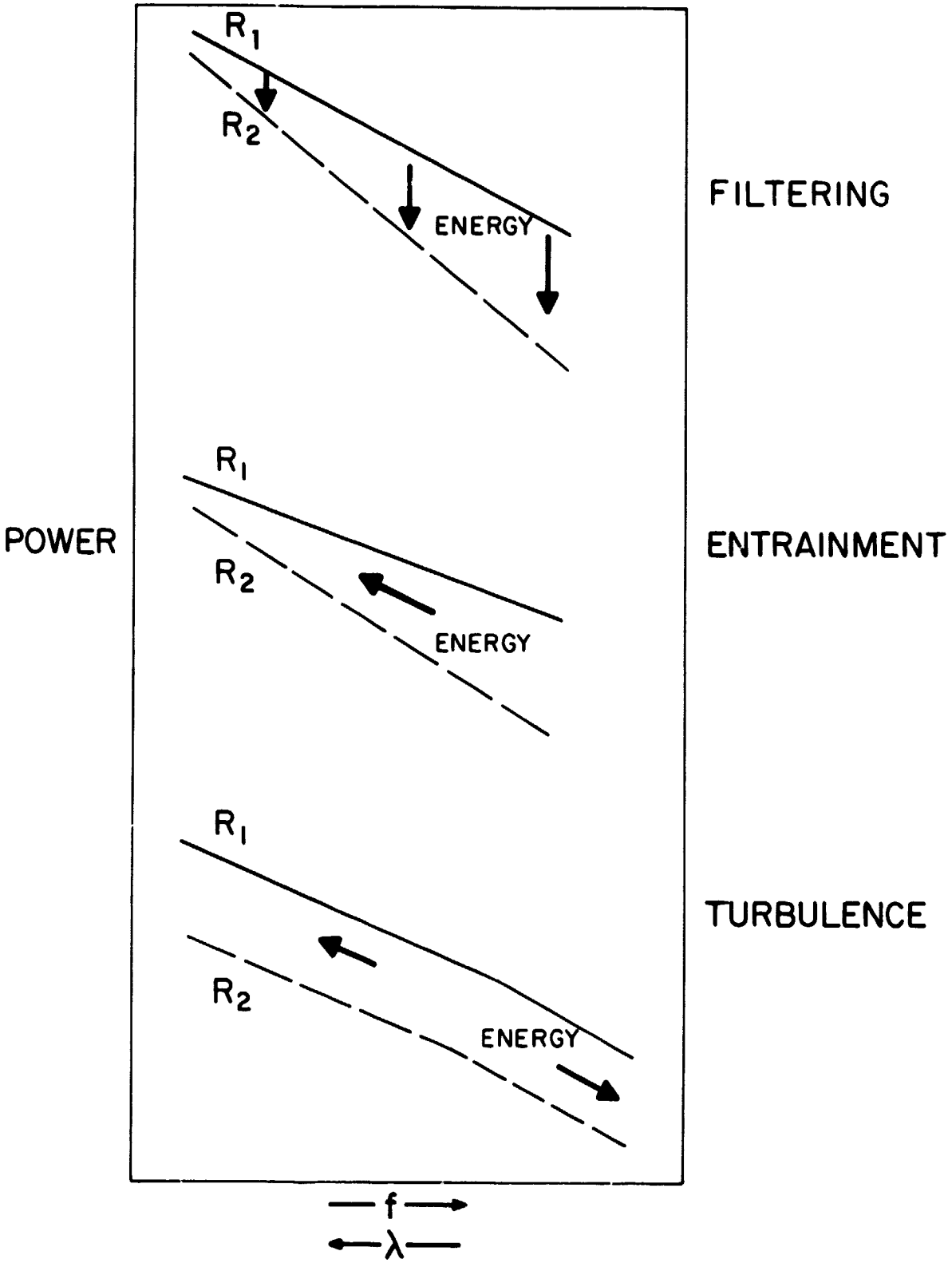

Figure 49